NASA TECHNICAL NOTE

NASA TN D-8212 ℓ. 1

NASA TN D-8212

APPLICATION OF THE AERODYNAMIC
ENERGY CONCEPT TO FLUTTER
SUPPRESSION AND GUST ALLEVIATION
BY USE OF ACTIVE CONTROLS

E. Nissim, A. Caspi, and I. Lottati

Langley Research Center
Hampton, Va. 23665

NATIONAL AERONAUTICS AND SPACE ADMINISTRATION • WASHINGTON, D. C. • JUNE 1976

1. Report No. NASA TN D-8212	2. Government Accession No.	3. Recipient's Catalog No.
4. Title and Subtitle APPLICATION OF THE AERODYNAMIC ENERGY CONCEPT TO FLUTTER SUPPRESSION AND GUST ALLEVIATION BY USE OF ACTIVE CONTROLS		5. Report Date June 1976
		6. Performing Organization Code
7. Author(s) E. Nissim, A. Caspi, and I. Lottati		8. Performing Organization Report No. L-10738
		10. Work Unit No. 512-53-01-05
9. Performing Organization Name and Address NASA Langley Research Center Hampton, Va. 23665		
		11. Contract or Grant No.
12. Sponsoring Agency Name and Address National Aeronautics and Space Administration Washington, D.C. 20546		13. Type of Report and Period Covered Technical Note
		14. Sponsoring Agency Code

15. Supplementary Notes

16. Abstract

The effects of active controls on flutter suppression and gust alleviation of two different types of subsonic aircraft (the Arava twin turboprop STOL transport and the Westwind twin-jet business transport) are investigated. The active control surfaces are introduced in pairs which include, in any chosen wing strip, a 20-percent chord leading-edge (L.E.) control and a 20-percent chord trailing-edge (T.E.) control. Each control surface is driven by a combined linear-rotational sensor system located on the activated strip. The control law is based on the concept of aerodynamic energy and utilizes previously optimized control law parameters based on two-dimensional aerodynamic theory. The best locations of the activated system along the span of the wing are determined for bending-moment alleviation, reduction in fuselage accelerations, and flutter suppression. The effectiveness of the activated system over a wide range of maximum control deflections is also determined. Two control laws are investigated. The first or basic control law utilizes both rigid-body and elastic contributions of the motion. The second or extended control law employs primarily the elastic contribution of the wing and leads to large increases in the activated control effectiveness as compared with the basic control law.

The results indicate that flutter speed can be significantly increased (over 70 percent increase) and that the bending moment due to gust loading can be almost totally eliminated by a control system of about 10 to 20 percent span with reasonable control-surface rotations. Large reductions in fuselage accelerations can also be obtained by a small number of activated L.E.-T.E. control systems.

17. Key Words (Suggested by Author(s)) Flutter suppression Gust alleviation Dynamic loads Aircraft design Active controls	18. Distribution Statement Unclassified — Unlimited Subject Category 39

19. Security Classif. (of this report) Unclassified	20. Security Classif. (of this page) Unclassified	21. No. of Pages 92	22. Price* $4.75

APPLICATION OF THE AERODYNAMIC ENERGY CONCEPT

TO FLUTTER SUPPRESSION AND GUST ALLEVIATION

BY USE OF ACTIVE CONTROLS

E. Nissim,[*] A. Caspi,[†] and I. Lottati[‡]
Langley Research Center

SUMMARY

The effects of active controls on flutter suppression and gust alleviation of two different types of subsonic aircraft (the Arava twin turboprop STOL transport and the Westwind twin-jet business transport) are investigated. The active control surfaces are introduced in pairs which include, in any chosen wing strip, a 20-percent chord leading-edge (L.E.) control and a 20-percent chord trailing-edge (T.E.) control. Each control surface is driven by a combined linear-rotational sensor system located on the activated strip. The control law is based on the concept of aerodynamic energy and utilizes previously optimized control law parameters based on two-dimensional aerodynamic theory. The best locations of the activated system along the span of the wing are determined for bending-moment alleviation, reduction in fuselage accelerations, and flutter suppression. The effectiveness of the activated system over a wide range of maximum control deflections is also determined. Two control laws are investigated. The first or basic control law utilizes both rigid-body and elastic contributions of the motion. The second or extended control law employs primarily the elastic contribution of the wing and leads to large increases in the activated control effectiveness as compared with the basic control law.

The results indicate that flutter speed can be significantly increased (over 70 percent increase) and that the bending moment due to gust loading can be almost totally eliminated by a control system of about 10 to 20 percent span with reasonable control-surface rotations. Large reductions in fuselage accelerations can also be obtained by a small number of activated L.E.-T.E. control systems.

[*]NRC-NASA Resident Research Associate, on leave from Technion — Israel Institute of Technology, Haifa, Israel.

[†]Israel Aircraft Industry, Lod, Israel, formerly with Technion — Israel Institute of Technology. Haifa, Israel.

[‡]Technion — Israel Institute of Technology, Haifa, Israel.

L

INTRODUCTION

The technological advances made in recent years in the field of control systems have stimulated considerable interest in evaluating the advantages of incorporating active control systems in aircraft. (See ref. 1.) The potentials of active controls for gust alleviation and mode stabilization have been analyzed for some specific aircraft such as the XB-70 (refs. 2 and 3) and the B-52 (refs. 4 and 5). Within the last few years, control systems that increase the damping of the lower frequency structural modes have evolved from analytical feasibility studies to production hardware. Such a system, which controls the response of the rigid-body mode and one elastic mode (first aft body bending) to gust inputs, has been successfully installed on the B-52G and B-52H fleets. A reduction in gust loads and a considerable extension of the fatigue life of the aircraft (ref. 6) have resulted. Some recently developed hardware indicates that flutter-suppression systems (controlling higher frequency unstable modes) are now technologically feasible. Analytical studies have shown that in many instances, weight savings by as much as 4 percent of the total structural weight of large aircraft like the supersonic transport or the Rockwell International B-1 can be achieved by suppressing flutter by active controls rather than by passive methods. This is a considerable weight saving when it is considered that the payload may be as small as 20 percent of the structural weight. (See refs. 7 and 8.)

A number of investigators have recently embarked on experimental flutter-suppression studies aimed at verifying analytical results. These studies provided experimental verification regarding the possibilities of suppressing flutter by active controls (refs. 9 to 15) and led to the pioneering flight-test demonstration using the B-52 airplane. (See ref. 16.)

One of the major difficulties which characterizes the introduction of active control systems into elastic structures lies in the need to determine a large number of parameters associated with the control system. An additional difficulty is introduced by the fact that an elastic structure, like an aircraft, cannot be considered as a fixed system since the properties of the system vary with the flight configuration, time of flight, etc. Hence, a proper optimization process must sweep over a very large number of parameters, including a large number of flight configurations. The determination of a satisfactory control law which copes with the variety of flight configurations can be seen to be a difficult task which requires considerable ingenuity from the control system designer.

In an attempt to reach an optimization procedure which does not exhibit sensitivity to flight configurations and to reduce to a minimum the number of arbitrary assumed parameters, the aerodynamic energy concept was developed. (See refs. 17 to 19.) The following general results are obtained by using the aerodynamic energy analysis:

(a) Optimum systems should include both leading-edge (L.E.) and trailing-edge (T.E.) control surfaces in each controlled strip.

(b) Optimum systems should be activated by both linear and rotational sensors located on the activated strip.

(c) Very general control laws can be assumed (based on the nature of the aerodynamic forces), and their coefficients determined for optimum performance irrespective of the type of aircraft, mass and stiffness distribution, center of gravity (c.g.) or elastic-axis locations, and reduced frequency or Mach number (within the subsonic range).

The remaining parameters such as the spanwise location of the active strips and some free gain parameters can be determined for specific aircraft together with the magnitude of the improvement obtained.

Flutter-suppression and gust-alleviation problems are closely interrelated and cannot be treated separately. This is true since flutter-suppression considerations impose no limitations on the values of the control law parameters whereas gust response considerations yield an upper bound to the control law values. This upper bound insures reasonable control-surface rotations over the flight envelope of the aircraft. Furthermore, the effects of the flutter-suppression system on the gust response characteristics of the aircraft need to be established. For this reason, the effects of the free parameters of this problem are investigated by bearing in mind both flutter-suppression and gust-alleviation problems. The purpose of the present work is to apply the initially optimized results, obtained through the use of the aerodynamic energy method, to flutter suppression and gust alleviation of specific aircraft. More specifically, the effects of the control parameters on the following aircraft characteristics are investigated:

(1) The maximum absolute value of the bending moment acting on the wing due to gust input,

(2) The acceleration at the center of gravity of the aircraft and along the fuselage due to gust input, and

(3) The flutter speed.

Some indication of the effects of the active control system on the short-period stability is included in this paper. However, no consideration is given to problems associated with controllability.

<div align="center">SYMBOLS</div>

b   semichord length

[C],[G],[R]   control law matrices defined by equation (1)

F_A aerodynamic forces

F_c control forces

F_I inertia forces

F_{RE} $= F_A + F_I$

h   displacement defined in sketch (a)

$\bar{h}$ $= h - h_r$

M_b bending moment

t   time

V   velocity

V_c design cruising speed of aircraft

V_g upgust velocity

α, β, δ rotations defined in sketch (a)

$\bar{\alpha}$ $= \alpha - \alpha_r$

δ_c value of δ when either bending moment or center-of-gravity acceleration of unalleviated aircraft reaches maximum value

ω circular frequency

$\omega_r, \omega_{r,1}, \omega_{r,2}$ reference frequencies

Subscripts:

cg   center of gravity

f   flutter

4

max   parameter relates to maximum value

r   parameter relates to reference section

Dots over symbols denote derivatives with respect to time.

CONTROL SYSTEM

The basic control system consists of a pair of leading- and trailing-edge control surfaces alined in the streamwise direction and having a width in the order of a tenth of a wing semispan. The control surfaces together with the wing surface between them are referred to as an activated strip. In the simplest form of the control concept, the deflections of the control surfaces are commanded to be proportional to the linear and rotational motion of the strip. A control system consists of one or more activated strips located on the wing and/or tail surfaces.

The aerodynamic forces acting on a wing section depend on the displacement h/b of a reference point along the chord (measured in semichord lengths b), the angle of rotation α as well as on their first and second time derivatives, that is, $\dot{h}/b$, $\dot{\alpha}$, $\ddot{h}/b$, and $\ddot{\alpha}$. (See sketch (a).) It can therefore be expected that the L.E. control rotation β and the T.E. control rotation δ will be a function of these parameters; that is,

Sketch (a)
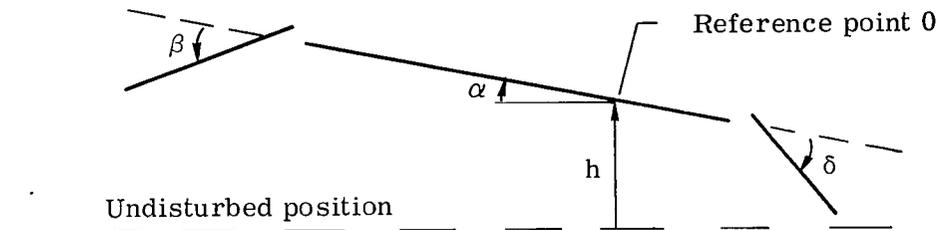
$$\begin{Bmatrix} \beta \\ \delta \end{Bmatrix} = [C]\begin{Bmatrix} h/b \\ \alpha \end{Bmatrix} + \frac{1}{\omega_r}[G]\begin{Bmatrix} \dot{h}/b \\ \dot{\alpha} \end{Bmatrix} + \frac{1}{\omega_{r,1}^2}[R]\begin{Bmatrix} \ddot{h}/b \\ \ddot{\alpha} \end{Bmatrix} \tag{1}$$

where $[C]$, $[G]$, and $[R]$ are square 2 by 2 matrices. The reference frequencies ω_r and $\omega_{r,1}$ are introduced to maintain the nondimensionality of equation (1) and can be used as free gain parameters. The matrix $[R]$ can be neglected since the aerodynamic inertia forces are relatively small at the usual range of flutter frequencies. Hence, the following basic control law will be used during the initial stages of this work (an extended control law is suggested later in this work):

$$\left\{ \begin{matrix} \beta \\ \delta \end{matrix} \right\} = [C] \left\{ \begin{matrix} h/b \\ \alpha \end{matrix} \right\} + \frac{1}{\omega_r} [G] \left\{ \begin{matrix} \dot{h}/b \\ \dot{\alpha} \end{matrix} \right\} \tag{2}$$

The aerodynamic energy analysis shows (ref. 17) that the optimum values of $[C]$ and $[G]$ are insensitive to the value of ω_r. Furthermore, the smaller ω_r is, the more effective the active controls become. Equation (2) can also be written as

$$\left\{ \begin{matrix} \beta \\ \delta \end{matrix} \right\} = [C] \left\{ \begin{matrix} h/b \\ \alpha \end{matrix} \right\} + i \frac{\omega}{\omega_r} [G] \left\{ \begin{matrix} h/b \\ \alpha \end{matrix} \right\} \tag{3}$$

The values recommended in reference 17 for the matrices $[C]$ and $[G]$ have been adopted in the present work; that is,

$$[C] = \begin{bmatrix} 0 & 5.6 \\ 0 & -1.4 \end{bmatrix}$$

$$[G] = \begin{bmatrix} 0 & 1.5 \\ -0.4 & 0.1 \end{bmatrix}$$

Changes are introduced in the values of G_{12} to reduce the maximum L.E. control rotation, whenever necessary, and to bring it closer to the maximum T.E. control rotation.

It is important to note here that unlike in reference 17, h/b is taken to be positive in the upward direction. This case requires a change of sign of the first column of each of the optimized matrices $[C]$ and $[G]$ which appear in reference 17. Modifications of the basic control law are introduced within the section "Supplementary Investigation" presented later.

APPROACH

Two methods are common in gust analysis — the discrete gust approach and the continuous gust approach. There are some distinct advantages to the continuous gust approach. It is not biased toward a specific gust frequency or gust shape since it uses atmospheric turbulence information as input. Furthermore, oscillatory aerodynamic coefficients (including control-surface coefficients) are used and these are readily available for both compressible and incompressible flows. Its main disadvantage lies, however, in the fact that statistical quantities are involved as response output. These

6

quantities do not lend themselves to an easy understanding of the physical side of the problem. The discrete gust approach enables one to follow the response of the aircraft in the time domain and thus promotes the understanding of the physical aspects of the problem. However, it has its own disadvantages. It has a distinct bias toward the gust input parameters, such as the gust frequency and gust velocity (often stipulated by federal aviation authorities), and the aerodynamic coefficients relating to control rotations or to unsteady compressible flow are not readily available. Nevertheless, the discrete gust approach has been adopted in this work since the physical aspects of the problem are considered to be very important.

Mathematical Model

The whole aircraft is treated as one dynamic system. It is assumed that the motion of the aircraft can be described by its rigid-body translation, rigid-body rotation, and the superposition of up to 10 elastic modes. The wing and horizontal tail are each permitted to accommodate up to 10 activated strips. Time lag in gust encounter between the wing and the horizontal tail is incorporated in the dynamic system.

Aerodynamics

The nonsteady aerodynamic forces arising due to a step deflection of either the L.E. or T.E. control surfaces are derived in the appendix for two-dimensional flow and zero Mach number. Nonsteady strip theory aerodynamics (involving the classical Wagner and Küssner functions) is employed throughout this work. The resulting aerodynamic forces are modified by introducing approximate finite-span effects through the square-root factor which yields the well-known wing-tip singularity. In addition, approximate compressibility effects are simulated through the introduction of the Prandtl-Glauert correction.

Computer Program

For any combination of activated control strips, the program provides the time histories of the motions of the airplane, elastic deformation of the structure, control-surface rotations, and the bending-moment loads. Flutter speed is determined from observations of the time history of the oscillation associated with the structural deformation.

APPLICATION

Description of the Aircraft

The complete geometric and dynamic data of two aircraft were made available to the writer for the purpose of the present investigation. These aircraft are the twin-boom

Arava STOL transport and the Westwind business jet transport. These two considerably different aircraft are briefly described in the following sections.

Arava aircraft.- The Arava (fig. 1) is a light-loading, low-speed, low-altitude STOL twin-turboprop transport (maximum mass 6800 kg). The high wings are hinged (in bending) at their roots and retained by struts which are attached to the wings at points lying ahead of the quarter-chord point around half the semispan. The twin-boom structure which carries the tail unit provides strong elastic coupling between wing and tail. In general, the aircraft is a highly elastic light transport.

Westwind aircraft.- The Westwind (fig. 2) is the Israel Aircraft Industry modified version of the Rockwell Jet Commander and has heavier loading, high-speed and high-altitude capability. It is a twin-jet business transport with a cantilevered wing (maximum mass 9400 kg). The wing is clean with engines fitted at the rear of the fuselage and carries empty tip tanks (chosen configuration).

Spanwise Location of Activated Strips

The wing of each aircraft is divided into 10 equally spaced strips as shown in figure 3. Each strip can accommodate a pair of active controls (that is, L.E.-T.E. controls). A strip with active controls is referred to as an activated strip. The strips located along the horizontal tail are allowed spans equal to one-third and one-tenth of the horizontal-tail semispan of the Arava and Westwind aircraft, respectively. (See fig. 3.) All leading- and trailing-edge control surfaces are 20 percent chord.

In an attempt to reduce labor, the effect of ω_r on the gust response of each aircraft is investigated at only five chosen spanwise locations along the wing and one location along the tail.

Gust and Flight Speeds

The gust disturbance is assigned a 1 - cos shape and its peak value is set to 9.1 m/s for the Arava and 15.2 m/s for the Westwind for flights at V_c (the design cruising speed which is taken everywhere in this work as the flight speed, except for the flutter investigation). The flight speed V_c of the Arava and Westwind are 85 m/s and 253 m/s, respectively.

Mention should be made here that the 1 - cos gust shape yields more information regarding the response of the aircraft as compared with the step gust case previously employed (ref. 20) and is therefore believed to be advantageous.

Calculations

The time histories of the airplane and control system responses (that is, h, α, β, δ, $\dot{h}$, $\dot{\alpha}$, $\dot{\beta}$, $\dot{\delta}$, $\ddot{h}$, $\ddot{\alpha}$, and wing bending moment) and the flutter speed are determined

for a range of values of ω_r. Since the flight and gust velocities are kept constant (except for the determination of the flutter speed), the response of the control system is directly related to the value of ω_r. In other words, the value of δ_{max}, for example, is directly related, under these conditions, to the value of ω_r.

The variation with ω_r of the peak root bending moment, for example, is equivalent and more meaningful when presented in terms of δ_{max}. In order to generalize the results obtained herein and permit their presentation in a condensed form, cross plotting of the response time histories is found to be necessary. The definition of some of the quantities involved is illustrated in the following sketches. (See sketch (b).)
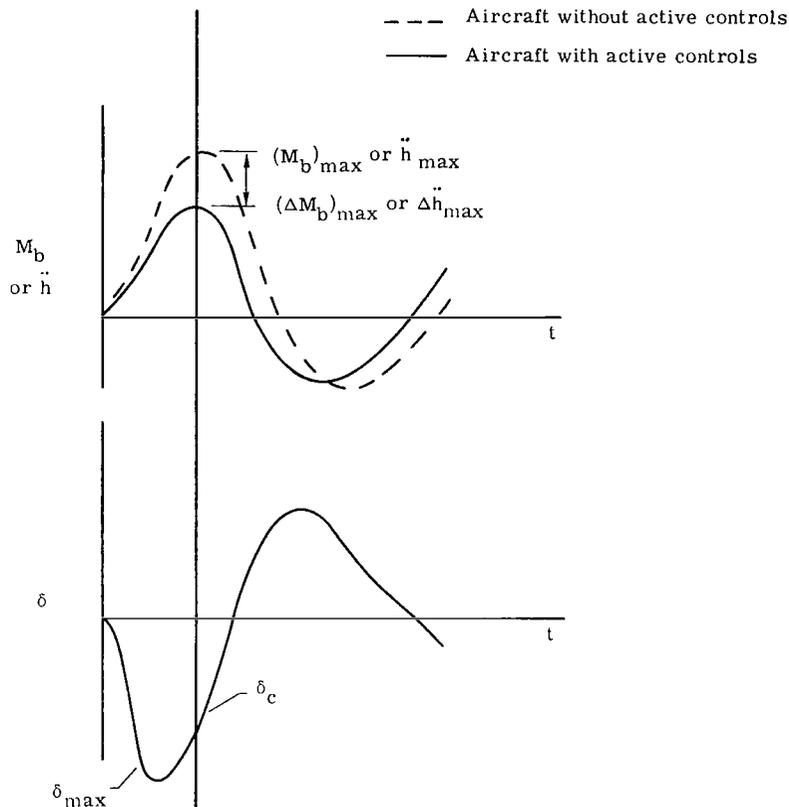
Sketch (b)

To a first order, the change in responses at the first peak $\left(\text{that is, } \left(\Delta M_b\right)_{max}, \Delta \ddot{h}_{max}\right)$ is directly proportional to δ_c and also to the gust velocity V_g. These can be made independent of the gust velocity if consideration is made of quantities such as $\left(\Delta M_b\right)_{max} \Big/ \left(M_b\right)_{max}$, $\Delta \ddot{h}_{max} \Big/ \ddot{h}_{max}$, and $\delta_c \Big/ \delta_{max}$. As already stated, the values of δ_c and δ_{max} are directly related to ω_r and, in turn, can be made independent of the gust

velocity when represented in terms of $\dfrac{\delta_c}{V_g/V_c}$ $\left(\text{or } \dfrac{\delta_{max}}{V_g/V_c}\right)$ provided the same flight speed is maintained.

Additional details regarding the general representation of the cross-plotted results, for both flutter suppression and gust alleviation, are given together with the presentation of the results.

Scope of the Analytical Investigation

Almost all the work reported herein relates to the activation of a single strip at different spanwise locations for each of the two aircraft. The results for each activated strip provide information regarding both gust alleviation and flutter suppression and are presented in a manner which enables some generalization to a multistrip activation (one example is included). Two control laws are investigated: the basic control law (presented under "Preliminary Investigation") which utilizes the total response of the airplane and the extended control law (presented under "Supplementary Investigation") which primarily employs the elastic responses of the structure. It is hoped that by treating two dynamically and widely different aircraft, as is the case in this paper, results are obtained which might be applicable to a wide variety of aircraft.

PRELIMINARY INVESTIGATION

The preliminary investigation is aimed at gaging the problems associated with the activation of a single preoptimized strip at different locations along the semispan of the wing and horizontal tail of both aircraft. The magnitude of the control-surface rotations is varied by changing the value of the free gain parameter $1/\omega_r$. The effects of these control rotations on the gust-alleviation characteristics and flutter speed of the aircraft is then determined.

In order to gain insight into the effect of active controls on the gust response of each aircraft, a sweep is made of a single activated strip along the five chosen wing stations of each aircraft. However, in order to maintain a common basis for comparisons, the parameter ω_r at each station is assigned a value which yields a maximum absolute value of control deflection of 0.5 rad. A generalization which covers a range of control-surface deflections is subsequently made.

Results and Discussion of Preliminary Investigation

The results are presented and discussed in three groups. These groups relate to the effect of active controls on the maximum bending moment of the wing, on the fuselage

accelerations, and on the flutter speed. Each such group contains the results available for both the Arava and the Westwind transports.

Bending-moment effects.- Figures 4 and 5 show the effects of the spanwise location of the activated strip on the maximum bending moment of the wing for maximum control deflections of 0.5 rad.   Mention should be made here that the maximum wing bending moment for the Arava transport is located at the inboard boundary of strip 5 where the struts join the wing. This location is unusual for conventionally built aircraft which have cantilevered wings and therefore develop maximum bending moment at the root of their wings. The Westwind, which is of conventional design, shows maximum values of bending moment at the inboard boundary of strip 10.

From figures 4 and 5 the following points emerge:

(a) The active strip, when located at the tip region of the wing is effective in reducing the positive bending moment but, at the same time, leads to an increase in the negative values of the bending moment. This may be explained in part by the fact that the external forces F_{RE} (fig. 6), which are comprised of aerodynamic forces F_A and inertia forces F_I (that is, reverse mass acceleration forces), act through an inboard section of the wing, whereas the control-surface reaction F_C to these forces acts through the activated strip located at the tip region. In addition, the control force F_C reduces the acceleration of the wing in proportion to ΔF_I. Such an arrangement promotes the bending of the wing and may lead, eventually, to a large bending moment. (Note that the $1 - \cos$ excitation is allowed for the duration of a single cycle only.) Figure 7 illustrates the case where the activated strip is located at the root of the wing. It can be seen that the contribution of F_C to the bending moment is negligible (in this case) whereas the reduction of ΔF_I leads to an increase in the maximum values of the positive bending moment. The best location of F_C to relieve the bending moment (for equal magnitudes of alleviated positive and negative peaks) is at the region of application of F_{RE} (that is, at the external forces center). When F_C is large and is brought about by a single activated strip located at the external forces center, it might shift the maximum bending-moment section toward the outboard of the wing (since the external forces are distributed over the whole of the wing). This case, however, is not realistic since the control deflections required to produce such magnitudes of F_C are beyond the practical range of a single strip. Figures 4 and 5 show that the external forces center of the Arava is located at around 55 percent of the span (just inboard of strip 5) whereas the external forces center of the Westwind is around the 35-percent span region (just inboard of strip 7). The Arava case is somewhat more complex when compared with the Westwind because of the influence of the strut's reaction. Nevertheless, the location of its external forces center can be determined from figure 4.

(b) The effectiveness of the activated controls is very different in the two aircraft treated; the Westwind shows a large reduction in the positive bending moment whereas the Arava shows a smaller reduction. The reason for this difference is threefold:

11

(1) The strut introduces a basic difference which pushes the external forces center to a region very near the maximum bending-moment section and hence reduces the effectiveness of the activated control for positive bending moment.

(2) The bending moment is a linear function of the gust angle V_g/V when the same flight speed is maintained. The activated control force is essentially a function of δ_c which designates the control deflection at the time the bending moment of the unactivated aircraft reaches its first positive peak value $\left(\left(M_b\right)_{max}\right)$. The effect of the L.E. control on the maximum bending moment is negligible compared with the effect of the T.E. control. Hence, for each station, the reduction in the positive peak value of the bending moment $\left(\left(\Delta M_b\right)_{max}\right)$ as a fraction of the positive peak bending moment (that is,

$\left(\Delta M_b\right)_{max}\Big/\left(M_b\right)_{max}$ will be approximately proportional to $\dfrac{\delta_c}{V_g/V_c}$. This relation implies that large values of $\dfrac{\delta_c}{V_g/V_c}$ should lead to larger reductions in the positive peak bending

moment. Hence, the effectiveness of a given δ_c value depends on the value of V_g/V_c. The smaller V_g/V_c is, the more effective the activated control becomes for a given δ_c. The value of V_g/V_c for the Westwind is around 0.06 whereas the corresponding value for the Arava is around 0.11; thus, the increased effectiveness of the Westwind is explained. In general, faster aircraft have smaller V_g/V_c values and this gives them an advantage over slower aircraft.

(3) The constraint on the control-surface rotation applies to the maximum value of rotation. It therefore follows that the larger δ_c/δ_{max} is, the more effective the active control becomes $\left(\left|\beta_{max}\right| \leqq \left|\delta_{max}\right|\right.$ in all cases being maintained through appropriate variation of $G_{12}\Big)$. The values of δ_c/δ_{max} for the Westwind are around 0.95 whereas the corresponding values for the Arava are around 0.65. This phenomenon further explains the reduced effectiveness of the Arava control as compared with the Westwind.

A logical outcome of this discussion is the representation of $\left(\Delta M_b\right)_{max}\Big/\left(M_b\right)_{max}$ as a function of $\dfrac{\delta_c}{V_g/V_c}$ and δ_c/δ_{max} as a function of $\dfrac{\delta_c}{V_g/V_c}$ at the different stations along the span of the wing. This representation is meaningful provided the activated controls do not act to promote increased bending response at later time intervals, that is, when the control forces act to the outboard of the external forces center. Hence, the results pertinent to $\left(\Delta M_b\right)_{max}\Big/\left(M_b\right)_{max}$ as a function of $\dfrac{\delta_c}{V_g/V_c}$ at strip 1, for example

(that is, at the wing tip), are meaningful provided the control surface at strip 1 is activated in conjunction with other active strips located along the span of the wing in a manner which insures that the resultant control force acts through the external forces center. Figures 8 and 9 show this variation of $\left(\Delta M_b\right)_{max}\big/\left(M_b\right)_{max}$ and δ_c/δ_{max} as a function of $\dfrac{\delta_c}{V_g/V_c}$ for both the Arava and the Westwind transports. The bending-moment curves show the expected linear relationship between $\left(\Delta M_b\right)_{max}\big/\left(M_b\right)_{max}$ and $\dfrac{\delta_c}{V_g/V_c}$ (except for very large bending-moment reductions which shift the activated maximum bending-moment curve toward the origin). The curves of δ_c/δ_{max} against $\dfrac{\delta_c}{V_g/V_c}$ for both aircraft show some slight nonlinear effects.

As already stated, the parameter δ_c/δ_{max} is very important since it has a strong effect on the effectiveness of the control rotations. It seems reasonable to expect that δ_c/δ_{max} will, in general, be a function of both the gust frequency and the natural frequencies of the aircraft. The gust frequency of the Westwind is around 5 Hz and is very near the first wing bending frequency ($\approx$6.5 Hz). In the Arava case, the gust frequency is around 1.7 Hz whereas the first wing bending frequency is around 6.5 Hz.

The effect of the values of airplane frequencies on the value of δ_c/δ_{max} is illustrated in the following discussion. Let δ_c/δ_{max} be equal to unity. This means that δ varies in phase with the bending moment. However, the bending moment itself varies almost in phase with the external forces acting on the aircraft. It therefore follows that by attempting to obtain $\delta_c/\delta_{max} = 1$, δ will vary in phase with the external forces. Equation (2) shows that if the extreme cases where ω_r is large are excluded, the second term in this equation can then be made dominant. This result implies that δ varies in phase with the velocity of the response. Hence, the stated object of having δ vary in phase with the external forces is equivalent to having the response velocity vary in phase with the external forces. Such a relationship exists only when the external forces excite the structure at one of its natural frequencies. The frequency of the rigid-body translation is zero; thus, the first wing bending frequency is left as the lowest natural frequency which might substantially affect δ_c/δ_{max}.

At this stage it is appropriate to draw attention to the fact that some rigid-body excitation will take place even when the gust frequency is identical to the wing natural frequency. This is particularly true since the gust excitation forces used in the present work (that is, 1 - cos) do not have a zero mean value. However, the large elastic response, in the latter case, is dominant and subsequently leads to large δ_c/δ_{max} values. Mention should also be made that the rotation of the controls introduce external

forces which lag both the control rotation and the response velocity. Therefore, these considerations relate to general trends only and permit some deviations whenever the secondary effects become larger.

Drawing attention to the gust frequency, it should be remembered that the Federal Aviation Regulations (F.A.R.) base this frequency on a 25-chord wavelength. Therefore, the faster the aircraft, the higher the value of the gust frequency. These higher gust frequencies, acting on faster flying aircraft, are thus brought closer to the first wing bending frequency and are generally responsible for the development of large gust loads. It is therefore interesting to note that the bending-moment alleviation using active controls is most effective $\left(\text{through the values of } \delta_c/\delta_{max} \text{ and } V_g/V_c\right)$ when the gust loads are largest. Similar conclusions can be obtained by using the continuous atmospheric turbulence approach since most of the turbulence frequencies lie within a frequency region which is strongly dependent on the flight speed.

The curves presented in figures 8 and 9 can readily be used to yield results for different values of δ_{max} and V_g. Take figure 9 (Westwind) as an example and determine δ_c so that δ_{max} will not exceed 1 rad at strip 1 when $V_g/V_c = 0.2$. Note that the slope of a straight line (through the origin) relative to the ordinate is given by $\dfrac{\delta_{max}}{V_g/V_c}$. In this example $\dfrac{\delta_{max}}{V_g/V_c} = 5$ and the straight line shown in figure 9 crosses the curve at point A to give $\dfrac{\delta_c}{V_g/V_c} = -4.4$. With this value of $\dfrac{\delta_c}{V_g/V_c}$, $\left(\Delta M_b\right)_{max}\Big/\left(M_b\right)_{max}$ can be determined from the same figure, which yields the value of -0.2 (that is, 20 percent reduction). The advantages of the graphical representation are now clearly evident.

Fuselage acceleration effects.- The various fuselage acceleration effects are presented in this section.

Center of gravity: The effect of the spanwise location of the activated strip on the center-of-gravity acceleration, for $\delta_{max} = 0.5$ rad is shown in figures 10 and 11. Here again it can be seen that the activated strips at the wing-tip region are relatively ineffective in reducing the center-of-gravity accelerations. The reason for this ineffectiveness originates from the fact that the activated strip at the tip region reduces the local wing acceleration and is unable to reduce the center-of-gravity acceleration because of the promotion of wing bending, as explained in an earlier section of this paper. The best spanwise location of the activated strip for maximum reduction in the center-of-gravity acceleration can be seen to lie at the wing-root section (strip 10), where the local aerodynamic coefficients per unit span are largest (because of the finite-span effect) and where direct bending effects are negligible.

14

In a manner similar to the bending-moment case, one can define a new value of δ_c which corresponds to the control-surface deflection when the center-of-gravity acceleration of the unactivated aircraft reaches its first maximum and can represent $\left(\Delta \ddot{h}_{cg}\right)_{max} \Big/ \left(\ddot{h}_{cg}\right)_{max}$ as a function of $\dfrac{\delta_c}{V_g/V_c}$ and δ_c/δ_{max} as a function of $\dfrac{\delta_c}{V_g/V_c}$. (See figs. 12 and 13.) The points previously discussed of the differences in effectiveness between the Westwind and the Arava transports due to the different $\dfrac{\delta_c}{V_g/V_c}$ and δ_c/δ_{max} values apply also to the center-of-gravity accelerations and confirm once again the advantages of fast aircraft over slower ones in regard to gust-alleviation problems.

It might be of interest to note that the peak value of $\ddot{h}_{cg}$ is almost in phase with the peak value of the bending moment; thus, almost identical δ_c values are obtained. For the Arava case, the curve representing δ_c/δ_{max} as a function of $\dfrac{\delta_c}{V_g/V_c}$ for the center-of-gravity accelerations is, in fact, identical to the one obtained from the bending-moment variation and is therefore not included in figure 12.

Acceleration at other stations along the fuselage: It is important to reduce the levels of accelerations not only at the center of gravity of the aircraft but also at different stations along the fuselage. Three points are chosen to indicate the accelerations of the fuselage. One of these points coincides with the center of gravity of each of the aircraft and has already been discussed. A second point, designated as point 1, is located along the axis of the fuselage aft of the center of gravity, and a third point, designated as point 2, is located along the same axis, forward of the center of gravity. For the Arava transport, points 1 and 2 are located at 3 m aft of and 3 m forward of the center of gravity. For the Westwind transport, points 1 and 2 are located 2.58 m aft of and 6.73 m forward of the center of gravity, respectively. Since both of the aircrafts under investigation are transport planes, a reduction in the accelerations at these three points, which span the length of the fuselage, has a strong influence on the ride comfort of the aircraft.

Figures 14 and 15 show the accelerations at points 1 and 2 for the two aircraft for maximum control rotations of 0.5 rad. The similarity between the accelerations at these points and the center-of-gravity acceleration is apparent and it shows the increased effectiveness of the inboard stations over the outboard ones. It can be seen that the accelerations at point 2 (forward of the center of gravity) are smaller than the center-of-gravity accelerations whereas the accelerations at point 1 (aft of the center of gravity) are larger than those of the center of gravity. Thus, the existence of a pitch-down acceleration is indicated.

Pitch acceleration: Figures 16 and 17 show the variation of the pitch-down accelerations around the center of gravity (rigid-body acceleration). It can be seen that the activated wing strips have little effect on the pitch accelerations.

Flutter speed effects.- It is useful to relate the flutter speed results with the gust response results through the representation of $\Delta V_f/V_f$ as a function of $\dfrac{\delta_c}{V_g/V_c}$, where ΔV_f represents the increase in the flutter speed due to the activated control, V_f represents the flutter speed of the unactivated airplane, and δ_c relates to the value of δ where the bending moment is maximum. For flutter speed calculations, the value of δ_c is irrelevant. However, it serves as a measure of ω_r and can be used to define the value of δ_{max} through the use of δ_c/δ_{max} as a function of $\dfrac{\delta_c}{V_g/V_c}$.

The flutter speeds for the unactivated Arava and Westwind aircraft are 233 m/s and 320 m/s, respectively. The high flutter speed of the Westwind leaves a very small margin for ΔV_f before crossing into the supersonic regime. Therefore, some changes in configuration were made (by essentially increasing the mass of the wings) which reduced the flutter speed to 240 m/s. Hence, the Westwind flutter results relate (unfortunately) to a different configuration and therefore, special computer runs were made to determine the variation of δ_c/δ_{max} with $\dfrac{\delta_c}{V_g/V_c}$ for this changed configuration. It should further be mentioned here that the activation of the control surfaces at high speed introduces, in the very low frequency range, an instability which looks like dynamic divergence. To counteract this instability, G_{11} is allowed a value of -0.4 for the Arava transport and a value of -1 for the Westwind. Figures 18 and 19 relate therefore to somewhat different control law parameters. Figures 18 and 19 show the variation of $\Delta V_f/V_f$ with $\dfrac{\delta_c}{V_g/V_c}$ and δ_c/δ_{max} with $\dfrac{\delta_c}{V_g/V_c}$ with the spanwise location of the activated strip. It can be seen that, as expected, the most effective location of the activated strip for flutter suppression is at the tip region. For purposes of illustration, imagine that maximum control-surface rotations of 0.18 rad at V_c are allowed. For the Westwind, this assumption yields a value of $\dfrac{\delta_{max}}{V_g/V_c}$ around -3. Figure 19 (strip 1) shows that for a slope of -3 with respect to the ordinate, a value of about -3 is obtained for $\dfrac{\delta_c}{V_g/V_c}$. With this value for $\dfrac{\delta_c}{V_g/V_c}$, figure 19 shows that an increase of about 70 percent in flutter speed is obtained.

Mention should be made here that significant values of $\Delta V_f/V_f$ bring the flutter speeds into the supersonic regime while subsonic aerodynamics is used. However, $\Delta V_f/V_f$ should be considered in those cases only as an indication of beneficial effects and should not be used quantitatively. It is very interesting to note that the introduction of G_{11} leads to large increases in the values of the flutter speed for both the Arava and Westwind transports. Further increase in the G_{11} values leads to a further increase in the flutter speeds. The parameter G_{11} is assigned the smallest value which stabilizes the divergence instability to the extent that the flutter speed can be determined. The effect of the parameter G_{11}, which is associated with the L.E. control, stresses once again the importance of the L.E. control.

Application of results to multistrip activation.- It can be seen that a single activated strip cannot be effective for flutter suppression without leading to a degradation in the bending-moment values. Furthermore, two or more activated strips are required to tackle both the flutter-suppression and gust-alleviation problems (that is, bending moment and center-of-gravity accelerations). These activated strips should be placed at the wing tip (for flutter suppression) and in the wing-root regions (for center-of-gravity acceleration) in a manner which insures that the resultant control force passes through the external forces center (for bending-moment alleviation). The representation of the results as a function of $\dfrac{\delta_c}{V_g/V_c}$ can also be used to estimate the joint effects of two or three neighboring activated strips. This case can best be illustrated by the following example:

Assume that it is desirable to find the effect of three activated strips located at strips 4, 5, and 6 of the Arava wing, maximum control deflections of 0.5 rad being allowed at each station. Since the resultant force of the three activated strips will pass around strip 5, it will be equivalent to a single force caused by a single activated strip located at strip 5, having a maximum control deflection of 1.5 rads (that is, 0.5×3). This condition leads to $\dfrac{\delta_{max}}{V_g/V_c} = 13.6$ which yields the value of $\dfrac{\delta_c}{V_g/V_c} = 9.9$. (This value is the same for both the bending moment and fuselage accelerations. See fig. 8.) The gust-alleviation and flutter-suppression effects follow from figures 8, 12, and 18 by using this value of $\dfrac{\delta_c}{V_g/V_c}$. These figures yield the following values:

$$\frac{\left(\Delta M_b\right)_{max}}{\left(M_b\right)_{max}} = -0.3 \qquad \text{(that is, 30 percent alleviation)}$$

$$\frac{\left(\Delta \ddot{h}_{cg}\right)_{max}}{\left(\ddot{h}_{cg}\right)_{max}} = -0.43 \qquad \text{(that is, 43 percent alleviation)}$$

The ratio $\Delta V_f / V_f$ was not calculated. Figure 20 shows the results obtained from a special computer run for the preceding three simultaneously activated controls. The agreement is seen to be extremely good; thus, the suggested procedure is confirmed.

Activation of a control strip along the horizontal tail.- Initial attempts to place an activated strip on the horizontal tail have led to a severe static longitudinal instability. This condition indicates that some changes will have to be introduced into the control law to permit the location of an activated strip (with no adverse effects) on the horizontal tail. This point is discussed in a subsequent section.

Summary of the Preliminary Investigation

The main points emerging from the preliminary investigation are as follows:

(1) A single activated strip promotes the bending of the wing when located at either the outboard region of the wing or at its root region.

(2) The optimum location of the activated strip for bending-moment alleviation is around the external forces center region.

(3) An activated strip located at the inboard region of the wing is most effective in reducing the center-of-gravity acceleration.

(4) An activated strip located at the outboard region of the wing is most effective for flutter suppression.

(5) The value of δ_c / δ_{max} tends to unity when the gust frequency approaches one of the wing's natural frequencies.

(6) The representation of $\left(\Delta M_b\right)_{max} / \left(M_b\right)_{max}$, $\left(\Delta \ddot{h}_{cg}\right)_{max} / \left(\ddot{h}_{cg}\right)_{max}$, and $\Delta V_f / V_f$, δ_c / δ_{max} as a function of $\dfrac{\delta_c}{V_g / V_c}$ allowed the generalization of the results over a wide range of conditions.

SUPPLEMENTARY INVESTIGATION

In the following section, the problems arising from the bending-moment degradation when locating a single activated strip at the wing-tip region are investigated and attempts are made to locate an activated strip on the horizontal tail with no adverse effects on the

longitudinal stability of the airplane. These attempts lead to the formulation of an extended control law which is subsequently applied to the basic problem of flutter suppression and gust alleviation.

Extended Control Law

It has already been mentioned, in previous sections, that the location of an activated control strip at the tip region of the wing leads to an increase in the absolute bending-moment values. This increase is clearly a result of the coupling (through the activated aerodynamic forces) between the rigid-body movements, due to the gust forces, and the wing elastic modes. These coupling effects promote the bending of the wing and require the addition of one or more active strips at the root region of the wing to force the resultant control force to pass through the external forces center. Furthermore, the rigid-body motion and these coupling effects introduce large wing responses due to gust, produce large control deflections, and thus limit ω_r to a relatively large value. This limitation of ω_r may eventually lead to a degraded performance of the activated strip at the flutter frequency since, in general, the effectiveness of the activated control increases with $1/\omega_r$ (except for those cases where ω_r is very small, as indicated in ref. 17). Hence, a control law which can either eliminate or reduce the rigid-body input to the control law or introduce some controlling elements to this latter input might prove to be superior. Such a reduction can be achieved by the following control law:

$$\begin{Bmatrix} \beta \\ \delta \end{Bmatrix} = [C]\begin{Bmatrix} \bar{h}/b \\ \bar{\alpha} \end{Bmatrix} + \frac{1}{\omega_r}[G]\begin{Bmatrix} \dot{\bar{h}}/b \\ \dot{\bar{\alpha}} \end{Bmatrix} + [C]\begin{Bmatrix} h_r/b \\ \alpha_r \end{Bmatrix} + \frac{1}{\omega_{r,2}}[G]\begin{Bmatrix} \dot{h}_r/b \\ \dot{\alpha}_r \end{Bmatrix} \tag{4}$$

where

$$\left.\begin{aligned} \bar{h} &= h - h_r \\ \bar{\alpha} &= \alpha - \alpha_r \end{aligned}\right\} \tag{5}$$

The values of h and α at the reference section are denoted in equation (5) as h_r and α_r.

The first two elements in equation (4) control the relative motion of the wing whereas the last two elements control the reference section movement. By using equation (5), equation (4) reduces to

$$\begin{Bmatrix} \beta \\ \delta \end{Bmatrix} = [C]\begin{Bmatrix} h/b \\ \alpha \end{Bmatrix} + \frac{1}{\omega_r}[G]\begin{Bmatrix} \dot{h}/b \\ \dot{\alpha} \end{Bmatrix} + \frac{1}{\omega_{r,2}}[G]\begin{Bmatrix} \dot{h}_r/b \\ \dot{\alpha}_r \end{Bmatrix} \tag{6}$$

19

In order to reduce the rigid-body contribution to the control-surface rotations, the root section is chosen as the reference section for control systems located along the wing.

It should be observed that when

$$\omega_{r,2} = \omega_r$$

equation (6) reduces to the basic control law (eq. (2)). This result implies that, in general, the reference section of an elastic structure can be controlled to a limited extent. If too large forces are applied on an elastic structure to control the motion of the reference section, dynamic instability might result. If, however, the magnitude of the forces which control the motion of the reference section is limited to values smaller than those defined by $\omega_r = \omega_{r,2}$, the stability of the system is expected to be maintained. It will therefore be postulated that stability will generally be maintained provided

$$\omega_{r,2} \geqq \omega_r \tag{7}$$

Hundreds of computer runs were made for the two aircraft by using a variety of combinations between ω_r and $\omega_{r,2}$ while maintaining equation (7). During those runs, no instability developed; thus, some measure of confirmation is provided to this postulation. The results obtained by using this extended control law are presented in the following sections.

Results and Discussion of Supplementary Investigation

The results obtained through the use of the extended control law are presented and discussed in three groups in much the same way as those relating to the ordinary control law. Each such group contains the results obtained for both the Arava and the Westwind transports and is accompanied by a discussion of these results. In all cases the value of $\omega_{r,2}$ is assigned large values compared with ω_r (at least one order of magnitude larger) in order to determine the effect of the extended control law near the extreme end of its range.

Bending-moment effects.- Figures 21 and 22 show the effects of the spanwise location of the activated strip on the maximum bending moment of the wing that are appropriate for a maximum control deflection of 0.5 rad. It should be observed that the results relating to the root section of both aircraft (strip 10) are not presented. The reason for this omission originates from the fact that since the root section of the wing has been chosen as the reference section, the extended control law reduces, in this particular case, to the ordinary control law which has already been treated. It should also be noted that the results relating to the activation of strip 8 of the Arava transport are not presented because of the extremely small values of ω_r required to produce moderate control

20

rotations. The results relating to strip 7 of the Westwind are very similar to those of strip 6 and have not been included here. The following discussion therefore relates to strips 1, 3, and 5 of the Arava and to strips 1, 4, and 6 of the Westwind. Figures 21 and 22 indicate that by eliminating the rigid-body velocities from the control law, the activated strip can be located at the tip region of the wing without promoting bending. The optimum location of the strip appears to be somewhat inboard of the wing-tip strip (strip 1). This result can clearly be seen in figure 22 which relates to the Westwind, where the results for strip 4 seem to indicate the optimality of this strip. Figure 21 which relates to the Arava, however, yields almost identical reductions in bending moment for both strips 1 and 3 and indicates that the optimum lies around strip 2. The reason for the inboard location of the optimum station is due to the finite-wing effects (elliptic distribution at the tip) and to the tapering of the wing (Westwind only) toward its tip.

A comparison between the results relating to the ordinary control law (figs. 4 and 5) and those relating to the extended control law (figs. 21 and 22) with a maximum control deflection of 0.5 rad in both cases shows the superiority of the extended control law. As an example, strip 4 of the Westwind shows almost a total reduction of the bending moment when using the extended control law, whereas the same strip with the same maximum control deflection yields only a reduction of about 60 percent. It should also be recalled that the 60-percent reduction in bending moment can be obtained provided other activated strips are located around the root section of the wing to insure that the resultant control force acts through the external forces center. It should further be recalled that the activated strips located inboard of the external forces center introduce detrimental effects regarding this positive bending-moment reduction and thus yield an overall bending-moment reduction which is smaller than 60 percent. It can therefore be seen that the basic control law (which enables the reduction of the bending moment, in this case, through the activation of more than one strip) is distinctly inferior to the extended control law in regard to bending-moment effects.

If a strict comparison on the basis of a single strip only is made, then the results relating to station 4 by use of the extended control law should be compared with those relating to station 7 (which almost coincide with the external forces center) by use of the basic control law. Figure 5 shows that for a maximum control deflection of 0.5 rad, the bending-moment reduction of the Westwind is around 35 percent; thus, the effectiveness of the extended control law is stressed. The extended control law is now investigated over a range of maximum control deflections and the results are summarized in figures 23 and 24 by using the same representation as adopted for the ordinary control law, that is, δ_c/δ_{max} as a function of $\dfrac{\delta_c}{V_g/V_c}$ and $(\Delta M_b)_{max}\Big/(M_b)_{max}$ as a function of $\dfrac{\delta_c}{V_g/V_c}$.

These remarks regarding the effectiveness of the extended control law can be seen to be appropriate over the entire range of control deflections. At the lower range of these

deflections, the relative effectiveness of the extended control law is somewhat diminished because of the reduction in the values of δ_c/δ_{max}. The reason for this reduction (in δ_c/δ_{max}) lies in the relative values of the various terms in equation (6). As already stated, $\omega_{r,2}$ is assigned large values compared with ω_r. As a result, the third term in equation (6) is very small in most cases. The first term in equation (6) has not been modified and is identical to the first term in equation (2). Thus, the second term of equation (6) represents the main difference between the basic control law and the extended control law. At this stage it becomes apparent that the second term in equation (6) must be substantially smaller than its equivalent counterpart in equation (2) (for identical values of ω_r and $[G]$) because of the smaller values of the relative velocities $\overset{.}{\overline{h}}$ and $\overset{.}{\overline{\alpha}}$ (employed in eq. (6)) compared with the space velocities $\dot{h}$ and $\dot{\alpha}$ (which are employed in eq. (2)). Thus, in order to obtain identical values of δ through the use of equations (2) and (6), the values of ω_r must be substantially reduced in equation (6) in order to compensate for the reduced response velocities $\overset{.}{\overline{h}}$ and $\overset{.}{\overline{\alpha}}$. If it is remembered, however, that the second term gives rise to aerodynamic damping forces, it follows that the stated reduction in ω_r leads to larger values of the aerodynamic damping coefficients (which are proportional to $\frac{1}{\omega_r}[G]$). It can therefore be stated that at the lower range of $\frac{\delta_c}{V_g/V_c}$, the values of ω_r are not small enough to render the second term in equation (6) dominant. At the upper range of $\frac{\delta_c}{V_g/V_c}$, this second term increases and leads to control rotations which are almost in phase with the relative response velocities $\overset{.}{\overline{h}}$ and $\overset{.}{\overline{\alpha}}$. For the remainder of the discussion, the argument regarding the conditions which yield large values of δ_c/δ_{max} follows along lines identical to those discussed earlier.

Figure 23 which relates to the Arava transport with the extended control law shows larger values of δ_c/δ_{max} (at the upper range of $\frac{\delta_c}{V_g/V_c}$) compared with those obtained through the use of the basic control law·(fig. 8). The reason for this increased effectiveness in δ_c/δ_{max} lies in the fact that the extended control law yields large damping coefficients which introduce large damping forces directly into the elastic modes and almost completely ignores the rigid-body velocities. These large damping forces lead to changes in the phase relationship between the exciting force and the response of the wing in such a direction that the response tends toward 90° phase lag, irrespective of the frequency of excitation. Such a phase lag is beneficial for the increase in δ_c/δ_{max}, as discussed earlier, and leads to the rapid decay of the response of the elastic modes.

It is interesting to note that it is almost impossible to increase $\dfrac{\delta_c}{V_g/V_c}$ $\Big($by reducing $\omega_r\Big)$ beyond the value which almost completely reduces the bending moment. This condition indicates that the activated control strip has introduced very large damping forces. Furthermore, within the range where δ_c/δ_{max} increases, there is a nonlinear relationship between the activated control effectiveness and the maximum control deflection. Thus, if the maximum control deflection is allowed to double its value, the effectiveness of the activated strip in reducing the bending moment will increase by a factor larger than 2. To illustrate this point, consider point A in figure 24 (relating to strip 1). This point corresponds to $\dfrac{\delta_{max}}{V_g/V_c} = -4.88$ and $\dfrac{\delta_c}{V_g/V_c} = -2$. The point designated as point B corresponds to $\dfrac{\delta_{max}}{V_g/V_c} = -9.76$ and $\dfrac{\delta_c}{V_g/V_c} = -9.3$. In passing from point A to point B, $\dfrac{\delta_{max}}{V_g/V_c}$ is allowed to double its value; in so doing, $\dfrac{\delta_c}{V_g/V_c}$ increases by a factor of 4.65. The resulting alleviation in the bending moment can be seen to increase from 23 percent (at point A) to 61 percent (at point B). This nonlinear dependence on δ_{max} gives, once again, an advantage to high-speed aircraft because of their relatively large values of $\dfrac{\delta_c}{V_g/V_c}$.

It should be stated however that ω_r assumes small values when yielding intermediate control-surface rotations leading to large values of ω/ω_r (eq. (3)). Reference 17 indicates that a deterioration in stability might develop at very large values of ω/ω_r. Subsequent work (ref. 21), however, indicates that some simple modifications can be introduced into the control law which may maintain the absolute stability of the control law even at very high values of ω/ω_r.

Fuselage acceleration effects.- Figures 25 and 26 show the effects of the spanwise location of the activated strip on the center-of-gravity acceleration for maximum control deflections of 0.5 rad. It can be seen, once again, that the optimum location of the activated strip for the maximum reduction of the center-of-gravity acceleration is near the root region of the wing. It should be remembered that at the root region itself, the extended control law reduces to the ordinary control law. In addition, at wing sections very near the root section, the values of ω_r required to produce reasonable control rotations become excessively small. Comparisons between figures 25 and 26 and figures 10 and 11 indicate that, in general, only minor differences can be detected between the two control laws. In those cases where the extended control law yields larger values

of δ_c/δ_{max}, the above-mentioned differences are favorable toward the extended control law (on the basis of limited control deflections). These remarks are mainly applicable to the Arava transport which shows relatively small values of δ_c/δ_{max} when the basic control law is used. Figures 27 and 28 confirm these stated trends in the representation of $\left(\Delta\ddot{h}_{cg}\right)_{max} \Big/ \left(\ddot{h}_{cg}\right)_{max}$ as a function of $\dfrac{\delta_c}{V_g/V_c}$ and δ_c/δ_{max} as a function of $\dfrac{\delta_c}{V_g/V_c}$ (for both aircrafts). It should be noted that the variation of δ_c/δ_{max} with $\dfrac{\delta_c}{V_g/V_c}$ for the Arava transport is identical to the one shown in figure 23. Figures 29 and 30 represent fuselage accelerations at points 1 and 2 that are appropriate for maximum control deflections of 0.5 rad.

Flutter speed effects.- By following identical lines as in the case of the basic control law, the representation of $\Delta V_f/V_f$ as a function of $\dfrac{\delta_c}{V_g/V_c}$ is shown in figures 31 and 32. For comparison purposes, G_{11} is assigned the same values in the supplementary investigation as those used in the preliminary investigation. The large advantages of the extended control law can immediately be seen upon comparison with the basic control law results. (See figs. 18 and 19.) This comparison indicates that there is a very close relationship between the flutter-suppression control law parameters and those relating to bending-moment alleviation. It is observed that the activated strips are most effective in suppressing flutter, when located at the tip region of the wing, at strips which are outboard of the optimum locations for maximum bending-moment reduction. It is observed (figs. 31 and 32) that at the wing tip, flutter is suppressed with very small control-surface rotations of a single activated strip. The Arava transport requires $\delta_{max} \approx 0.07$ rad whereas the Westwind transport requires $\delta_{max} \approx 0.2$ rad. The higher gains required for substantial bending-moment alleviation will also result in increased flutter-suppression effectiveness.

It should be noted that most of the wind-tunnel tests which are performed with the purpose of investigating the effects of active controls on the flutter speed relate to models attached to a rigid support. (See refs. 11, 12, 14, and 15.) This condition is equivalent to using the extended control law, as presented in this paper. Hence, large differences may be observed between "free flying" models and the "clamped" ones.

Finally, it is important to note that the use of the extended control law either eliminates the dynamic divergence instability or else considerably reduces its effect. It seems therefore that this dynamic divergence instability arises because of the coupling between rigid-body and elastic modes. Best results are obtained when $\omega_{r,2}$ is made very large and, as a result, flutter-suppression effectiveness is increased and control rotations are

reduced. A reduced effectiveness can be observed in figure 31 (strip 5). Here $\omega_{r,2} = 2.5$ whereas in all other cases $\omega_{r,2}$ assumes larger values (either 20 or 100). This value of $\omega_{r,2}$ explains the relatively large values of $\dfrac{\delta_c}{V_g/V_c}$ appearing in figure 31. It appears therefore that the complete elimination of the contributions of the rigid-body motions from equation (4), by leaving only the first two terms, is likely to yield best results for both flutter suppression and the elimination of the dynamic divergent instability; that is,

$$\left\{ \begin{matrix} \beta \\ \delta \end{matrix} \right\} = [C] \left\{ \begin{matrix} \bar{h}/b \\ \bar{\alpha} \end{matrix} \right\} + \frac{1}{\omega_r} [G] \left\{ \begin{matrix} \dot{\bar{h}}/b \\ \dot{\bar{\alpha}} \end{matrix} \right\} \tag{8}$$

Activation of a control strip on the horizontal tail.- It has been pointed out (ref. 17) that the two-dimensional control law, derived through the use of the aerodynamic energy concept, activates the controls in such a way as to counteract any lift build-up on the strip and provide large damping forces. This reduction in lift build-up eventually leads to both a reduction in the bending moment acting on the wing and a reduction in the acceleration sensed at the center of gravity of the aircraft. However, when placing the activated strip on the horizontal tail of the aircraft, the resulting reduction in the lift build-up due to a rigid-body motion clearly reduces the effectiveness of the horizontal tail and leads to a deterioration in the longitudinal static stability of the aircraft. To counteract these detrimental effects on the static stability, the following control law, which completely eliminates the responses of the reference section, is suggested by equation (8).

For gust-alleviation work, the reference point is chosen along the wing-root section which corresponds to the center-of-gravity location of the airplane. This choice implies that a simple rigid-body pitch movement will lead to $\bar{\alpha} = 0$ and thus neutralize the activation of the control due to this movement. The gains associated with $\bar{h}$ in the $[C]$ matrix are zero whereas the gain associated with $\dot{\bar{h}}$ and $\dot{\bar{\alpha}}$ lead to dissipative forces which may introduce some sluggishness into the pitch movement of the aircraft with no subsequent degradation in the static stability. For horizontal-tail flutter problems, the movement of the center of gravity of the aircraft is generally unimportant in controlling the instability and the activated strip should therefore maintain its effectiveness (since the elastic deformations are fully maintained in $\bar{h}$, $\bar{\alpha}$, and their derivatives).

The suggested control law is applied to both the Arava and the Westwind transports and the results relating to an activated strip located near the center-line region of the horizontal tail (strip 11) are shown in figures 33 to 36. Figures 33 and 34 show the fuselage accelerations and the maximum bending-moment variation following the activation of the tail strip with $\delta_{max} = 0.5$ rad $\left(\text{the Arava transport results relate to } \delta_{max} = 0.25 \text{ rad}\right)$.

It can be seen that the pitch accelerations have been reduced $\left(\text{leading to a reduction in } h_1\right.$ and an increase in $\left. h_2\right)$, with particular reductions in the absolute peak negative values. Furthermore, a reduction can also be observed in the center-of-gravity acceleration and, here again, the largest reductions relate to the peak negative values. The bending-moment variation shows a slight increase in the peak positive bending moment with a substantial reduction in the peak negative value of the bending-moment curve. Figures 35 and 36 summarize the results relating to the variation of $\left(\Delta M_b\right)_{max/min}\Big/\left(M_b\right)_{max/min}$, $\left(\Delta \ddot{h}_{cg}\right)_{max/min}\Big/\left(\ddot{h}_{cg}\right)_{max/min}$, $\left(\Delta \ddot{h}_1\right)_{max/min}\Big/\left(\ddot{h}_1\right)_{max/min}$, and $\left(\Delta \ddot{h}_2\right)_{max/min}\Big/\left(\ddot{h}_2\right)_{max/min}$ as functions of $\dfrac{\delta_c}{V_g/V_c}$ for the two aircraft. (The subscript max/min denotes that either the maximum or minimum values for the ratio are taken.)

No problems relating to horizontal-tail flutter could be simulated on the two aircraft treated and therefore, active flutter suppression of tail surfaces could not be considered. However, when tail flutter problems exist, the tail root section is believed to provide the best location for the reference point. It can therefore be seen that the suggested control law provides the necessary means for flutter suppression and gust alleviation by using activated strips on the tail surfaces.

Remarks on extended control law.- The supplementary investigation included the introduction of an extended control law, based on the elimination of some of the rigid-body contributions from the active control input. This elimination of the rigid-body movements cannot be regarded as the normal filtering process widespread in control theory. The Westwind case is best suited for the purpose of illustrating this point; both the gust frequency and the first natural wing bending frequency are approximately 5 Hz. Hence, if it is desired to filter out the rigid-body response to gust input, the first wing bending frequency must be filtered out as well. Thus the activated controls are prevented from reacting to the fluttering oscillation which takes place at ≈ 5 Hz. On the other hand, the flutter frequency of the Arava is ≈ 12 Hz whereas the bulk of the gust frequencies is ≈ 1.7 Hz. This value of the frequency allows the rigid-body responses to be filtered, and the free elastic modes are left to be controlled by the active system. In this latter case, however, one cannot directly tackle the gust-alleviation problem or take advantage of the flutter-suppression active system to control the gust loads (because of the filtering out of the rigid-body frequencies). It can therefore be seen that both the extended control law and the tail activation introduce new elements by considering the relative movement of the structure as inputs to the control system (as against the elimination of all the input signals below a certain frequency).

Finally, it should be mentioned that the two aircraft treated in the present work have negligible wing sweep angles. It is expected that when large sweep angles exist, rigid-body

26

pitching angles may activate the wing-tip strips, based on the extended law, in much the same way as it activates the strips on the horizontal tail. It can thus be seen that some measure of rigid-body pitch control can be obtained from the activated strips located on the wing. A control over these pitching forces can readily be obtained by moving the reference point backward along the root chord. If necessary, each wing strip can be allowed a different reference point (for the extended control law) along the root chord; thus, the complete elimination of the rigid responses is insured.

Summary of Supplementary Investigation

The main points emerging from the supplementary investigation are as follows:

(1) The extended control law introduces large damping forces directly into the elastic modes while being only slightly affected by the rigid-body response of the aircraft.

(2) The effectiveness of the activated strip using the extended control law is greatly increased for both bending-moment alleviation and flutter suppression.

(3) The extended control law appears to be somewhat more effective than the basic control law for outboard wing sections in regard to fuselage accelerations. This point is true for outboard strip locations since it leads to comparatively larger values.of δ_c/δ_{max}.

(4) The optimum strip location for maximum reduction in fuselage accelerations is at the inboard region of the wing (but clearly not on the reference strip).

(5) The optimum strip location for maximum bending-moment reductions is in the tip region of the wing inboard of the tip strip.

(6) The extended control law eliminates the need to define the external forces center.

(7) The optimum strip location for maximum increase in flutter speed is at the wing-tip strip.

(8) The extended control law, with the reference section defined as the tail root section, can be used to suppress tail flutter.

(9) Activation of a strip on the horizontal tail with the wing chord taken as the reference section can be used mainly to reduce the absolute negative values of the bending moment and center-of-gravity acceleration (if necessary).

CONCLUDING REMARKS

The effectiveness of activated leading-edge and trailing-edge control systems on flutter suppression and gust alleviation has been determined in the present work. Most of the results have already been summarized in previous sections of this work. However, it is felt appropriate to mention here some of the major points which emerge from the present work:

(1) The activated system introduces strong coupling effects between the rigid-body response of the aircraft (to gust inputs) and the wing bending modes. These coupling effects impose severe restrictions on the location of the activated systems along the span of the wing (their resultant should pass through the external forces center) when bending-moment loads are important.

(2) The coupling between the rigid-body modes and elastic modes, introduced by the activated system, leads to large control deflections and to a greatly reduced overall effectiveness of the control system. This effect is particularly pronounced when the activated system is located at the outboard wing region, and it introduces severe limitations on bending-moment alleviation and flutter-suppression capabilities of the activated system.

(3) The extended control law, which is based on the wing elastic deformation only, appears to overcome these limitations and leads to almost complete decoupling between the rigid-body responses, elastic responses, and the activated control forces. As a result, considerable improvements in both bending-moment alleviation and flutter suppression are obtained.

(4) The extended control law permits the suppression of tail flutter without leading to losses in the static longitudinal stability of the aircraft.

(5) It is found that the effectiveness of the activated control system ultimately depends on the value of the ratio between the maximum trailing-edge control deflection δ_{max} and the gust angle V_g/V_c, that is, $\dfrac{\delta_{max}}{V_g/V_c}$. It is therefore very easy to present excellent gust-alleviation results for small δ_{max} values whenever V_g/V_c is assigned very small values $\left(\text{to yield large values of } \dfrac{\delta_{max}}{V_g/V_c}\right)$. Comparison between the performance of various control systems should therefore be made only at comparable values of $\dfrac{\delta_{max}}{V_g/V_c}$.

(6) It is found that activated control systems are more effective in gust alleviation and flutter suppression of fast flying aircraft when compared with slow flying aircraft.

(7) Free flying wind-tunnel models might show a greatly reduced performance as compared with clamped models unless some form of an extended control law is used.

(8) The basic control law is best suited for reducing the acceleration levels along the fuselage provided it is applied to activated strips located very near the root of the wing. Deterioration in bending-moment levels may result unless the resultant of these activated control forces is made to pass through the external forces center or a compensation based on the extended control law is made by placing an activated strip at the outboard end of the wing.

Many graphical results have been presented in the present work with the hope of contributing toward a better insight into the problem of flutter suppression and gust alleviation and with the purpose of showing the strong interrelations that exist when attempting to treat separately only some of the aspects associated with the wider problem. Additional work is, however, required which incorporates the actuator dynamic characteristics, continuous gust inputs, three-dimensional aerodynamics, and performance at supersonic speeds. Nevertheless, it is very encouraging to discover the large effectiveness of the activated control systems in flutter suppression and gust alleviation. It also appears remarkable that a "utility" type, preoptimized control law, which is based on the concept of aerodynamic energy, brings about such stable and powerful control systems.

Langley Research Center
National Aeronautics and Space Administration
Hampton, Va. 23665
April 27, 1976

APPENDIX

DERIVATION OF THE GENERALIZED AERODYNAMIC FORCES OF A
LEADING-EDGE AND TRAILING-EDGE SYSTEM DUE TO A
UNIT STEP ROTATION OF THE CONTROL SURFACES

In addition to the symbols given in the body of the paper, the following symbols are used in the derivation:

e   distance between midchord and leading edge of control surface $\left(\text{also designated as } \ell_8\right)$

$F(\omega)$ Fourier transform function defined by equation (A17)

$F(k)$ real part of Theodorsen function

$G(k)$ imaginary part of Theodorsen function

$h, \overline{\overline{h}}$ displacements defined in sketches (c) and (d), respectively

I, I_j integrals defined by equations (A21) and (A24), respectively

J_j integral defined by equation (A25)

k reduced frequency, $\omega b/V$

$\left.\begin{array}{l}L, M, T, \\ P, Q, R\end{array}\right\}$ aerodynamic forces defined in sketch (d)

$\left.\begin{array}{l}L_j, M_j, T_j, \\ P_j, Q_j, R_j\end{array}\right\}$ constituents of L, M, T, P, Q, and R, respectively, comprised in $\left[A_0\right]$

$\left.\begin{array}{l}\ell_1, \ell_2, \ell_3, \\ \ell_4, \ell_8\end{array}\right\}$ distances defined in sketch (d)

p $= -\dfrac{1}{3}\left(1 - 4b^2\right)^{3/2}$

APPENDIX

$\left.\begin{array}{l} Q_{h/b}, Q_{\alpha}, \\ Q_{\beta}, Q_{\delta} \end{array}\right\}$ generalized aerodynamic force along h/b, α, β, and δ, respectively

q_i ith generalized coordinate

s nondimensional distance, Vt/b

T_j jth Theodorsen T function

t time

$\left.\begin{array}{l} W_{h/b}, W_{\alpha}, \\ W_{\beta}, W_{\delta} \end{array}\right\}$ virtual work along coordinates h/b, α, β, and δ, respectively

$\bar{\bar{\alpha}}, \bar{\bar{\beta}}, \bar{\bar{\delta}}$ rotations defined in sketch (d)

$\phi(s)$ Wagner function

ρ fluid density

Matrices:

$\left[A_0\right]$ aerodynamic coefficients matrix defined by equation (A11b)

$\left[A_1\right], \left[A_2\right]$ aerodynamic matrices defined by equations (A40) and (A41), respectively

$\left[B_1\right], \left[B_2\right]$ aerodynamic matrices defined by equations (A42) and (A43), respectively

$[D]$ transformation matrix, defined by equation (A11a)

$[E]$ aerodynamic matrix defined by equations (A44)

$\left[H_0\right], \left[H_1\right]$ matrices of aerodynamic coefficients defined by equations (A13) and (A14), respectively

Notation:

$[\ ]^T$ transposed matrix

31

Subscripts:

s   step-type variation

δ parameter relates to δ

Dots over symbols denote derivatives with respect to time.

First consider the determination of the aerodynamic oscillatory forces acting on the leading- and trailing-edge system shown in sketch (c). Assume that the oscillatory
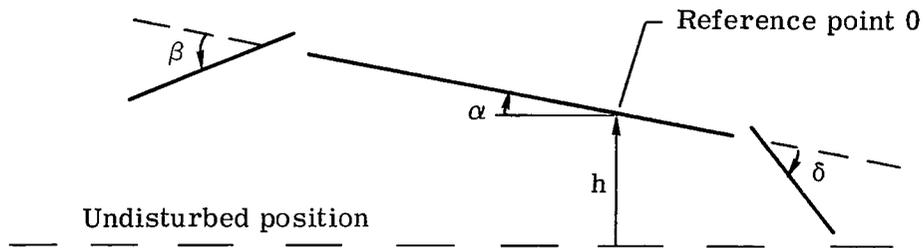
Sketch (c)

forces acting on a somewhat similar trailing edge and tab system (as used in refs. 22 and 23) described in sketch (d) are known. Note the difference between the h, α, β, and δ coordinates and the $\bar{\bar{h}}$, $\bar{\bar{\alpha}}$, $\bar{\bar{\beta}}$, and $\bar{\bar{\delta}}$ coordinates. The arrows in each sketch indicate the direction of positive displacements, forces, and distances.
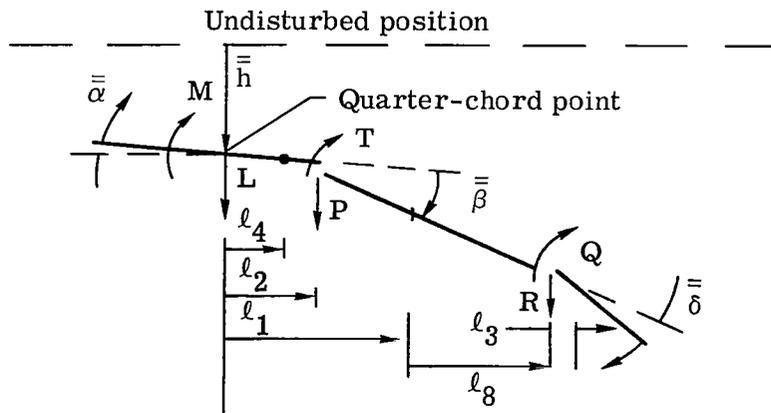
Sketch (d)

The symbols L and M denote, respectively, the total lift and pitching moment and L is assumed to act through the quarter-chord point. The force acting on the trailing-edge and tab combination through the leading-edge point is denoted by P and the aileron tab moment is denoted by T. The force acting on the tab moment is Q.

APPENDIX

The forces in sketch (d), their direction, and points of application are identical with those of Smilg, Wasserman, et al. (See refs. 22 and 23.)

As a first stage of the following analysis, the oscillatory generalized forces acting along the h, α, β, and δ coordinates are determined through the application of the principle of virtual work.

The virtual work W_h in the h coordinate is given by

$$W_h = -b\,\frac{h}{b}\,L \tag{A1}$$

where b represents the semichord length. Denoting the generalized forces by subscripted Q's yields from equation (A1)

$$Q_{h/b} = \frac{\delta W_h}{\delta(h/b)} = -bL \tag{A2a}$$

Similarly, the virtual work W_α in the α coordinate is given by

$$W_\alpha = M\alpha - L\ell_1\alpha$$

or

$$Q_\alpha = \frac{\delta W_\alpha}{\delta\alpha} = M - L\ell_1 \tag{A2b}$$

The virtual work W_β in the β coordinate is given by

$$W_\beta = -\left(M - T - P\ell_2\right)\beta + (L - P)\ell_4\beta$$

and hence,

$$Q_\beta = \frac{\delta W_\beta}{\delta\beta} = P\left(\ell_2 - \ell_4\right) + L\ell_4 + T - M \tag{A3}$$

Similarly,

$$W_\delta = Q\delta - R\ell_3\delta$$

or

$$Q_\delta = \frac{\delta W_\delta}{\delta\delta} = Q - R\ell_3 \ldots \tag{A4}$$

33

APPENDIX

These equations can be condensed into the following matrix equation:

$$
\begin{Bmatrix} Q_{h/b} \\ Q_\alpha \\ Q_\beta \\ Q_\delta \end{Bmatrix} = \begin{bmatrix} -b & 0 & 0 & 0 & 0 & 0 \\ -\ell_1 & 1 & 0 & 0 & 0 & 0 \\ \ell_4 & -1 & 1 & \ell_2 - \ell_4 & 0 & 0 \\ 0 & 0 & 0 & 0 & 1 & -\ell_3 \end{bmatrix} \begin{Bmatrix} L \\ M \\ T \\ P \\ Q \\ R \end{Bmatrix} \tag{A5}
$$

but the forces are of the form

$$
\begin{Bmatrix} L \\ M \\ T \\ P \\ Q \\ R \end{Bmatrix} = \pi\rho\omega^2 \begin{bmatrix} b^3 \\ & b^4 \\ & & b^4 \\ & & & b^3 \\ & & & & b^4 \\ & & & & & b^3 \end{bmatrix} \begin{bmatrix} A_0 \end{bmatrix} \begin{Bmatrix} \bar{\bar{h}}/b \\ \bar{\bar{\alpha}} \\ \bar{\bar{\beta}} \\ \bar{\bar{z}}/b \\ \bar{\bar{\delta}} \\ \bar{\bar{y}}/b \end{Bmatrix} \tag{A6}
$$

where $\begin{bmatrix} A_0 \end{bmatrix}$ is a 6×6 matrix and $\bar{\bar{z}}$ and $\bar{\bar{y}}$ define the hinge locations and are given by

$$
\bar{\bar{z}} = \left(\ell_2 - \ell_4\right)\bar{\bar{\beta}}
$$

$$
\bar{\bar{y}} = -\ell_3\bar{\bar{\delta}}
$$

Therefore, one can write the following equation based on the latter two equations:

34

$$
\begin{Bmatrix} \bar{\bar{h}}/b \\ \bar{\bar{\alpha}} \\ \bar{\bar{\beta}} \\ \bar{\bar{z}}/b \\ \bar{\bar{\delta}} \\ \bar{\bar{y}}/b \end{Bmatrix} = \begin{bmatrix} 1 & 0 & 0 & 0 \\ 0 & 1 & 0 & 0 \\ 0 & 0 & 1 & 0 \\ 0 & 0 & \dfrac{\ell_2 - \ell_4}{b} & 0 \\ 0 & 0 & 0 & 1 \\ 0 & 0 & 0 & \dfrac{-\ell_3}{b} \end{bmatrix} \begin{Bmatrix} \bar{\bar{h}}/b \\ \bar{\bar{\alpha}} \\ \bar{\bar{\beta}} \\ \bar{\bar{\delta}} \end{Bmatrix} \tag{A7}
$$

Comparison between the coordinates h, α, β, and δ and $\bar{\bar{h}}$, $\bar{\bar{\alpha}}$, $\bar{\bar{\beta}}$, and $\bar{\bar{\delta}}$ yields the following relations:

$$
\bar{\bar{h}} = -\left(h + \ell_1 \alpha - \ell_4 \beta \right)
$$

$$
\bar{\bar{\alpha}} = \alpha - \beta
$$

$$
\bar{\bar{\beta}} = \beta
$$

$$
\bar{\bar{\delta}} = \delta
$$

These expressions reduce to

$$
\begin{Bmatrix} \bar{\bar{h}}/b \\ \bar{\bar{\alpha}} \\ \bar{\bar{\beta}} \\ \bar{\bar{\delta}} \end{Bmatrix} = \begin{bmatrix} -1 & -\ell_1/b & \ell_4/b & 0 \\ 0 & 1 & -1 & 0 \\ 0 & 0 & 1 & 0 \\ 0 & 0 & 0 & 1 \end{bmatrix} \begin{Bmatrix} h/b \\ \alpha \\ \beta \\ \delta \end{Bmatrix} \tag{A8}
$$

Substitution of equation (A8) into equation (A7) yields

$$
\begin{Bmatrix} \bar{\bar{h}}/b \\ \bar{\bar{\alpha}} \\ \bar{\bar{\beta}} \\ \bar{\bar{z}}/b \\ \bar{\bar{\delta}} \\ \bar{\bar{y}}/b \end{Bmatrix} = \begin{bmatrix} -1 & -\dfrac{\ell_1}{b} & \dfrac{\ell_4}{b} & 0 \\ 0 & 1 & -1 & 0 \\ 0 & 0 & 1 & 0 \\ 0 & 0 & \dfrac{\ell_2 - \ell_4}{b} & 0 \\ 0 & 0 & 0 & 1 \\ 0 & 0 & 0 & \dfrac{-\ell_3}{b} \end{bmatrix} \begin{Bmatrix} h/b \\ \alpha \\ \beta \\ \delta \end{Bmatrix} \tag{A9}
$$

Substituting equations (A6) and (A9) into equation (A5) yields the following relation between the generalized forces and the displacements of the L.E.-T.E. system

$$
\begin{Bmatrix} Q_{h/b} \\ Q_\alpha \\ Q_\beta \\ Q_\delta \end{Bmatrix} = \pi\rho\omega^2 b^4 [D]^T [A_0] [D] \begin{Bmatrix} h/b \\ \alpha \\ \beta \\ \delta \end{Bmatrix} \tag{A10}
$$

where

$$
[D] = \begin{bmatrix} -1 & -\dfrac{\ell_1}{b} & \dfrac{\ell_4}{b} & 0 \\ 0 & 1 & -1 & 0 \\ 0 & 0 & 1 & 0 \\ 0 & 0 & \dfrac{\ell_2 - \ell_4}{b} & 0 \\ 0 & 0 & 0 & 1 \\ 0 & 0 & 0 & -\dfrac{\ell_3}{b} \end{bmatrix} \tag{A11a}
$$

Letting

$$
\begin{bmatrix} A_0 \end{bmatrix} =
\begin{bmatrix}
L_1 & L_2 & L_3 & L_4 & L_5 & L_6 \\
M_1 & M_2 & M_3 & M_4 & M_5 & M_6 \\
T_1 & T_2 & T_3 & T_4 & T_5 & T_6 \\
P_1 & P_2 & P_3 & P_4 & P_5 & P_6 \\
Q_1 & Q_2 & Q_3 & Q_4 & Q_5 & Q_6 \\
R_1 & R_2 & R_3 & R_4 & R_5 & R_6
\end{bmatrix}
\tag{A11b}
$$

and using equation (A10) yields

$$
\left\{ \begin{matrix} Q_{h/b} \\ Q_\alpha \end{matrix} \right\} = \pi \rho \omega^2 b^4 \left(\begin{bmatrix} H_0 \end{bmatrix} \left\{ \begin{matrix} h/b \\ \alpha \end{matrix} \right\} + \begin{bmatrix} H_1 \end{bmatrix} \left\{ \begin{matrix} \beta \\ \delta \end{matrix} \right\} \right)
\tag{A12}
$$

where

$$
\begin{bmatrix} H_0 \end{bmatrix} =
\begin{bmatrix}
\begin{bmatrix} L_1 \end{bmatrix} & \begin{bmatrix} L_1 \dfrac{\ell_1}{b} - L_2 \end{bmatrix} \\
\begin{bmatrix} L_1 \dfrac{\ell_1}{b} - M_1 \end{bmatrix} & \begin{bmatrix} \dfrac{\ell_1}{b}\left(L_1 \dfrac{\ell_1}{b} - L_2 \right) - M_1 \dfrac{\ell_1}{b} + M_2 \end{bmatrix}
\end{bmatrix}
\tag{A13}
$$

and

$$
\begin{bmatrix} H_1 \end{bmatrix} =
\begin{bmatrix}
H_1(1,1) & H_1(1,2) \\
H_1(2,1) & H_1(2,2)
\end{bmatrix}
$$

where

$$
\left.
\begin{aligned}
H_1(1,1) &= -\left(L_1 \frac{\ell_4}{b} - L_2 + L_3 + L_4 \frac{\ell_2 - \ell_4}{b} \right) \\[2ex]
H_1(1,2) &= -L_5 + L_6 \frac{\ell_3}{b} \\[2ex]
H_1(2,1) &= M_1 \frac{\ell_4}{b} - M_2 + M_3 + M_4 \frac{\ell_2 - \ell_4}{b} - \frac{\ell_1}{b}\left(L_1 \frac{\ell_4}{b} - L_2 + L_3 + L_4 \frac{\ell_2 - \ell_4}{b} \right) \\[2ex]
H_1(2,2) &= M_5 - M_6 \frac{\ell_3}{b} - \frac{\ell_1}{b}\left(L_5 - L_6 \frac{\ell_3}{b} \right)
\end{aligned}
\right\}
\tag{A14}
$$

Equation (A14) can be written as

$$\left[H_1\right] = \left[T_A\right][A]\left[T_P\right] \qquad (A15)$$

where

$$\left[T_A\right] = \begin{bmatrix} 1 & 0 \\ \dfrac{\ell_1}{b} & -1 \end{bmatrix}$$

$$\left[T_P\right] = \begin{bmatrix} -\dfrac{\ell_4}{b} & 0 \\ 1 & 0 \\ -1 & 0 \\ \dfrac{-\left(\ell_2 - \ell_4\right)}{b} & 0 \\ 0 & -1 \\ 0 & \dfrac{\ell_3}{b} \end{bmatrix}$$

and

$$[A] = \begin{bmatrix} L_1 & L_2 & L_3 & L_4 & L_5 & L_6 \\ M_1 & M_2 & M_3 & M_4 & M_5 & M_6 \end{bmatrix}$$

In order to compute the forces due to control-surface step rotations, Fourier integrals are used to superimpose the various sinusoidal forces into step forces; that is,

$$q_i(t) = \frac{1}{2\pi} \int_{-\infty}^{\infty} F(\omega) \, e^{i\omega t} \, d\omega \qquad (A16)$$

$$F(\omega) = \int_{-\infty}^{\infty} q_i(t) \, e^{-i\omega t} \, dt \qquad (A17)$$

where $q_i(t)$ is the generalized ith coordinate. For a q_i step function of amplitude $q_{i,s}$, equation (A17) yields a frequency spectrum of

$$F(\omega) = \frac{q_{i,s}}{i\omega} \qquad (A18)$$

with amplitudes, as given by equation (A16), that is,

$$dq_i = \frac{1}{2\pi} F(\omega) \, e^{i\omega t} \, d\omega$$

or

$$dq_i = \frac{q_{i,s}}{2\pi} \frac{e^{i\omega t}}{i\omega} \, d\omega \qquad (A19)$$

Equation (A12) yields the aerodynamic forces for any frequency. Hence, substituting equation (A19) into equation (A12) and integrating over the whole spectrum, which constitutes a step variation in amplitude yields

$$\begin{Bmatrix} Q_{h/b} \\ Q_\alpha \end{Bmatrix}_s = \pi \rho b^4 \int_{-\infty}^{\infty} \frac{\omega^2 \, e^{i\omega t}}{2\pi i \omega} \left(\begin{bmatrix} H_0 \end{bmatrix} \begin{Bmatrix} h_{s/b} \\ \alpha_s \end{Bmatrix} + \begin{bmatrix} H_1 \end{bmatrix} \begin{Bmatrix} \beta_s \\ \alpha_s \end{Bmatrix} \right) d\omega \qquad (A20)$$

where the subscript s refers to step variation. Equation (A20) requires the evaluation of integrals of the type

$$\left. \begin{array}{l} I = q_{r,s} \displaystyle\int_{-\infty}^{\infty} L_j \, \frac{\omega^2 \, e^{i\omega t}}{2\pi i \omega} \, d\omega \\[4mm] I = q_{r,s} \displaystyle\int_{-\infty}^{\infty} M_j \, \frac{\omega^2 \, e^{i\omega t}}{2\pi i \omega} \, d\omega \end{array} \right\} \qquad (A21)$$

The functions L_j and M_j can be represented in their most general form by the following quadratic expression in $1/k$ $\left(\text{illustrated for } L_j\right)$:

$$L_j = \begin{bmatrix} a_0 + (F + iG) \, d_0 \end{bmatrix} + \begin{bmatrix} a_1 + (F + iG) \, d_1 \end{bmatrix}\frac{1}{k} + \begin{bmatrix} a_2 + (F + iG) \, d_2 \end{bmatrix}\frac{1}{k^2} \qquad (A22)$$

where the a_j's and d_j's are constants and $(F + iG)$ represents the Theodorsen function which varies with k. Hence, the evaluation of equations (A21) requires the evaluation of the following basic integrals:

$$I_j = q_{r,s} a_j \int_{-\infty}^{\infty} \frac{\omega^2 e^{i\omega t} d\omega}{2\pi i \omega (k)^j}$$

$$J_j = q_{r,s} d_j \int_{-\infty}^{\infty} \frac{(F + iG)\omega^2 e^{i\omega t} d\omega}{2\pi i \omega (k)^j}$$

(A23)

Remembering that

$$\omega = \frac{V}{b} k$$

and letting

$$s = \frac{Vt}{b}$$

leads to

$$\omega t = ks$$

Thus,

$$I_j = q_{r,s} a_j \frac{V^2}{b^2} \int_{-\infty}^{\infty} \frac{k^2 e^{iks}}{2\pi i k (k)^j} dk \qquad (j = 0, 1, 2) \qquad (A24)$$

$$J_j = q_{r,s} d_j \frac{V^2}{b^2} \int_{-\infty}^{\infty} \frac{(F + iG)k^2 e^{iks}}{2\pi i k (k)^j} dk \qquad (j = 0, 1, 2) \qquad (A25)$$

By remembering also that

$$\int_{-\infty}^{\infty} \frac{e^{iks}}{2\pi i k} dk = H(s)$$

where $H(s)$ is the unit step function, and that

$$\int_{-\infty}^{\infty} \frac{(F + iG) e^{iks}}{2\pi i k} dk = \phi(s)$$

where $\phi(s)$ is the Wagner function, equations (A24) and (A25) yield the following relationships:

$$
\left.\begin{aligned}
I_0 &= -a_0 \ddot{q}_{r,s} \\[2mm]
J_0 &= -d_0\ \phi(s)\ \ddot{q}_{r,s} \\[2mm]
I_1 &= -ia_1 \frac{V}{b}\ \dot{q}_{r,s} \\[2mm]
J_1 &= -id_1 \frac{V}{b}\ \phi(s)\ \dot{q}_{r,s} \\[2mm]
I_2 &= a_2 \frac{V^2}{b^2}\ q_{r,s} \\[2mm]
J_2 &= d_2 \frac{V^2}{b^2}\ \phi(s)\ q_{r,s}
\end{aligned}\right\} \tag{A26}
$$

where $\dot{q}_{r,s}$ and $\ddot{q}_{r,s}$ represent, respectively, step-type variations in velocity and acceleration of the rth generalized coordinate.

In the following equations, $L_j q_r$ and $M_j q_r$ are presented (as taken from refs. 22 and 23) together with the respective results of step integration, denoted by $\left(\omega^2 L_j q_r\right)_s$ and $\left(\omega^2 M_j q_r\right)_s$:

$$
L_1 q_r = \left[1 - i\frac{2}{k}(F + iG)\right] q_r
$$

$$
\left(\omega^2 L_1 q_r\right)_s = -\ddot{q}_{r,s} - 2\ \phi(s)\frac{V}{b}\dot{q}_{r,s} \tag{A27}
$$

$$
L_2 q_r = \left\{\frac{1}{2} - \frac{i}{k}[1 + 2(F + iG)] - \frac{2}{k^2}(F + iG)\right\} q_r
$$

$$
\left(\omega^2 L_2 q_r\right)_s = -\frac{1}{2}\ddot{q}_{r,s} - \left[\frac{V}{b}(1 + 2\ \phi(s))\right]\dot{q}_{r,s} - \frac{2V^2}{b^2}\ \phi(s)\ q_{r,s} \tag{A28}
$$

$$
L_3 q_r = \left[-\frac{T_1}{\pi} + \frac{i}{k}\frac{T_4}{\pi} - \frac{i}{k}\frac{T_{11}}{\pi}(F + iG) - \frac{2}{k^2}\frac{T_{10}}{\pi}(F + iG)\right] q_r
$$

$$
\left(\omega^2 L_3 q_r\right)_s = \frac{T_1}{\pi}\ddot{q}_{r,s} + \frac{V}{b}\left(\frac{T_4}{\pi} - \frac{T_{11}}{\pi}\ \phi(s)\right)\dot{q}_{r,s} - \frac{V^2}{b^2}2\frac{T_{10}}{\pi}\ \phi(s)\ q_{r,s} \tag{A29}
$$

$$L_4 q_r = \left[-i\, \frac{2}{k}(F + iG)\, \frac{\phi_1}{\pi} + \frac{\phi_3}{\pi} \right] q_r$$

$$\left(\omega^2 L_4 q_r \right)_s = -2\, \frac{V}{b}\, \frac{\phi_1}{\pi}\, \phi(s)\, \dot{q}_{r,s} - \frac{\phi_3}{\pi}\, \ddot{q}_{r,s} \tag{A30}$$

$$\left(\omega^2 L_5 q_r \right)_s = \frac{T_{1\delta}}{\pi}\, \ddot{q}_{r,s} + \frac{V}{b}\left(\frac{T_{4\delta}}{\pi} - \frac{T_{11\delta}}{\pi}\, \phi(s) \right) \dot{q}_{r,s} - \frac{V^2}{b^2}\, 2\, \frac{T_{10\delta}}{\pi}\, \phi(s)\, q_{r,s} \tag{A31}$$

$$\left(\omega^2 L_6 q_r \right)_s = -2\, \frac{V}{b}\, \frac{\phi_{1\delta}}{\pi}\, \phi(s)\, \dot{q}_{r,s} - \frac{\phi_{3\delta}}{\pi}\, \ddot{q}_{r,s} \tag{A32}$$

$$M_1 q_r = \frac{1}{2}\, q_r$$

$$\left(\omega^2 M_1 q_r \right)_s = -\frac{1}{2}\, \ddot{q}_{r,s} \tag{A33}$$

$$M_2 q_r = \left(\frac{3}{8} - \frac{i}{k} \right) q_r$$

$$\left(\omega^2 M_2 q_r \right)_s = -\frac{3}{8}\, \ddot{q}_{r,s} - \frac{V}{b}\, \dot{q}_{r,s} \tag{A34}$$

$$M_3 q_r = \left[-\frac{T_7}{\pi} - \left(e + \frac{1}{2} \right) \frac{T_1}{\pi} + \frac{i}{k}\left(\frac{2p + T_4}{\pi} \right) - \frac{1}{k^2}\left(\frac{T_4 + T_{10}}{\pi} \right) \right] q_r$$

$$\left(\omega^2 M_3 q_r \right)_s = \left[\frac{T_7}{\pi} + \left(e + \frac{1}{2} \right)\frac{T_1}{\pi} \right] \ddot{q}_{r,s} + \frac{V}{b}\left(\frac{2p + T_4}{\pi} \right) \dot{q}_{r,s} - \frac{V^2}{b^2}\left(\frac{T_4 + T_{10}}{\pi} \right) q_{r,s} \tag{A35}$$

$$M_4 q_r = \left(-\frac{i}{k}\, \frac{\phi_5}{\pi} + \frac{1}{4}\, \frac{\phi_6}{\pi} \right) q_r$$

$$\left(\omega^2 M_4 q_r \right)_s = -\frac{V}{b}\, \frac{\phi_5}{\pi}\, \dot{q}_{r,s} - \frac{\phi_6}{4\pi}\, \ddot{q}_{r,s} \tag{A36}$$

$$\left(\omega^2 M_5 q_r \right)_s = \left[\frac{T_{7\delta}}{\pi} + \left(e_\delta + \frac{1}{2} \right)\frac{T_{1\delta}}{\pi} \right] \ddot{q}_{r,s} + \frac{V}{b}\left(\frac{2p_\delta + T_{4\delta}}{\pi} \right) \dot{q}_{r,s} - \frac{V^2}{b^2}\left(\frac{T_{4\delta} + T_{10\delta}}{\pi} \right) q_{r,s}$$

$$\tag{A37}$$

$$\left(\omega^2 M_6 q_r\right)_s = -\frac{V}{b}\frac{\phi_{5\delta}}{\pi}\dot{q}_{r,s} - \frac{\phi_{6\delta}}{4\pi}\ddot{q}_{r,s} \tag{A38}$$

Substituting equations (A27) to (A38) into the second term of equation (A20) yields the contribution of the controls to the generalized step forces. This relationship can be written in the form

$$\left\{\begin{array}{c} Q_{h/b} \\ Q_\alpha \end{array}\right\}_s = \pi\rho b^2 V^2 \left(\phi(s)\left[A_1\right] + \left[A_2\right]\right)\left\{\begin{array}{c} \beta_s \\ \delta_s \end{array}\right\} + \pi\rho b^3 V\left(\phi(s)\left[B_1\right] + \left[B_2\right]\right)\left\{\begin{array}{c} \dot{\beta}_s \\ \dot{\delta}_s \end{array}\right\} + \pi\rho b^4 [E]\left\{\begin{array}{c} \ddot{\beta}_s \\ \ddot{\delta}_s \end{array}\right\} \tag{A39}$$

where

$$\left[A_1\right] = \begin{bmatrix} \left(-2 + 2\,\dfrac{T_{10}}{\pi}\right) & \dfrac{2}{\pi}\,T_{10\delta} \\[2em] \dfrac{\ell_1}{b}\left(-2 + 2\,\dfrac{T_{10}}{\pi}\right) & 2\,\dfrac{\ell_1}{b}\,\dfrac{T_{10\delta}}{\pi} \end{bmatrix} \tag{A40}$$

$$\left[A_2\right] = \begin{bmatrix} 0 & 0 \\[2em] -\left(\dfrac{T_4 + T_{10}}{\pi}\right) & -\left(\dfrac{T_{4\delta} + T_{10\delta}}{\pi}\right) \end{bmatrix} \tag{A41}$$

$$\left[B_1\right] = \begin{bmatrix} \left[\dfrac{2\ell_4}{b} - 2 + \dfrac{T_{11}}{\pi} + \dfrac{2\phi_1}{\pi}\dfrac{\ell_2 - \ell_4}{b}\right] & \left[\dfrac{T_{11\delta}}{\pi} - \dfrac{2\phi_{1\delta}}{\pi}\dfrac{\ell_3}{b}\right] \\[2em] \left[\dfrac{\ell_1}{b}\left(\dfrac{2\ell_4}{b} - 2 + \dfrac{T_{11}}{\pi} + \dfrac{2\phi_1}{\pi}\dfrac{\ell_2 - \ell_4}{b}\right)\right] & \left[\dfrac{\ell_1}{b}\left(\dfrac{T_{11\delta}}{\pi} - \dfrac{2\phi_{1\delta}}{\pi}\dfrac{\ell_3}{b}\right)\right] \end{bmatrix} \tag{A42}$$

$$\left[B_2\right] = \begin{bmatrix} B_2(1,1) & B_2(1,2) \\[1em] B_2(2,1) & B_2(2,2) \end{bmatrix} \tag{A43}$$

where

$$B_2(1,1) = -1 - \frac{T_4}{\pi}$$

$$B_2(1,2) = -\frac{T_{4\delta}}{\pi}$$

$$B_2(2,1) = -\frac{\ell_1}{b}\left(1 + \frac{T_4}{\pi}\right) + 1 + \frac{2p + T_4}{\pi} - \frac{\phi_5}{\pi}\frac{\ell_2 - \ell_4}{b}$$

$$B_2(2,2) = -\frac{\ell_1}{b}\frac{T_{4\delta}}{\pi} + \frac{2p_\delta + T_{4\delta}}{\pi} + \frac{\phi_{5\delta}}{\pi}\frac{\ell_3}{b}$$

$$[E] = \begin{bmatrix} E(1,1) & E(1,2) \\ E(2,1) & E(2,2) \end{bmatrix}$$

where

$$E(1,1) = \frac{\ell_4}{b} - \frac{1}{2} - \frac{T_1}{\pi} + \frac{\phi_3}{\pi}\frac{\ell_2 - \ell_4}{b}$$

$$E(1,2) = -\frac{T_{1\delta}}{\pi} - \frac{\phi_{3\delta}}{\pi}\frac{\ell_3}{b}$$

$$E(2,1) = \frac{\ell_1}{b}\left[\frac{\ell_4}{b} - \frac{1}{2} - \frac{T_1}{\pi} + \frac{\phi_3}{\pi}\frac{\ell_2 - \ell_4}{b}\right] - \frac{1}{2}\frac{\ell_4}{b} + \frac{3}{8} + \frac{T_7}{\pi} + \left(e + \frac{1}{2}\right)\frac{T_1}{\pi} - \frac{\phi_6}{4\pi}\frac{\ell_2 - \ell_4}{b}$$

$$E(2,2) = \frac{\ell_1}{b}\left(-\frac{T_{1\delta}}{\pi} - \frac{\phi_{3\delta}}{\pi}\frac{\ell_3}{b}\right) + \frac{T_{7\delta}}{\pi} + \left(e_\delta + \frac{1}{2}\right)\frac{T_{1\delta}}{\pi} + \frac{\phi_{6\delta}}{4\pi}\frac{\ell_3}{b}$$

(A44)

REFERENCES

1. Davis, H. Max; and Swaim, Robert L.: Controlling Dynamic Response in Rough Air. AIAA Paper No. 66-997, Nov.- Dec. 1966.

2. Wykes, John H.; and Mori, Alva S.: Techniques and Results of an Analytical Investigation Into Controlling the Structural Modes of Flexible Aircraft. AIAA Symposium on Structural Dynamics and Aeroelasticity, Aug.-Sept. 1965, pp. 419-433.

3. Wykes, John H.; and Mori, Alva S.: An Analysis of Flexible Aircraft Structural Mode Control. AFFDL-TR-65-190, Pt. I, U.S. Air Force, June 1966. (Available from DDC as AD 486 794.)

4. Dempster, John B.; and Roger, Kenneth L.: Evaluation of B-52 Structural Response to Random Turbulence With Stability Augmentation Systems. J. Aircraft, vol. 4, no. 6, Nov.-Dec. 1967, pp. 507-512.

5. Rohling, Walter J.: Flying Qualities: An Integral Part of a Stability Augmentation System. J. Aircraft, vol. 6, no. 6, Nov.-Dec. 1969, pp. 510-515.

6. Dempster, John B.; and Arnold, James I.: Flight Test Evaluation of an Advanced Stability Augmentation System for the B-52 Aircraft. AIAA Paper No. 68-1068, Oct. 1968.

7. Thompson, Glenn O.; and Kass, Gerald J.: Active Flutter Suppression — An Emerging Technology. J. Aircraft, vol. 9, no. 3, Mar. 1972, pp. 230-235.

8. Topp, L. J.: Potential Performance Gains by Use of a Flutter Suppression System. Paper No. 7-B3, 1971 Joint Automatic Control Conference (St. Louis, Mo.), Aug. 1971.

9. Abel, Irving; and Sandford, Maynard C.: Status of Two Studies on Active Control of Aeroelastic Response. NASA TM X-2909, 1973.

10. Redd, L. T.; Gilman, J., Jr.; Cooley, D. E.; and Sevart, F. D.: Wind-Tunnel Investigation of a B-52 Model Flutter Suppression System. J. Aircraft, vol. 11, no. 11, Nov. 1974, pp. 659-663.

11. Sandford, Maynard C.; Abel, Irving; and Gray, David L.: Transonic Study of Active Flutter Suppression Based on an Energy Concept. J. Aircraft, vol. 12, no. 2, Feb. 1975, pp. 72-77.

12. Sandford, Maynard C.; Abel, Irving; and Gray, David L.: Development and Demonstration of a Flutter-Suppression System Using Active Controls. NASA TR R-450, 1975.

13. Thompson, G. O.; and Sevart, F. D.: Wind Tunnel Investigation of Control Configured Vehicle Systems. Flutter Suppression and Structural Load Alleviation, AGARD-CP-175, Apr. 1975, pp. 4-1 — 4-8.

14. Destuynder, Roger: Essai en Soufflerie d'un Suppresseur de Flottement sur une Aile Droite. Flutter Suppression and Structural Load Alleviation, AGARD-CP-175, Apr. 1975, pp. 6-1 – 6-3.

15. Cwach, Emil; and Stearman, Ronald O.: Suppression of Flutter on Interfering Lifting Surfaces by the Use of Active Controls. AIAA Paper No. 74-404, Apr. 1974.

16. Roger, Kenneth L.; Hodges, Garold E.; and Felt, Larry: Active Flutter Suppression – A Flight Test Demonstration. AIAA Paper No. 74-402, Apr. 1974.

17. Nissim, E.: Flutter Suppression Using Active Controls Based on the Concept of Aerodynamic Energy. NASA TN D-6199, 1971.

18. Garrick, I. E.: Perspectives in Aeroelasticity. Israel J. Technol., vol. 10, no. 1-2, 1972, pp. 1-22.

19. Garrick, I. E.: Aeroelasticity – Frontiers and Beyond. AIAA Paper No. 76-219, Jan. 1976.

20. Nissim, E.: Flutter Suppression and Gust Alleviation Using Active Controls. TAE Rep. No. 198, Technion – Israel Inst. Technol., 1974. (Available as NASA CR-138658.)

21. Nissim, E.: Active Flutter Suppression Using Trailing-Edge and Tab Control Surfaces. AIAA Paper No. 75-822, May 1975.

22. Smilg, Benjamin; and Wasserman, Lee S.: Application of Three-Dimensional Flutter Theory to Aircraft Structures. ACTR No. 4798, Material Div., Army Air Corps, July 9, 1942.

23. Wasserman, Lee S.; Mykytow, Walter J.; and Spielberg, Irvin: Tab Flutter Theory and Applications. AAF TR No. 5153, Air Technical Service Command, Army Air Forces, Sept. 1, 1944.

Wing mean chord, 2.09 m

Wing aspect ratio, 10

12.88 m

5.20 m

4.62 m

5.20 m

20.90 m

4.00 m
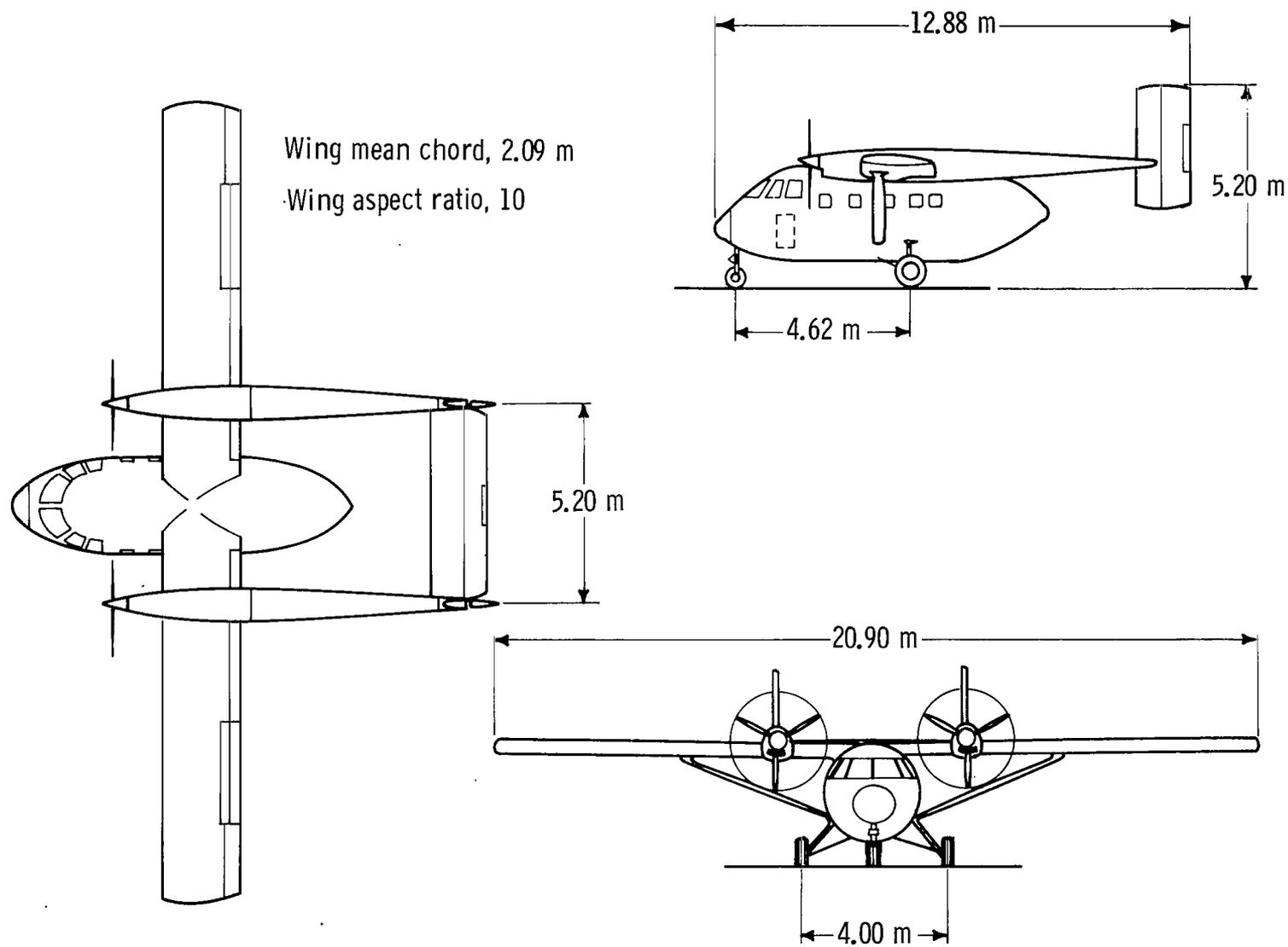
Figure 1.- General view and dimensions of Arava STOL transport.

Wing mean chord, 2.08 m
Wing aspect ratio, 6.51

1.57 m

6.40 m

3.05 m

3.57 m

2.73 m

4.81 m

1.83 m

13.65 m

3.35 m
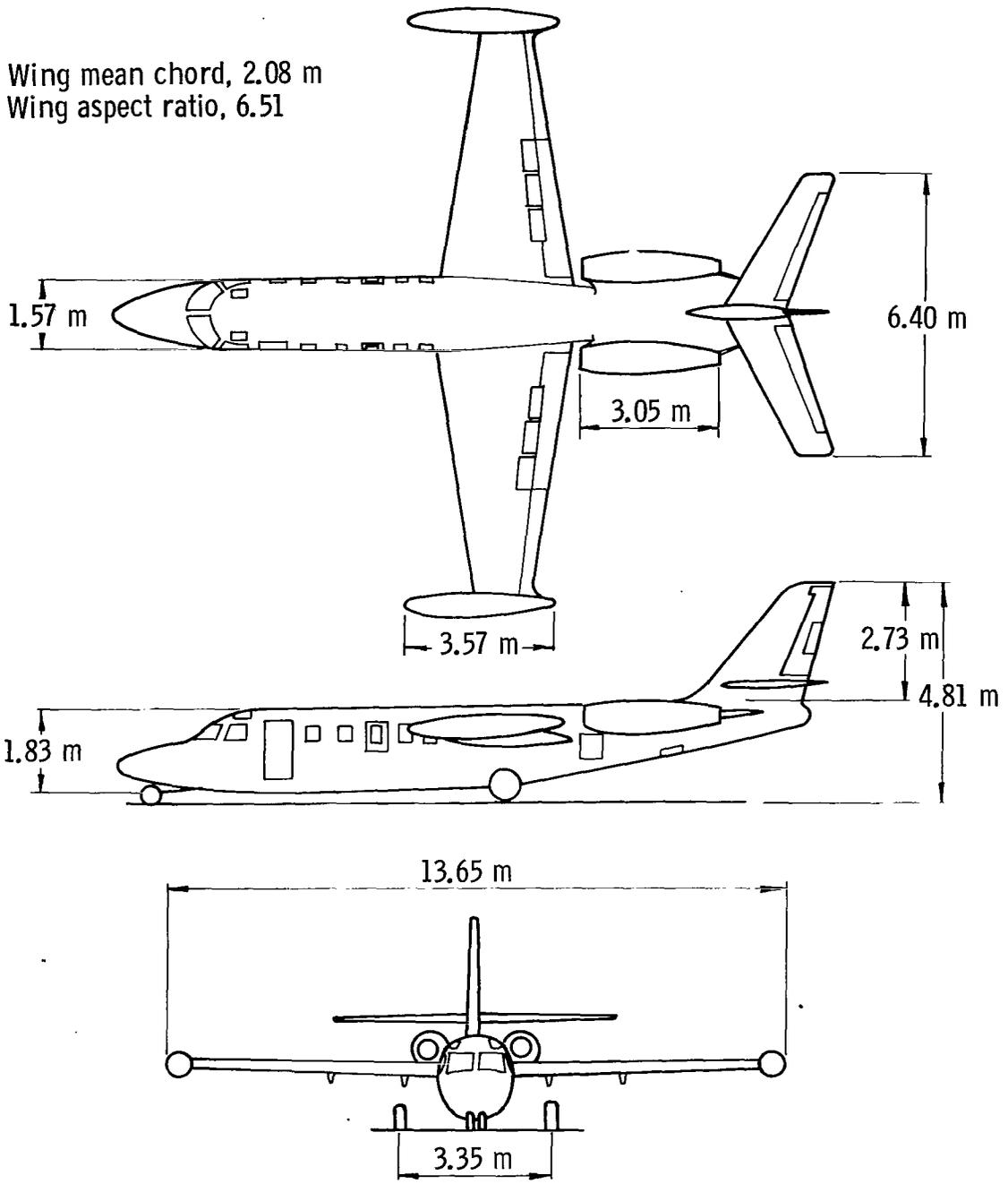
Figure 2.- General view and dimensions of Westwind business jet transport.

Arava fuselage center line

Boom center line

10 9 8 7 6 5 4 3 2 1

11
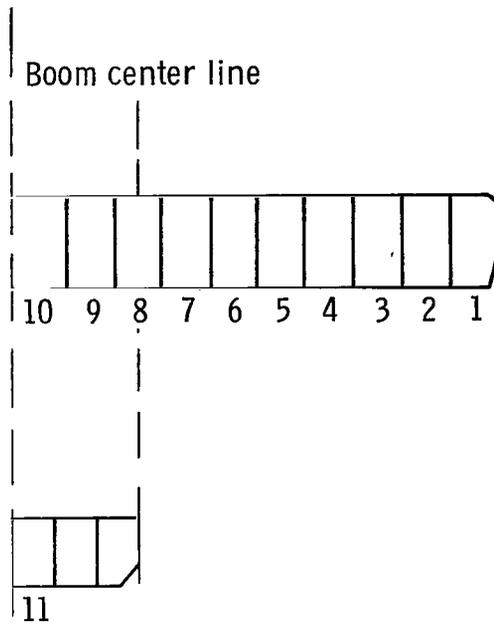
Westwind fuselage center line

10 9 8 7 6 5 4 3 2 1

11
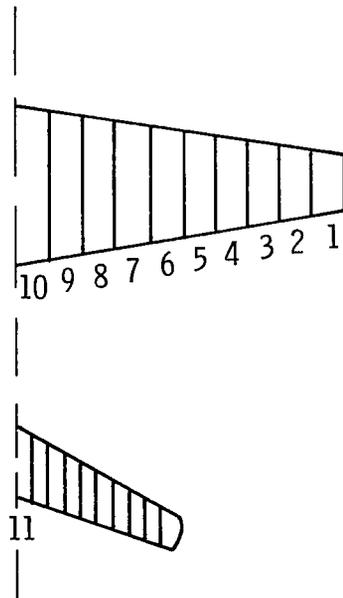
Figure 3.- Strip allocations along wing and horizontal tail of
Arava and Westwind aircraft.
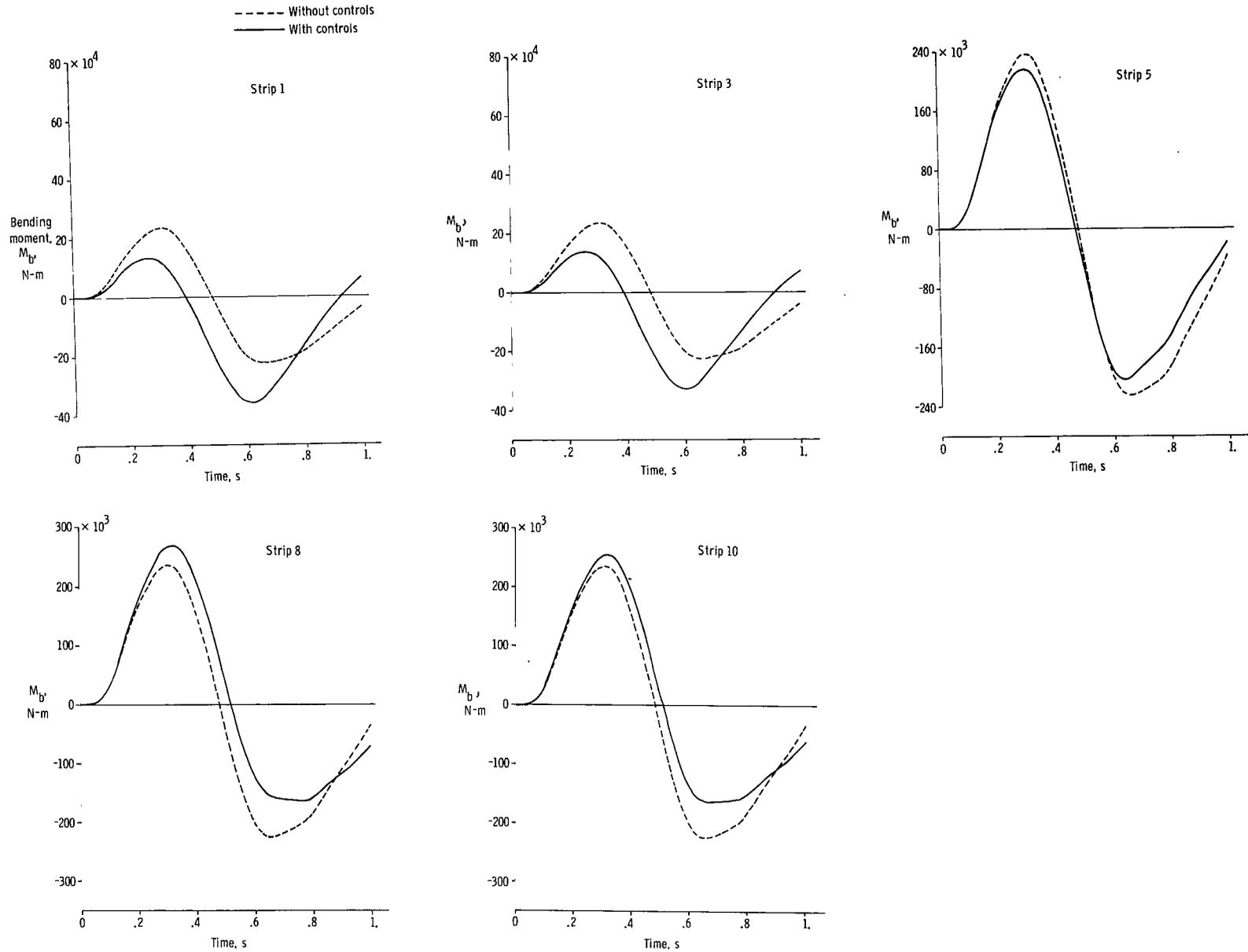
Figure 4.- Variation with time of wing bending moment at station 5 due to a (1 - cos) upgust. Arava transport with a single L.E.-T.E. active control system located at various strips along wing and with $\delta_{max} = 0.5$ rad.
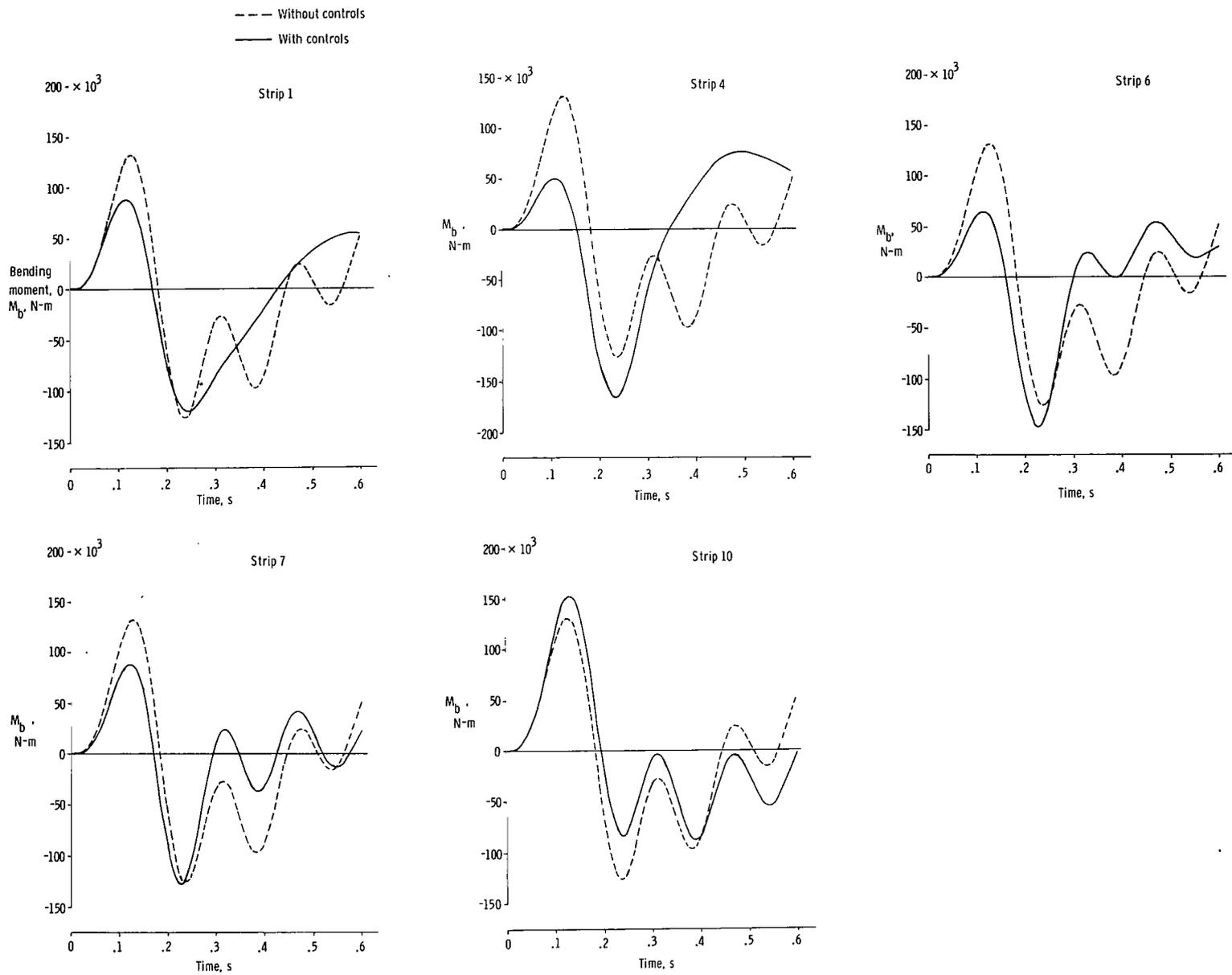
Figure 5.- Variation with time of wing bending moment at station 10 due to a (1 - cos) upgust. Westwind transport with a single L.E.-T.E. active control system located at various strips along wing and with $\delta_{max} = 0.5$ rad.
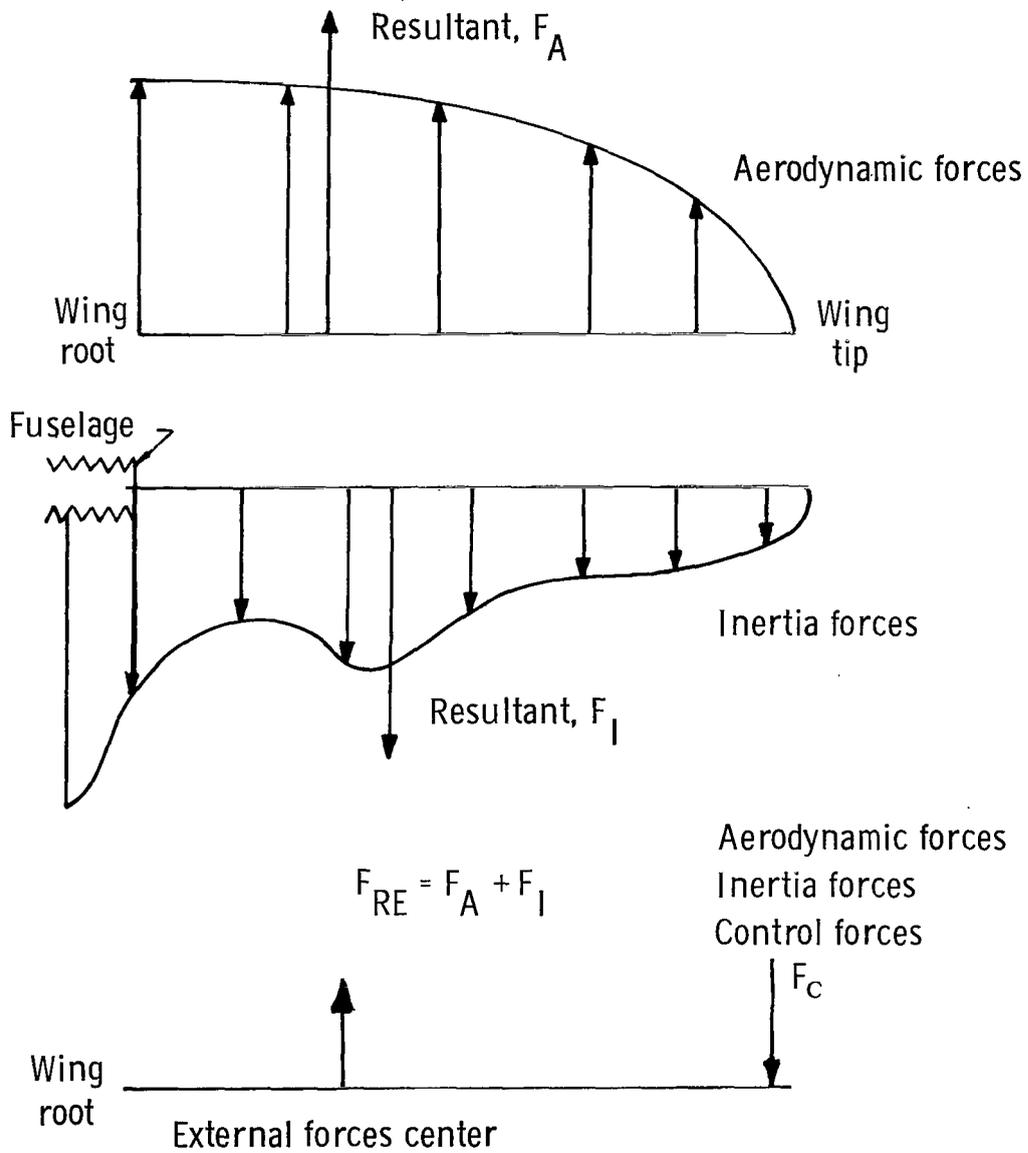
Figure 6.- Distribution of various forces acting along wing and locations of their resultants illustrating promotion of bending moment due to rigid-body—control-force interaction.

$$F_{RE} = F_A + F_I$$
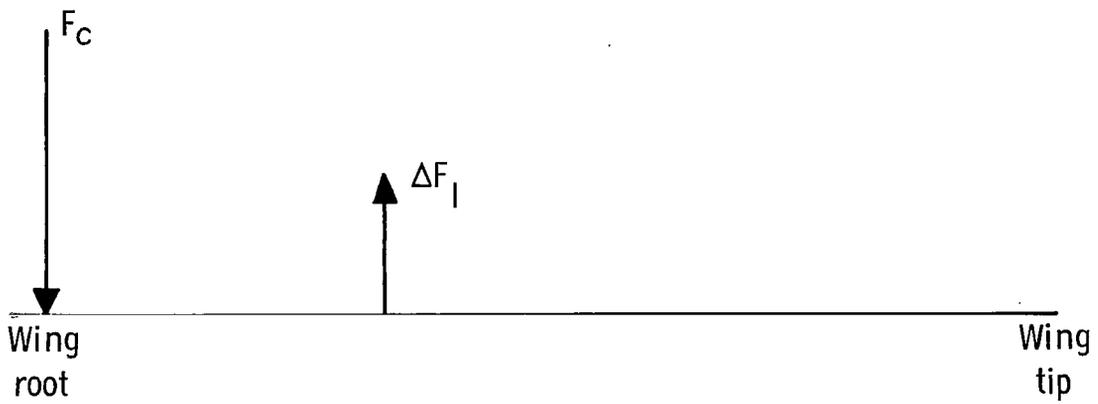
Figure 7.- Promotion of bending moment due to changes in inertia forces resulting from control forces acting at root of wing.
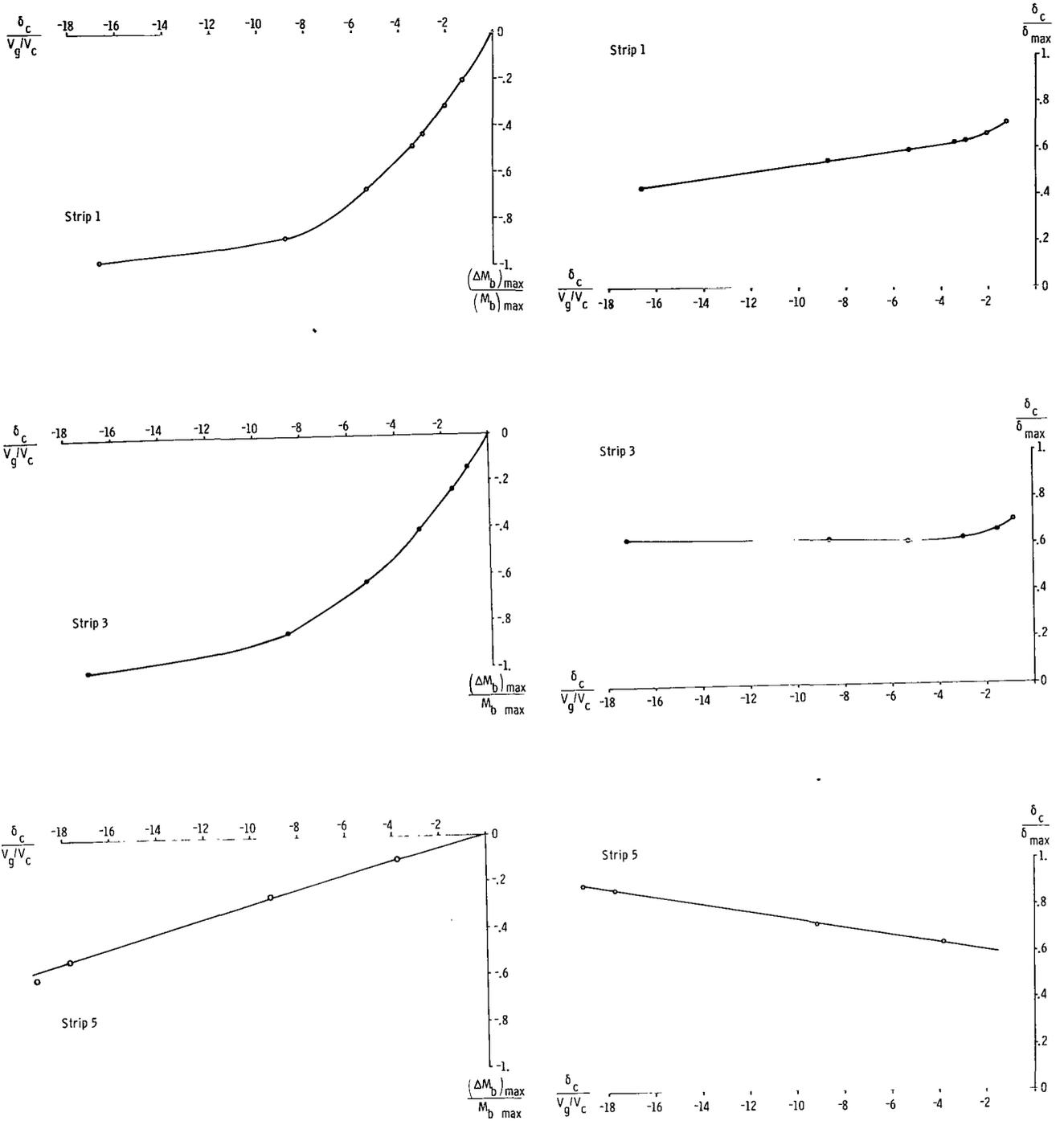
Figure 8.- Variation with control rotation parameter $\dfrac{\delta_c}{V_g/V_c}$ of bending-moment alleviation ratio at station 5 and maximum control rotation ratio. Arava transport with a single L.E.-T.E. active control system located at various strips along wing.
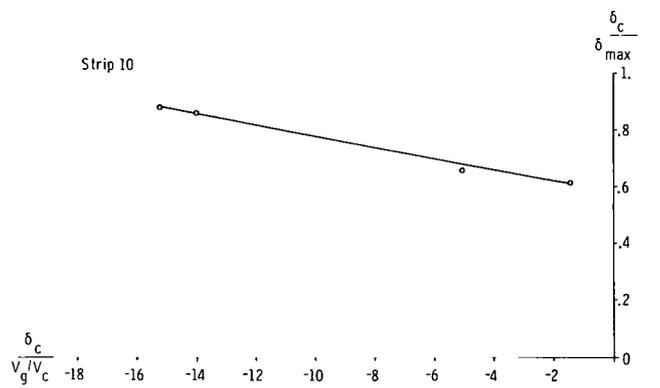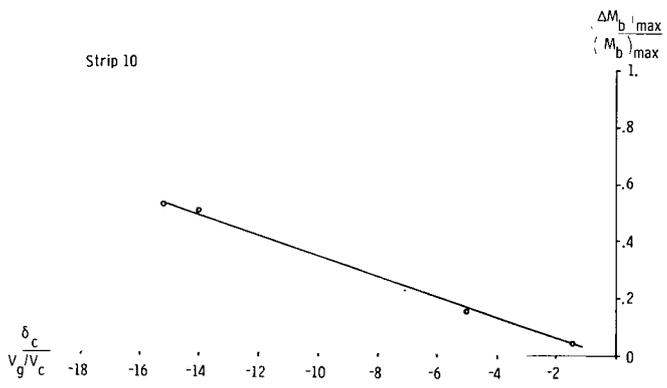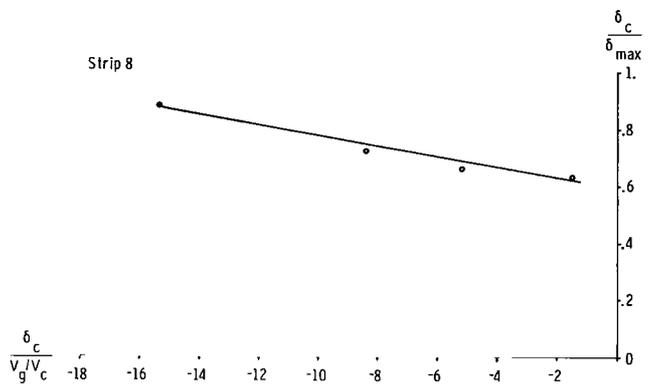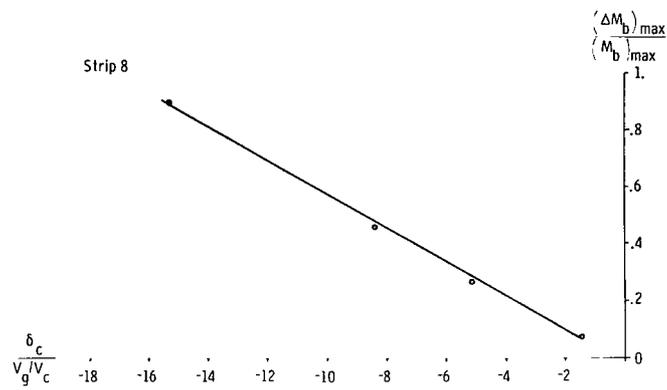
Figure 8.- Concluded.
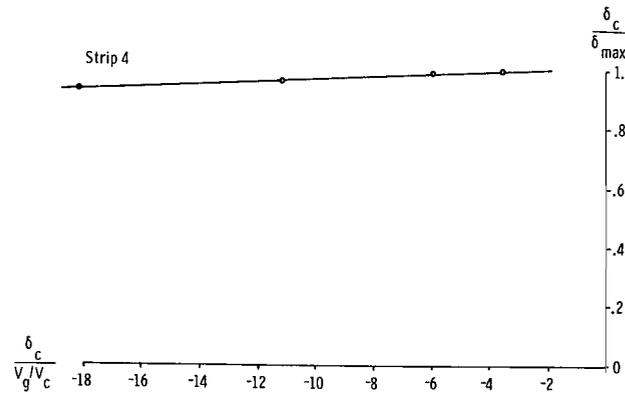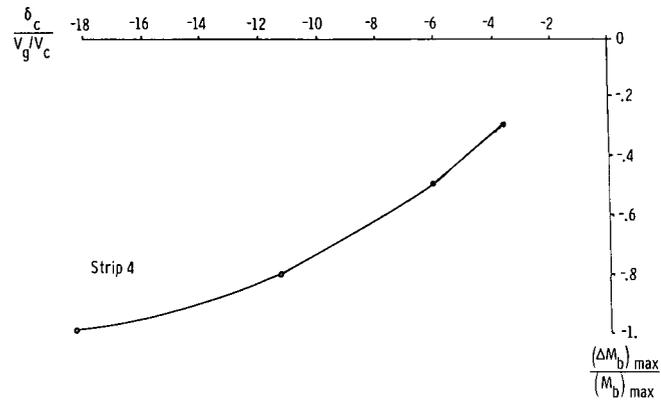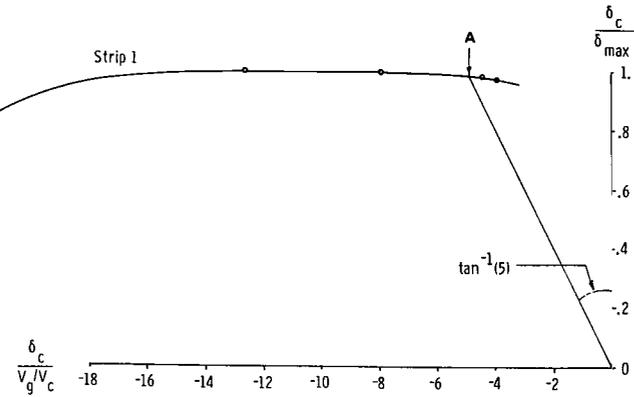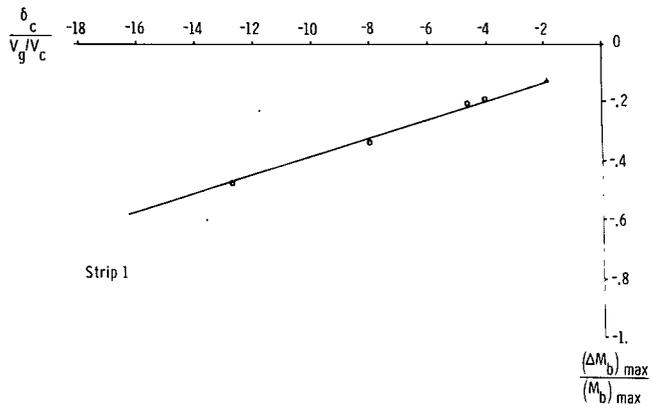
Figure 9.- Variation with control rotation parameter $\dfrac{\delta_c}{V_g/V_c}$ of bending-moment alleviation ratio at

station 10. Westwind transport with a single L.E.-T.E. active control system located at various strips along wing.

Figure 9.- Continued.

Strip 10

$\dfrac{(\Delta M_b)_{max}}{(M_b)_{max}}$

1.

.8

.6

.4

.2

0

$\dfrac{\delta_c}{V_g/V_c}$ -18 -16 -14 -12 -10 -8 -6 -4 -2

Strip 10

$\dfrac{\delta_c}{\delta_{max}}$

1.

.8

.6

.4

.2

0

$\dfrac{\delta_c}{V_g/V_c}$ -18 -16 -14 -12 -10 -8 -6 -4 -2
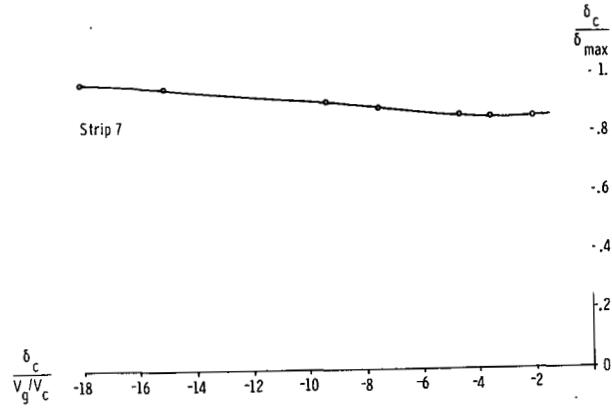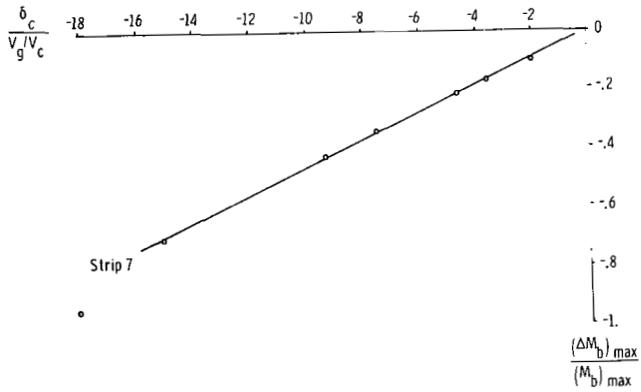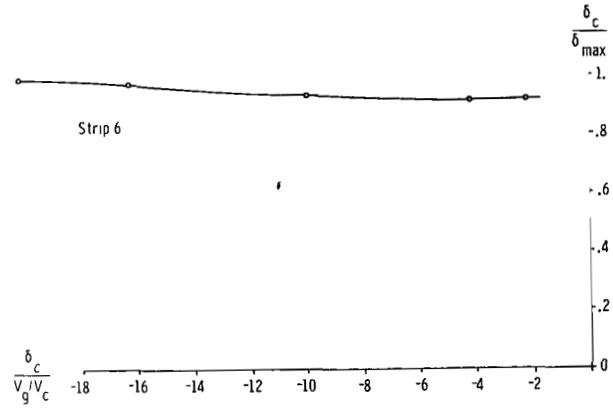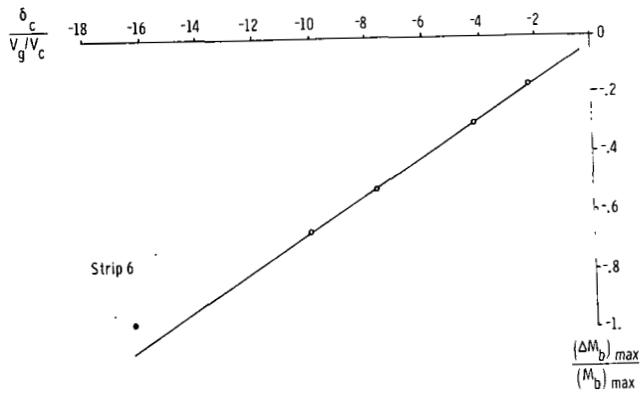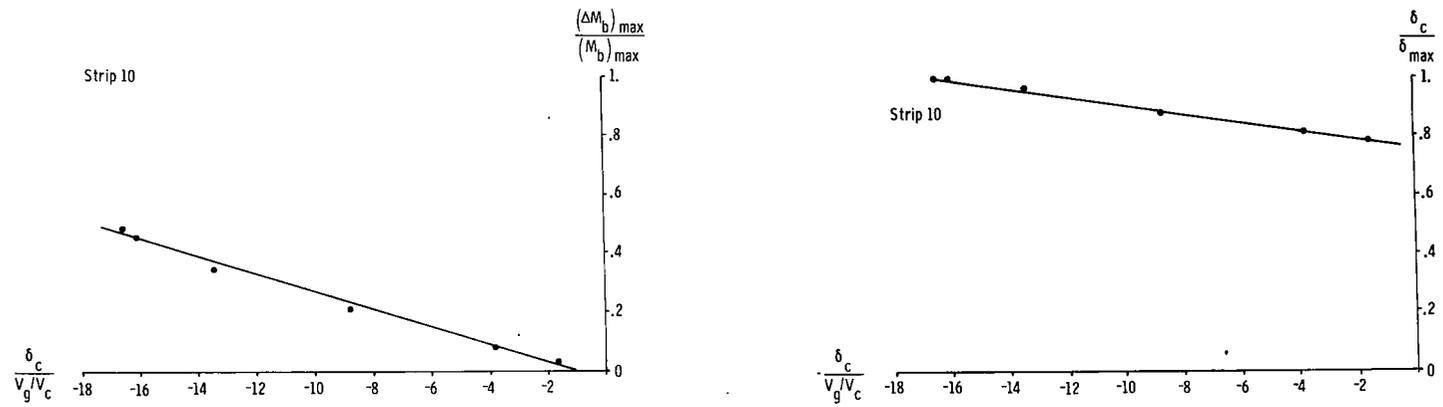
Figure 9.- Concluded.
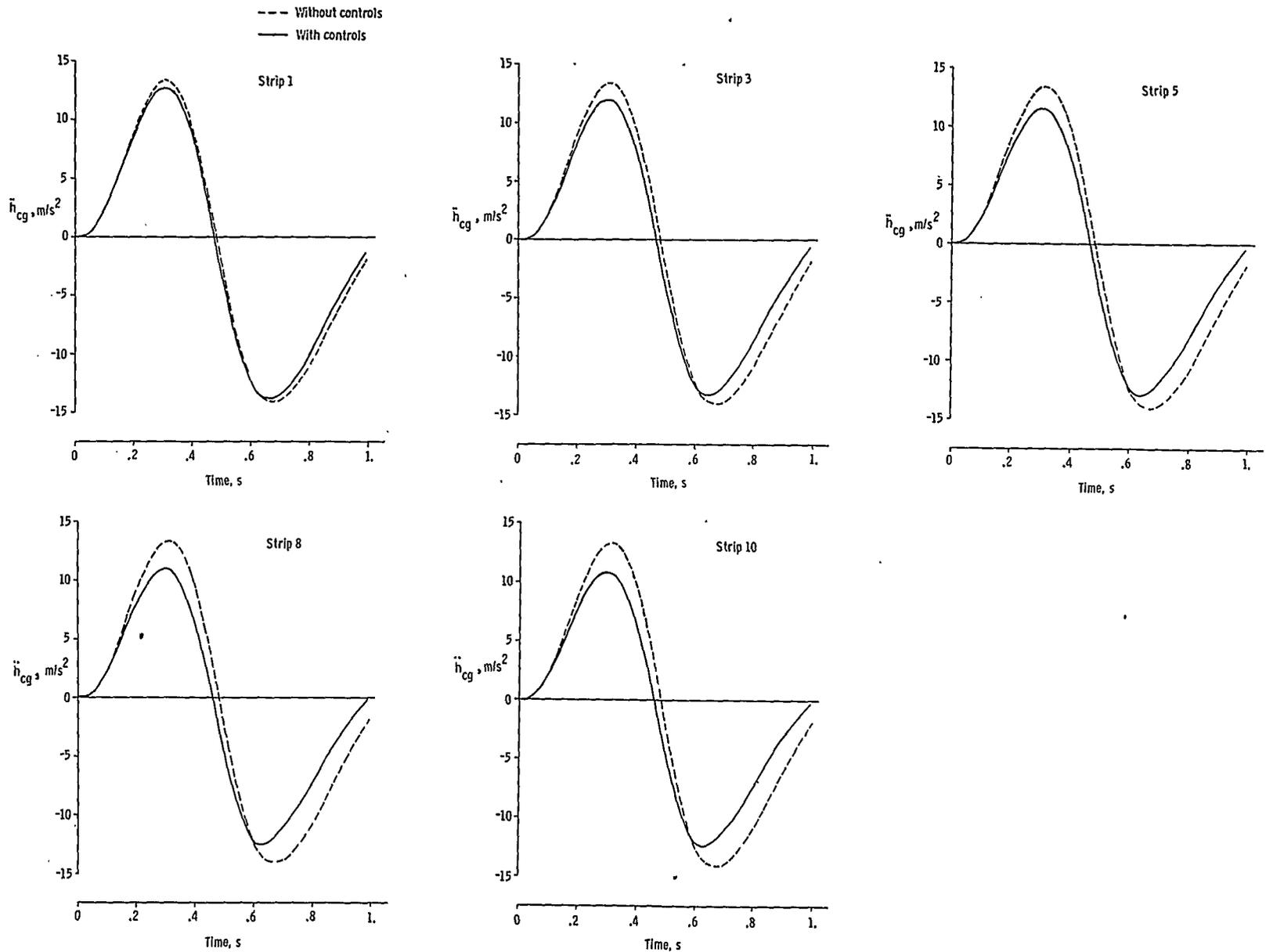
Figure 10.- Variation with time of linear acceleration at center of gravity due to a (1 - cos) upgust. Arava transport with a single L.E.-T.E. active control system located at various strips along wing and with δ_{max} = 0.5 rad.
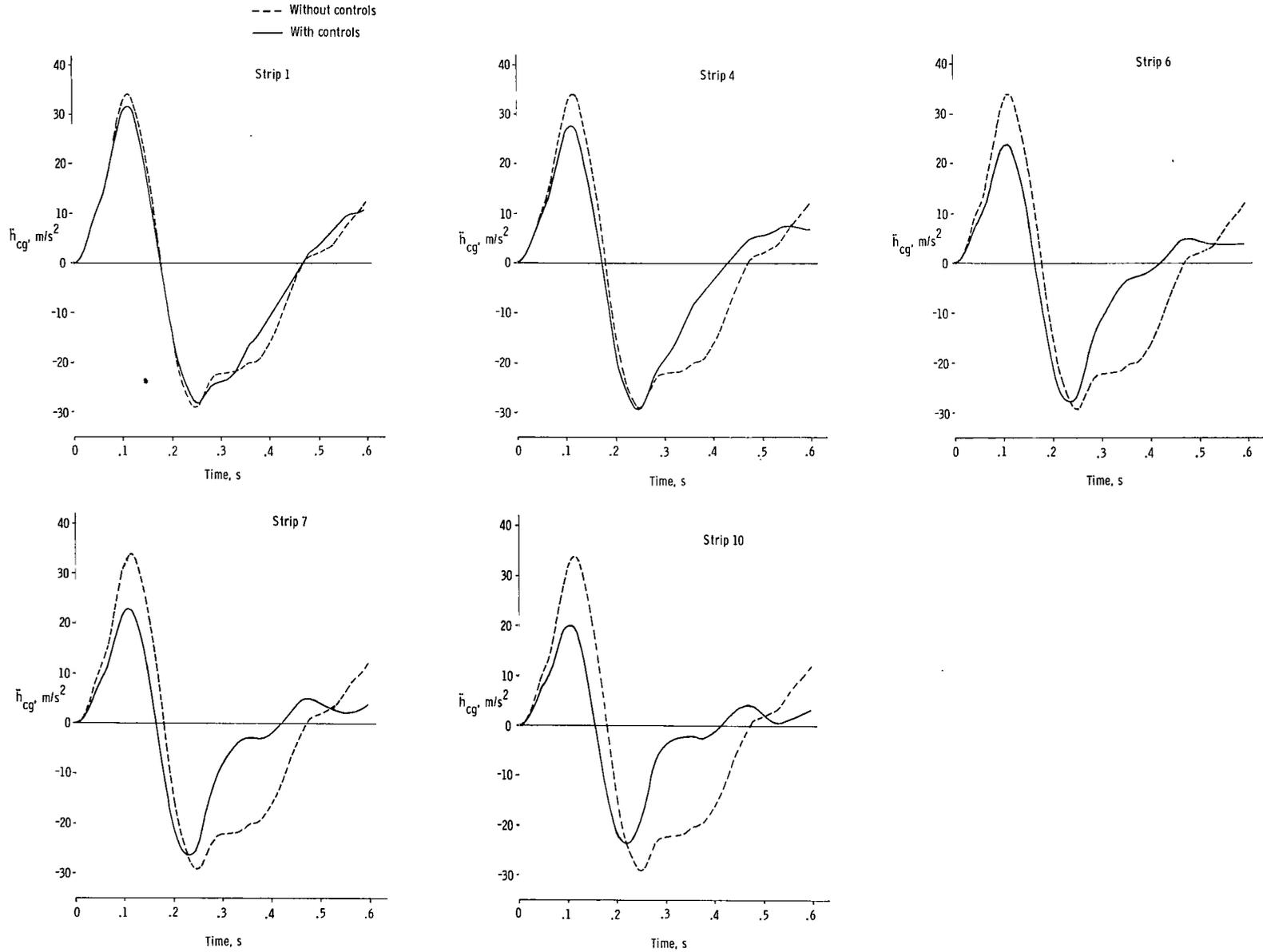
Figure 11.- Variation with time of linear acceleration at center of gravity due to a (1 - cos) upgust. Westwind transport with a single L.E.-T.E. active control system located at various strips along wing and with $\delta_{max} = 0.5$ rad.
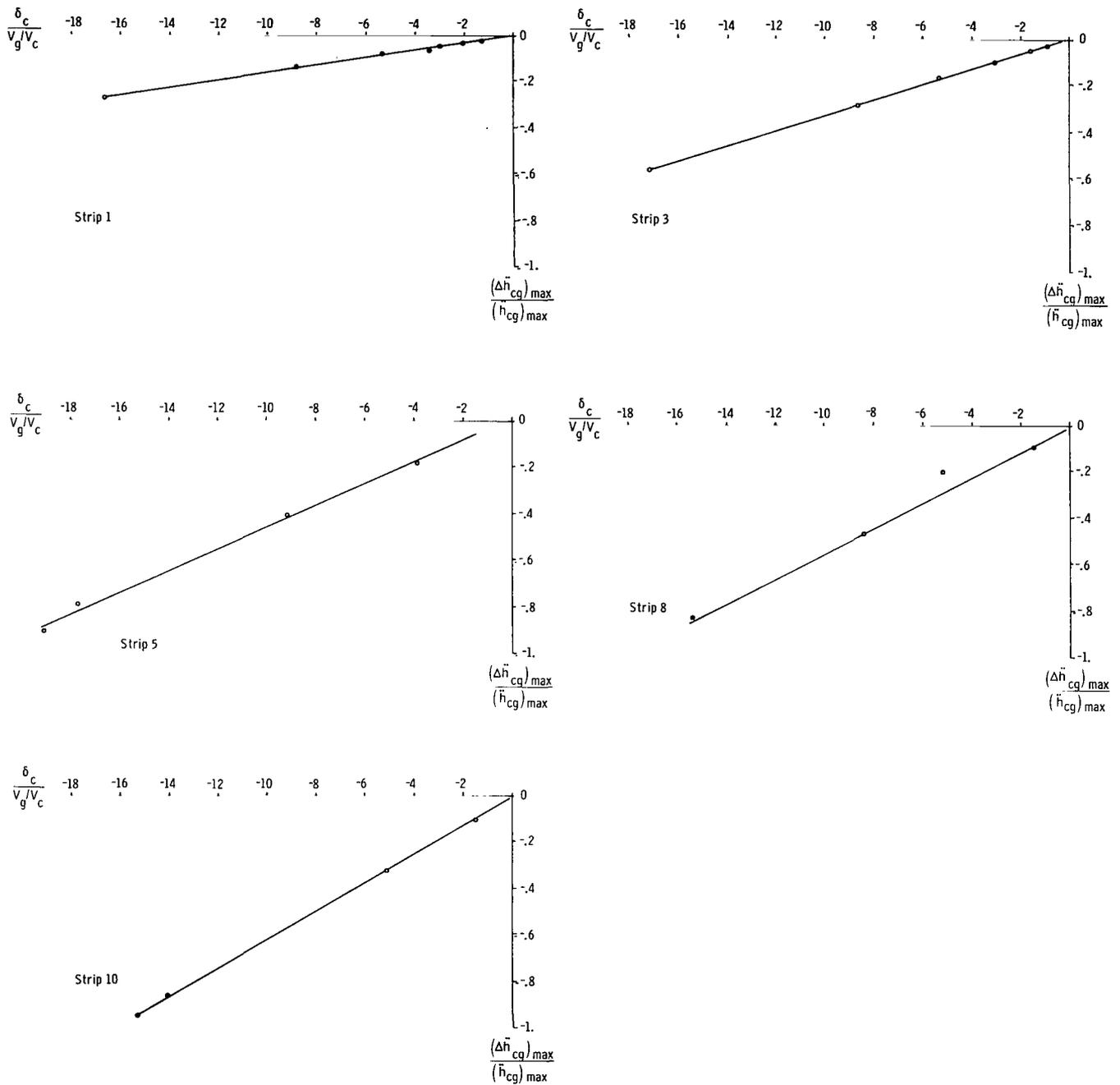
Figure 12.- Variation with control rotation parameter $\dfrac{\delta_c}{V_g/V_c}$ of acceleration alleviation ratio at center of gravity and maximum control rotation ratio. Arava transport with a single L.E.-T.E. active control system located at various strips along wing.
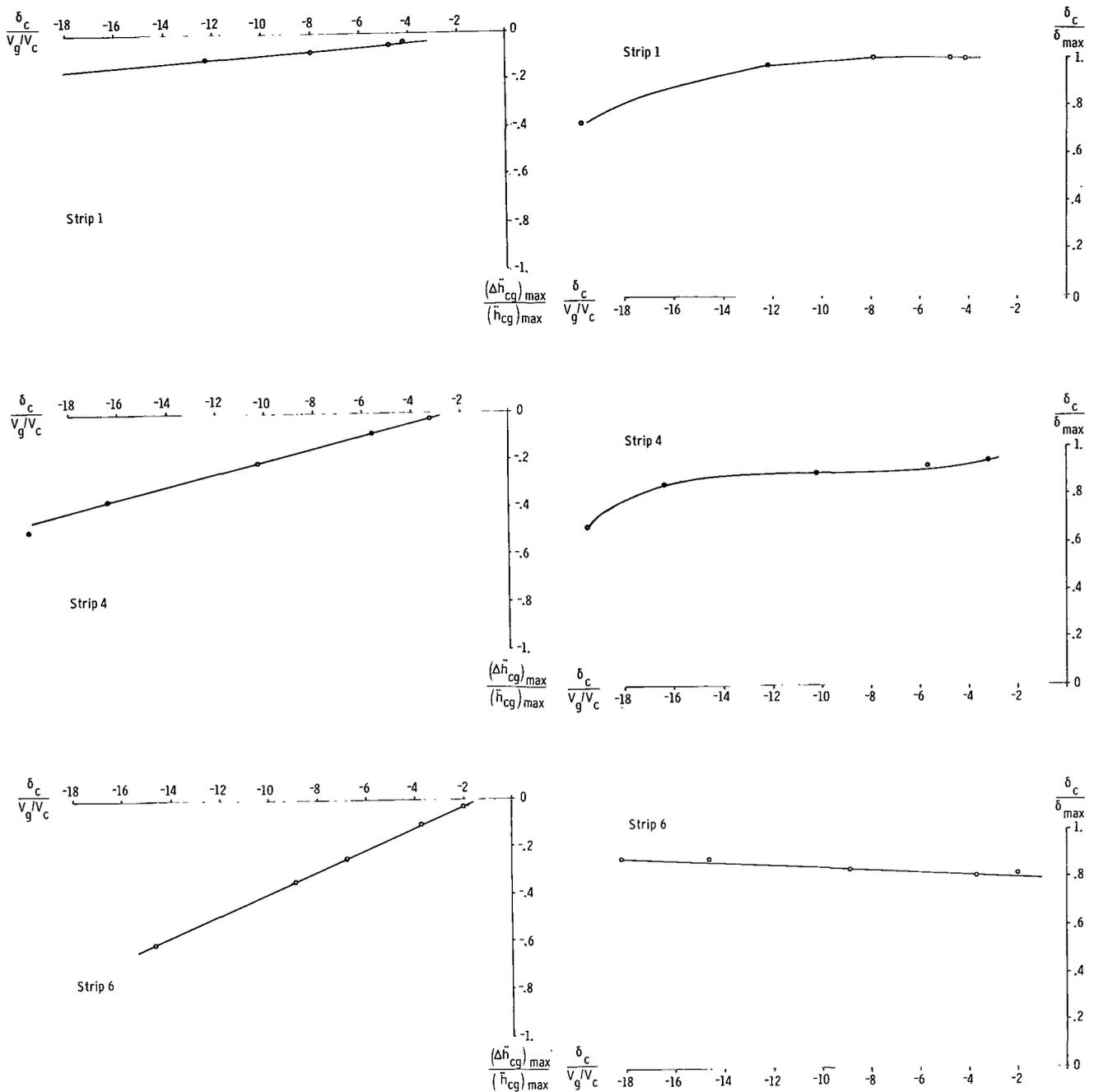
Figure 13.- Variation with control rotation parameter $\dfrac{\delta_c}{V_g/V_c}$ of acceleration alleviation ratio at center of gravity and maximum control rotation ratio. Westwind transport with a single L.E.-T.E. active control system located at various strips along wing.
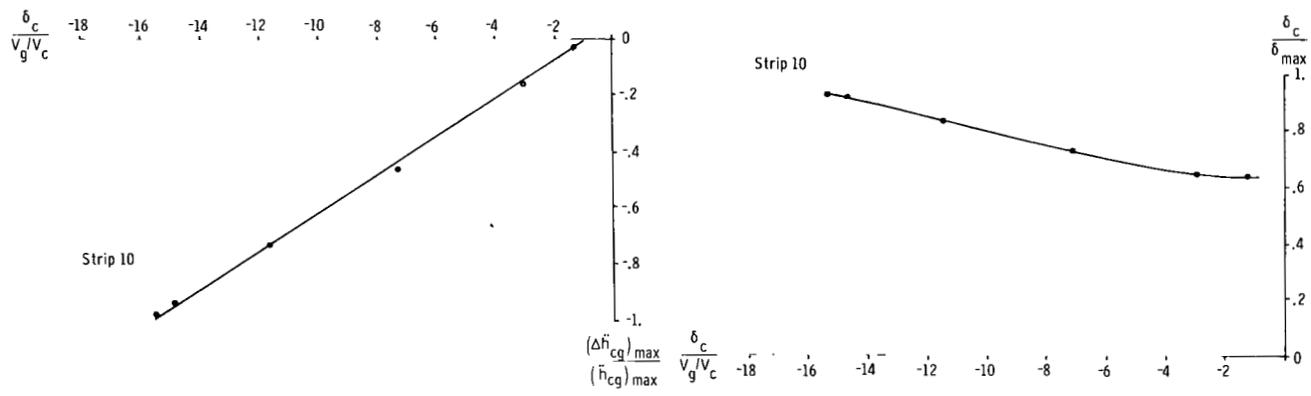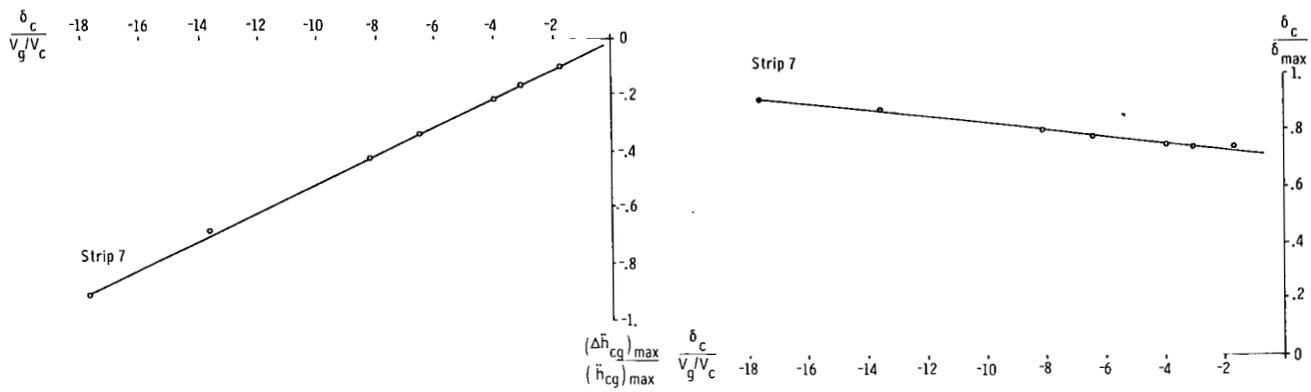
Figure 13.- Concluded.
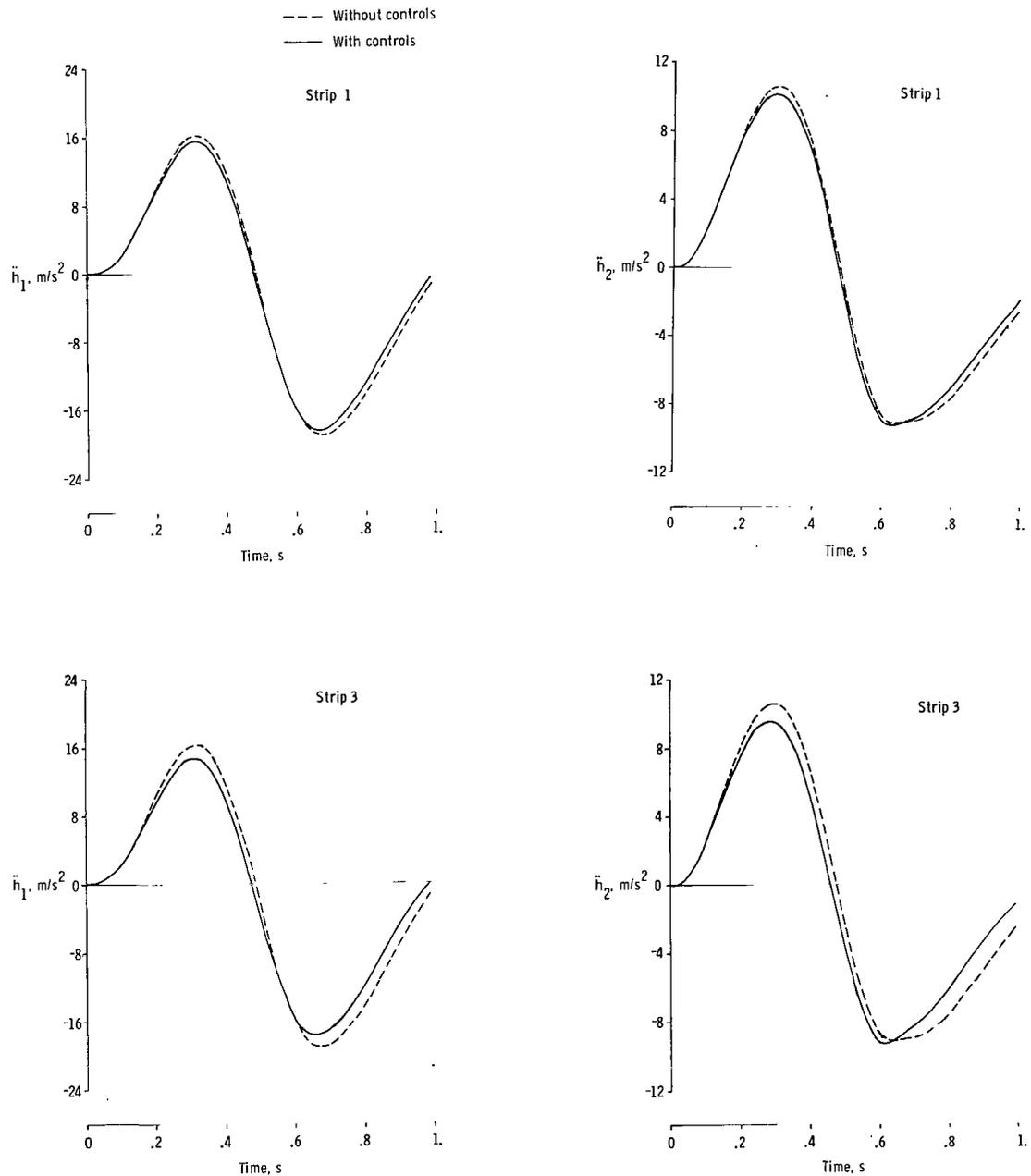
Figure 14.- Variation with time of linear acceleration at point 1 and point 2 due to a (1 - cos) upgust. Arava transport with a single L.E.-T.E. active control system located at various strips along wing and with $\delta_{max} = 0.5$ rad.
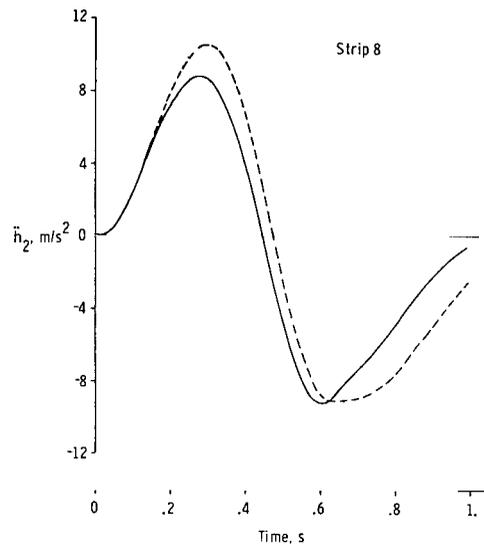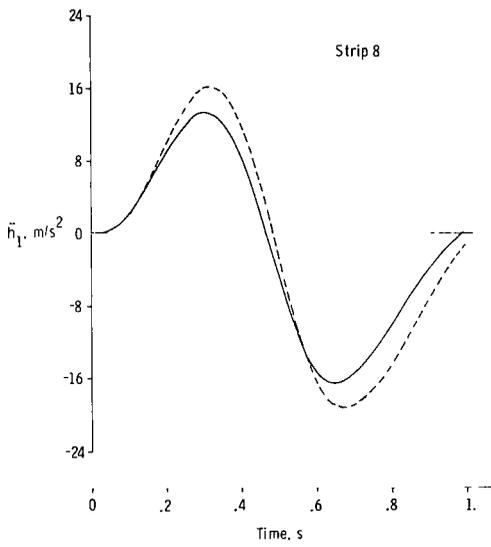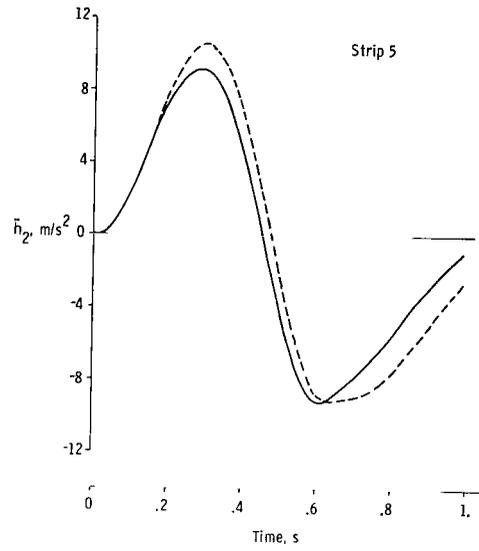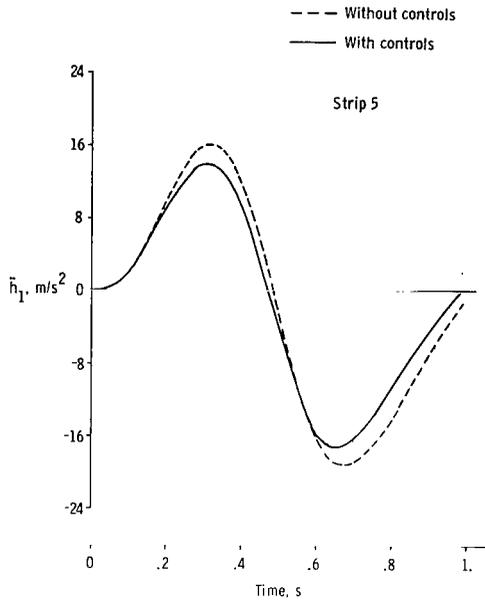
Figure 14.- Continued.
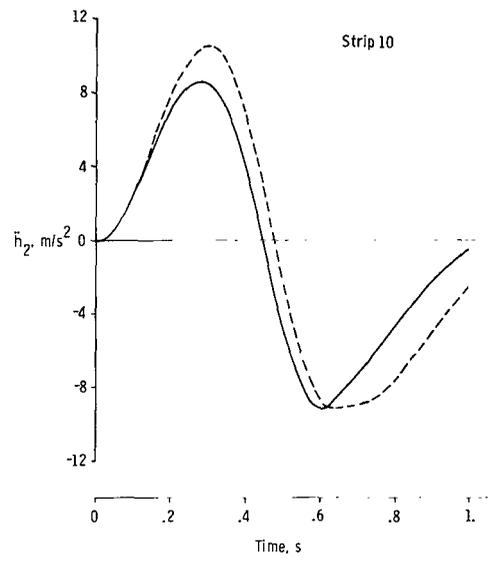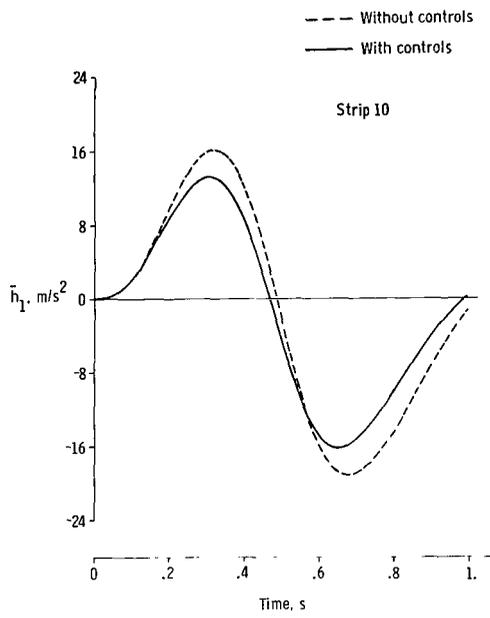
Figure 14.- Concluded.
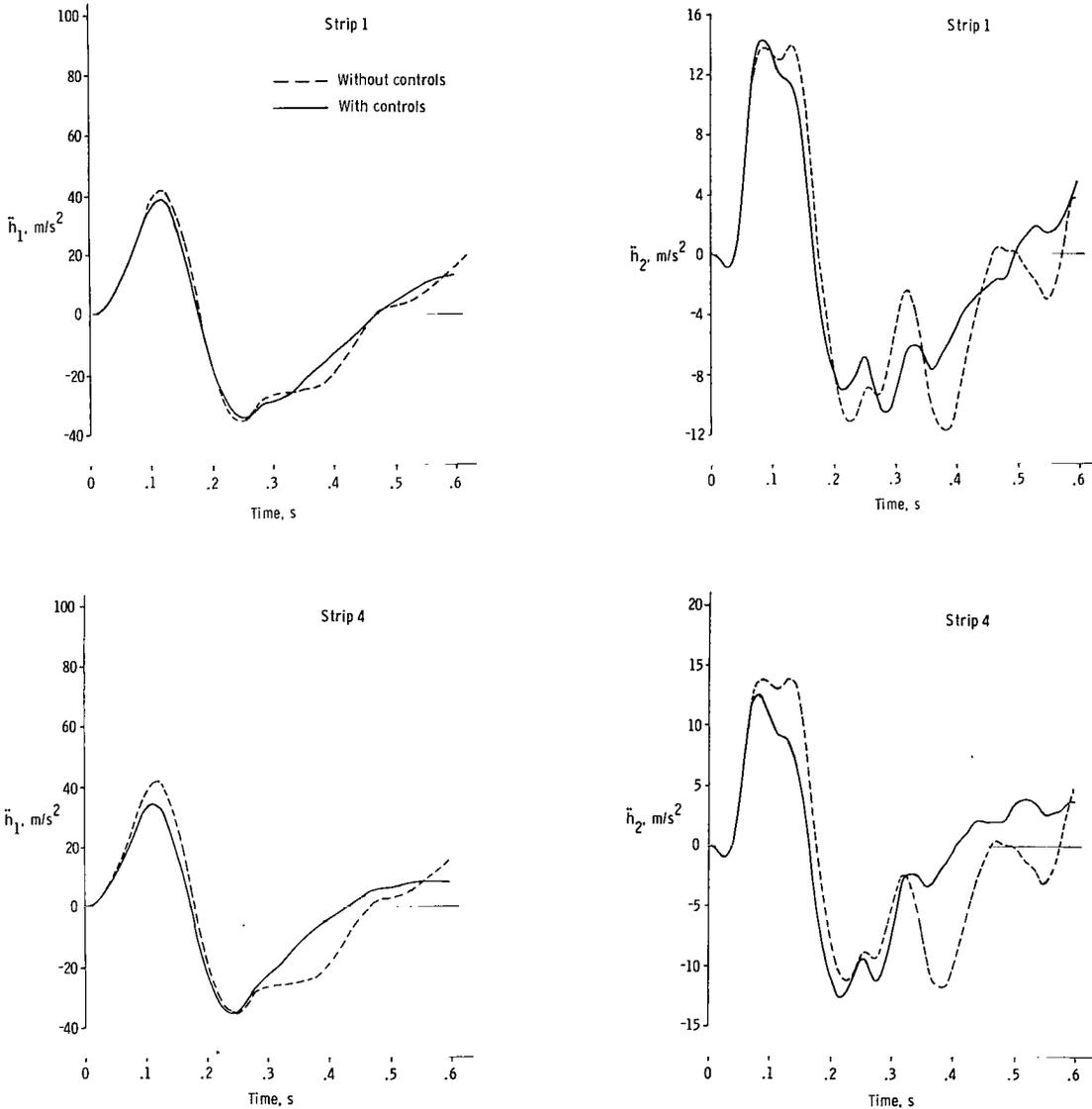
Figure 15.- Variation with time of linear acceleration at point 1 and point 2 due to a
(1 - cos) upgust. Westwind transport with a single L.E.-T.E. active control
system located at various strips along wing and with $\delta_{max} = 0.5$ rad.
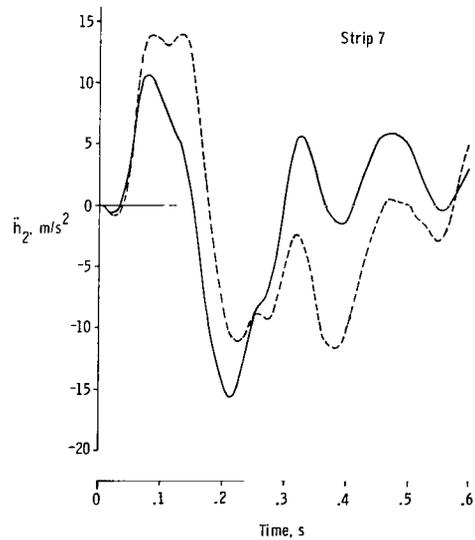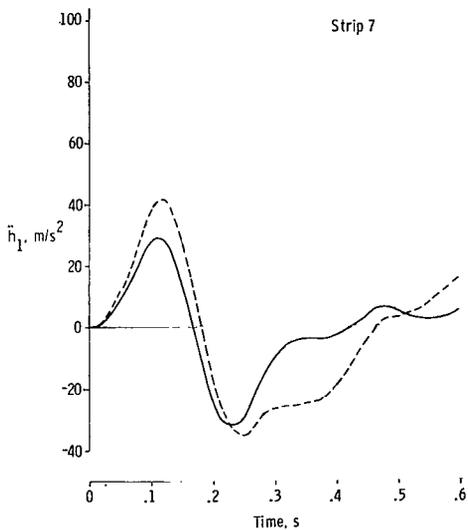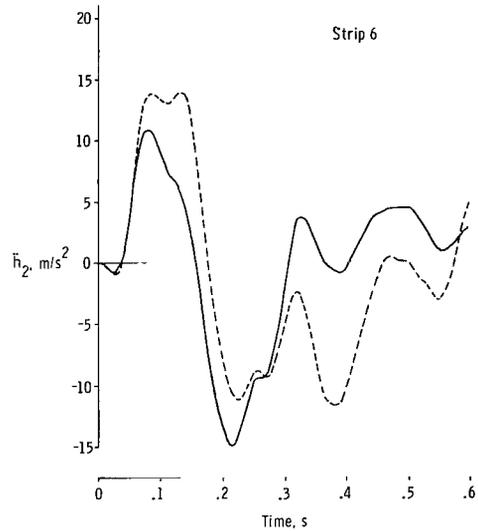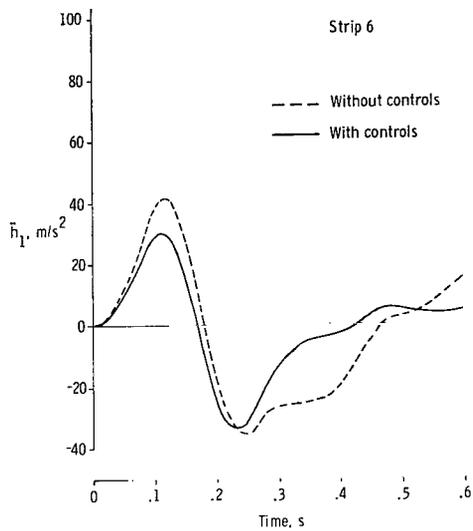
Figure 15.- Continued.
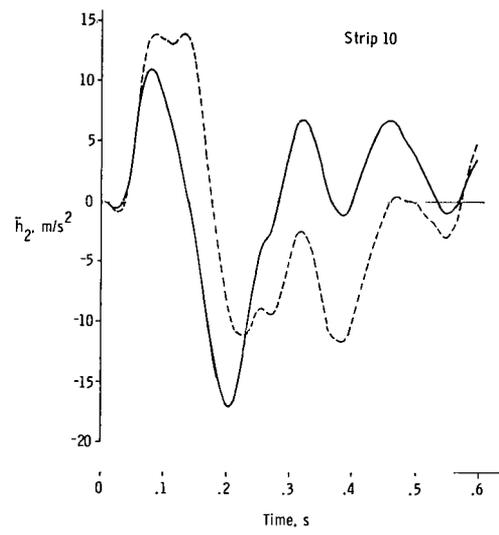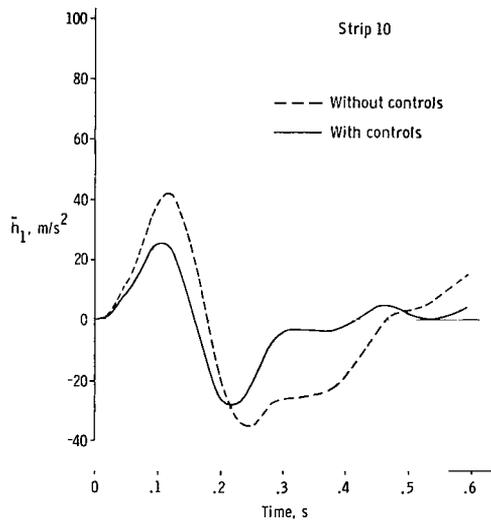
Figure 15.- Concluded.
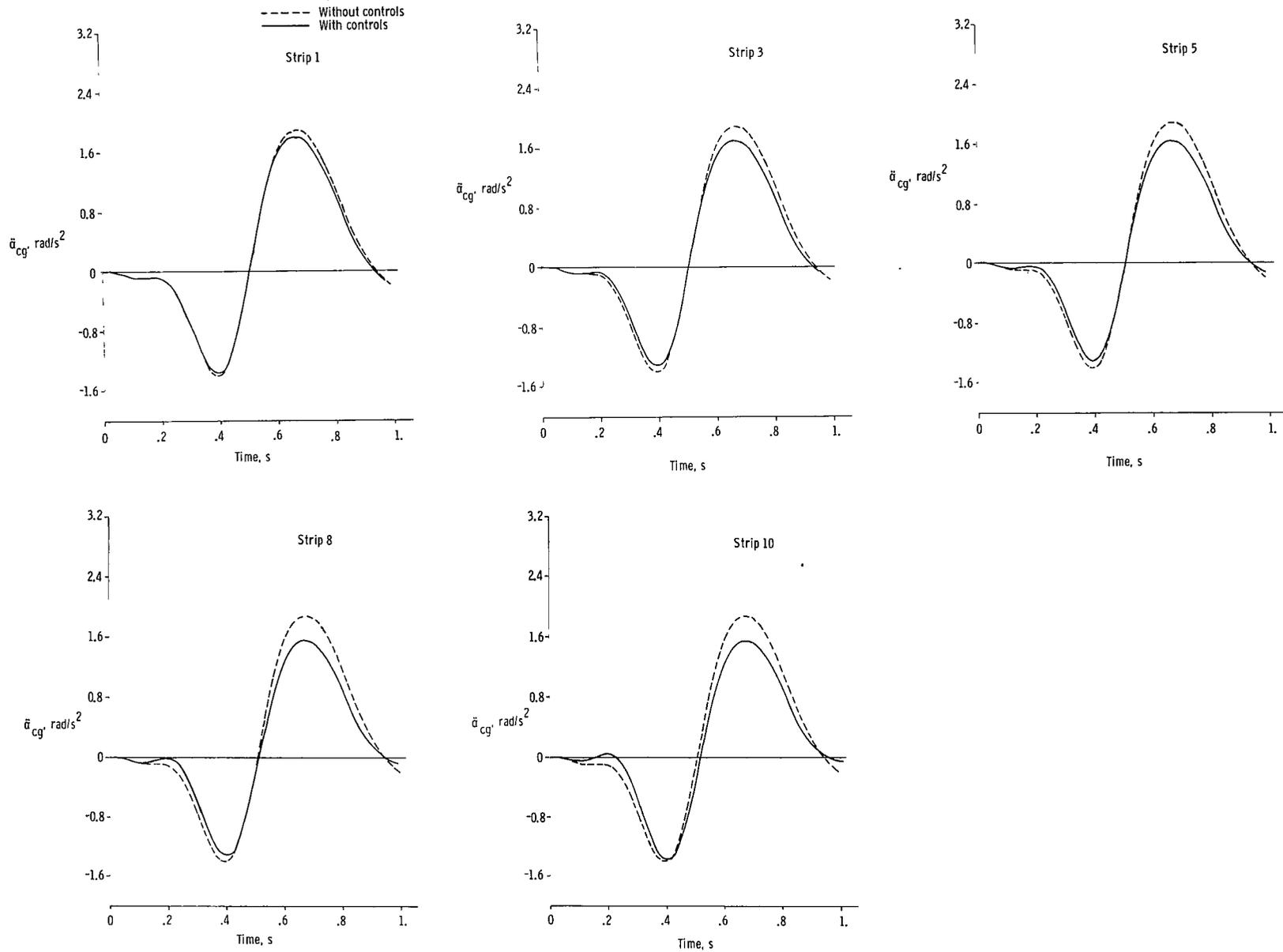
Figure 16.- Variation with time of rotational acceleration at center of gravity due to a (1 - cos) upgust. Arava transport with a single L.E.-T.E. active control system located at various strips along wing and with $\delta_{max} = 0.5$ rad.
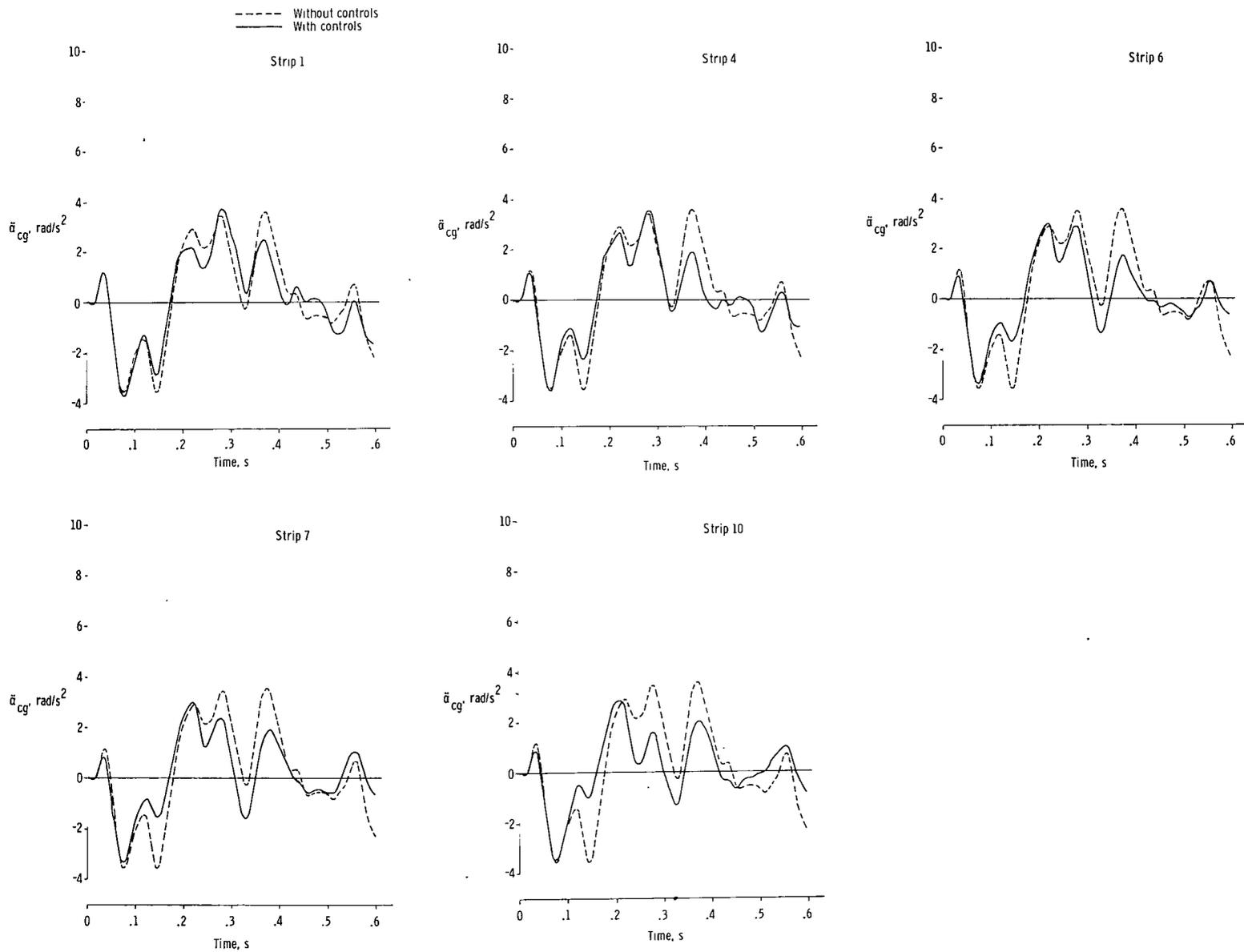
Figure 17.- Variation with time of rotational acceleration at center of gravity due to a (1 - cos) upgust. Westwind transport with a single L.E.-T.E. active control system located at various strips along wing and with δ_{max} = 0.5 rad.

71
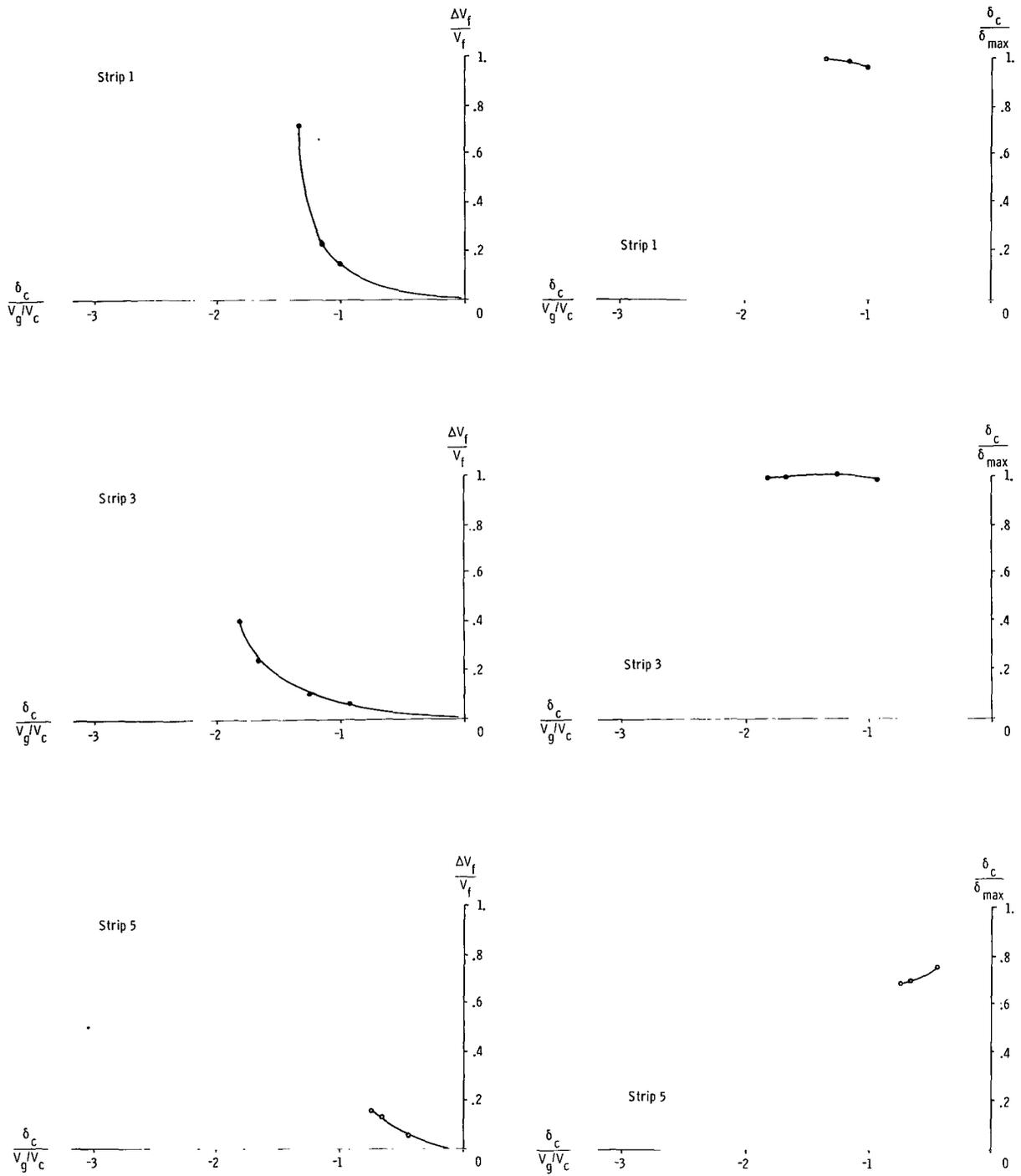
Figure 18.- Variation with control rotation parameter $\dfrac{\delta_c}{V_g/V_c}$ of flutter speed increase ratio and maximum control rotation ratio. Arava transport with a single L.E.-T.E. active control system located at various strips along wing.
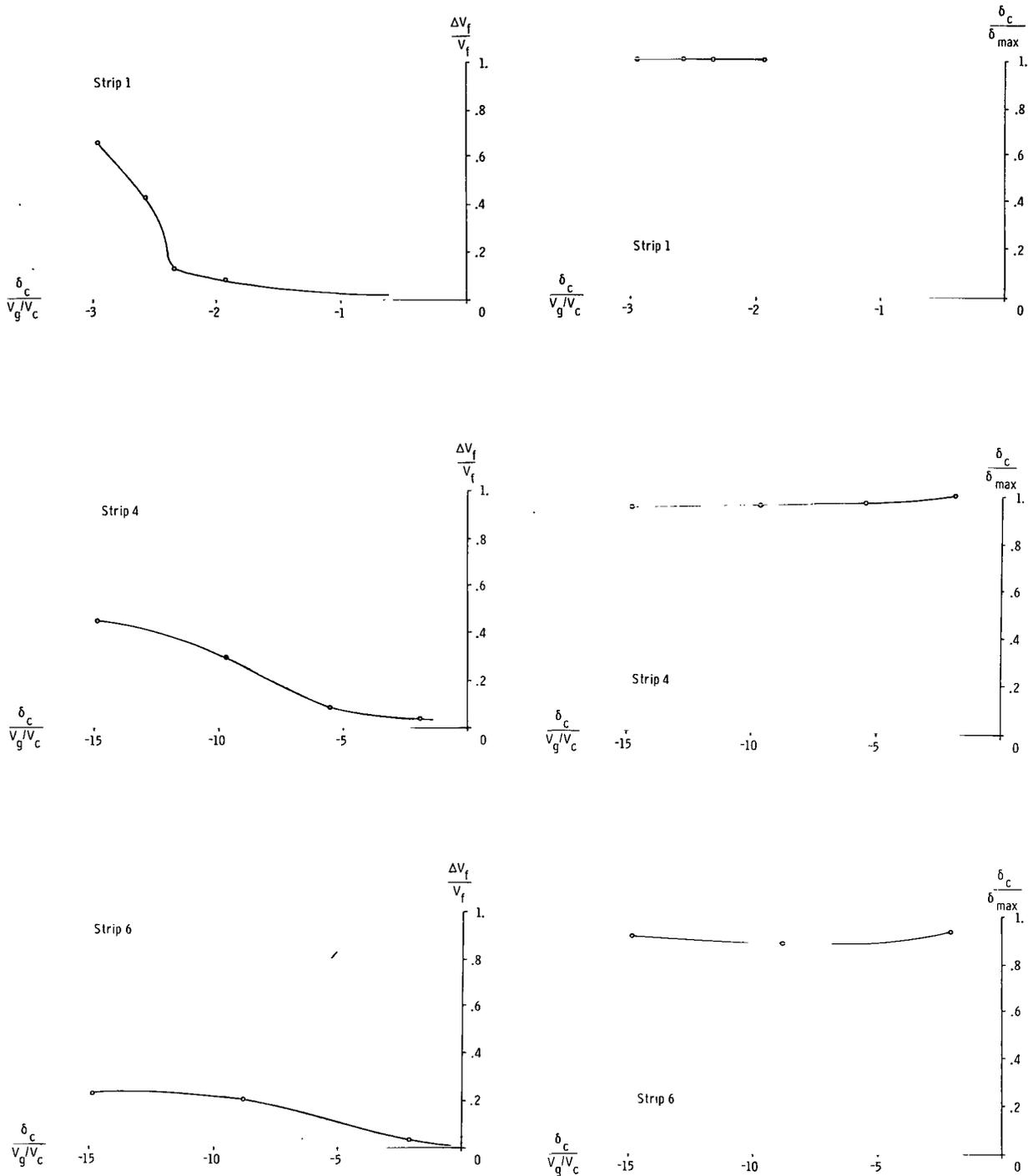
Figure 19.– Variation with control rotation parameter $\dfrac{\delta_c}{V_g/V_c}$ of flutter speed increase ratio and maximum control rotation ratio. Westwind transport with a single L.E.-T.E. active control system located at various strips along wing.
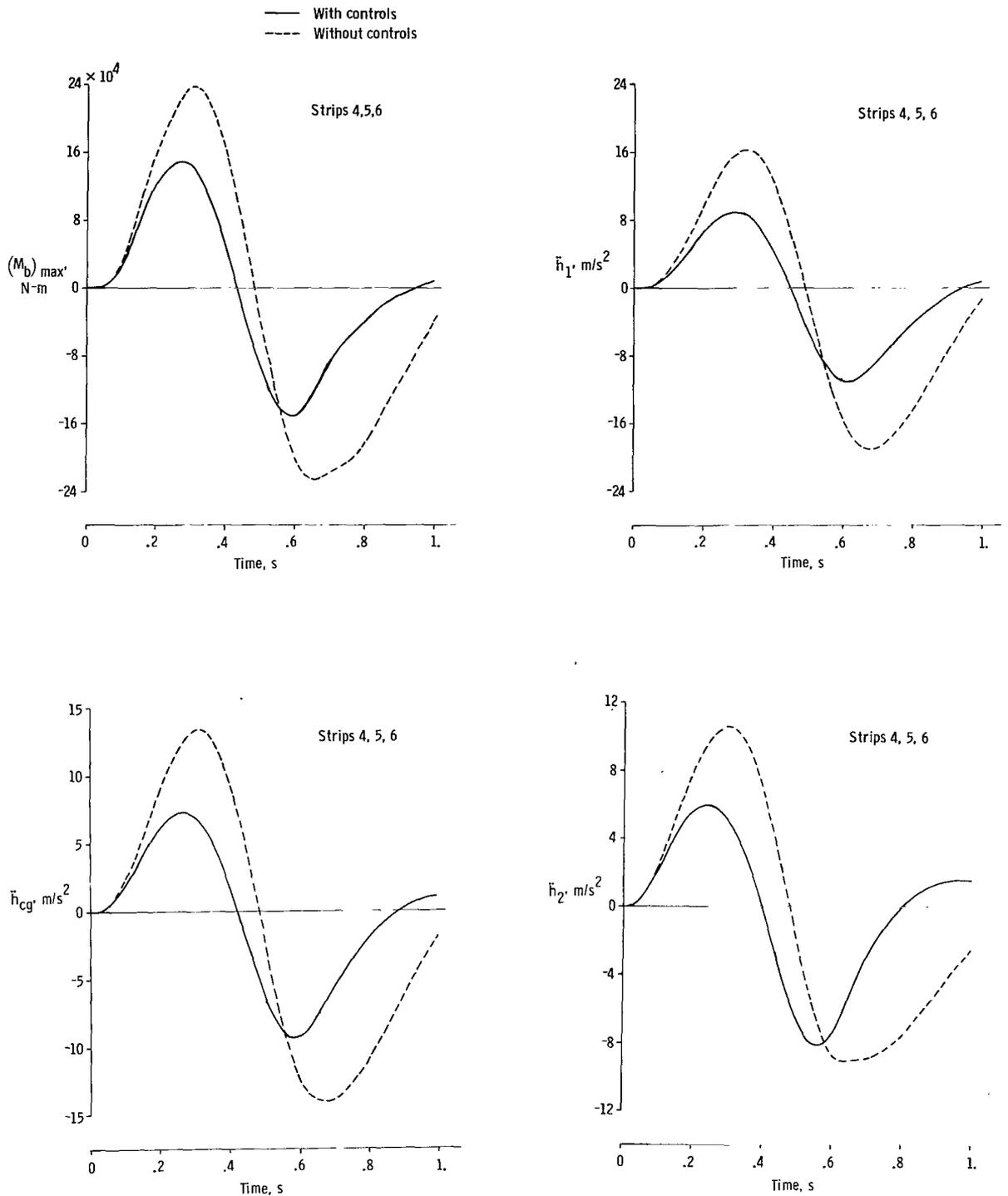
Figure 20.- Variation with time of various gust response parameters due to a (1 - cos) upgust. Arava transport with three L.E.-T.E. active control systems located at strips 4, 5, and 6 along wing and with $\delta_{max} = 0.5$ rad.
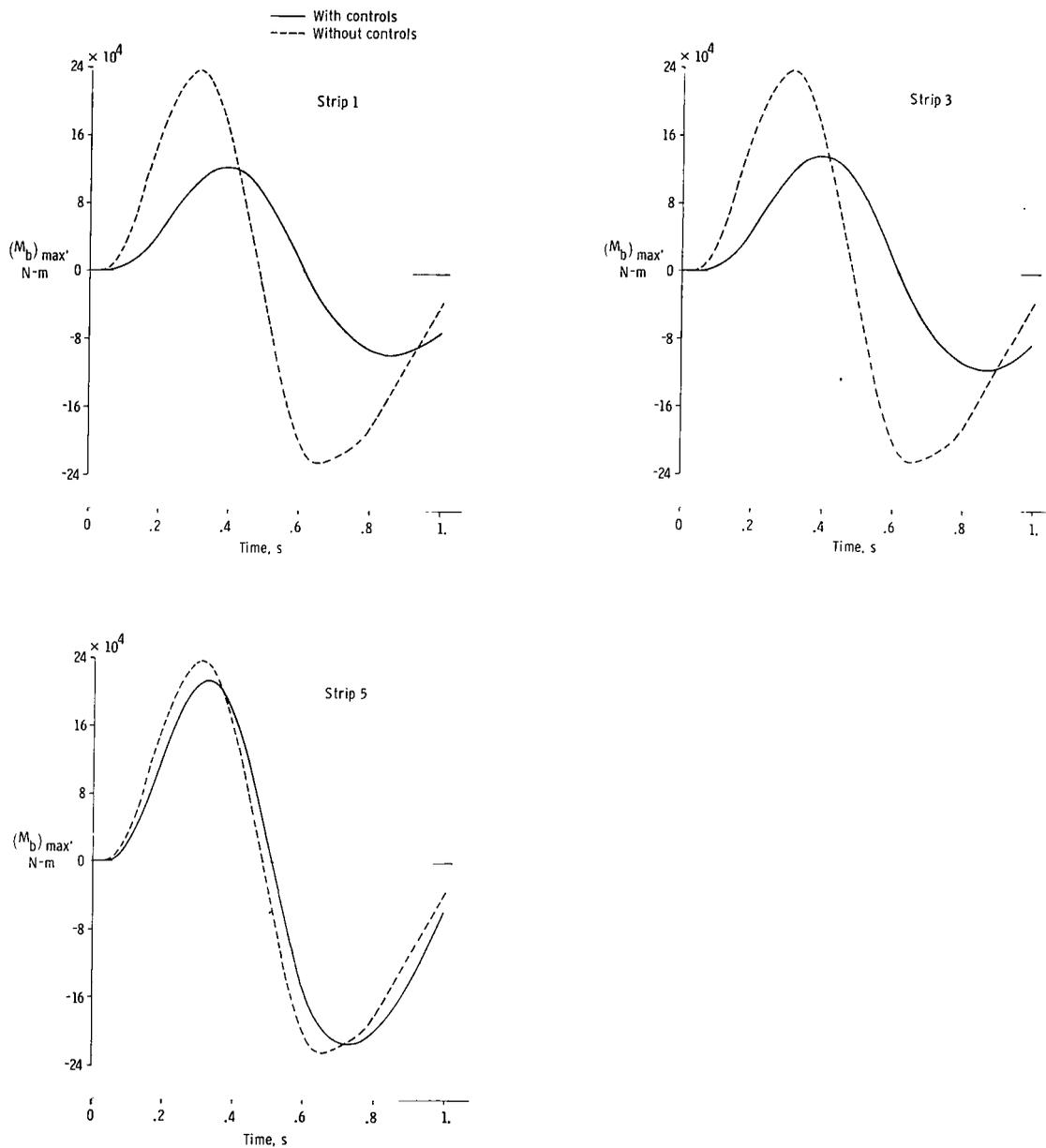
Figure 21.- Variations with time of wing bending moment at station 5 due to a (1 - cos) upgust. Arava transport with a single L.E.-T.E. active control system (using extended control law) located at various strips along wing and with δ_{max} = 0.5 rad.
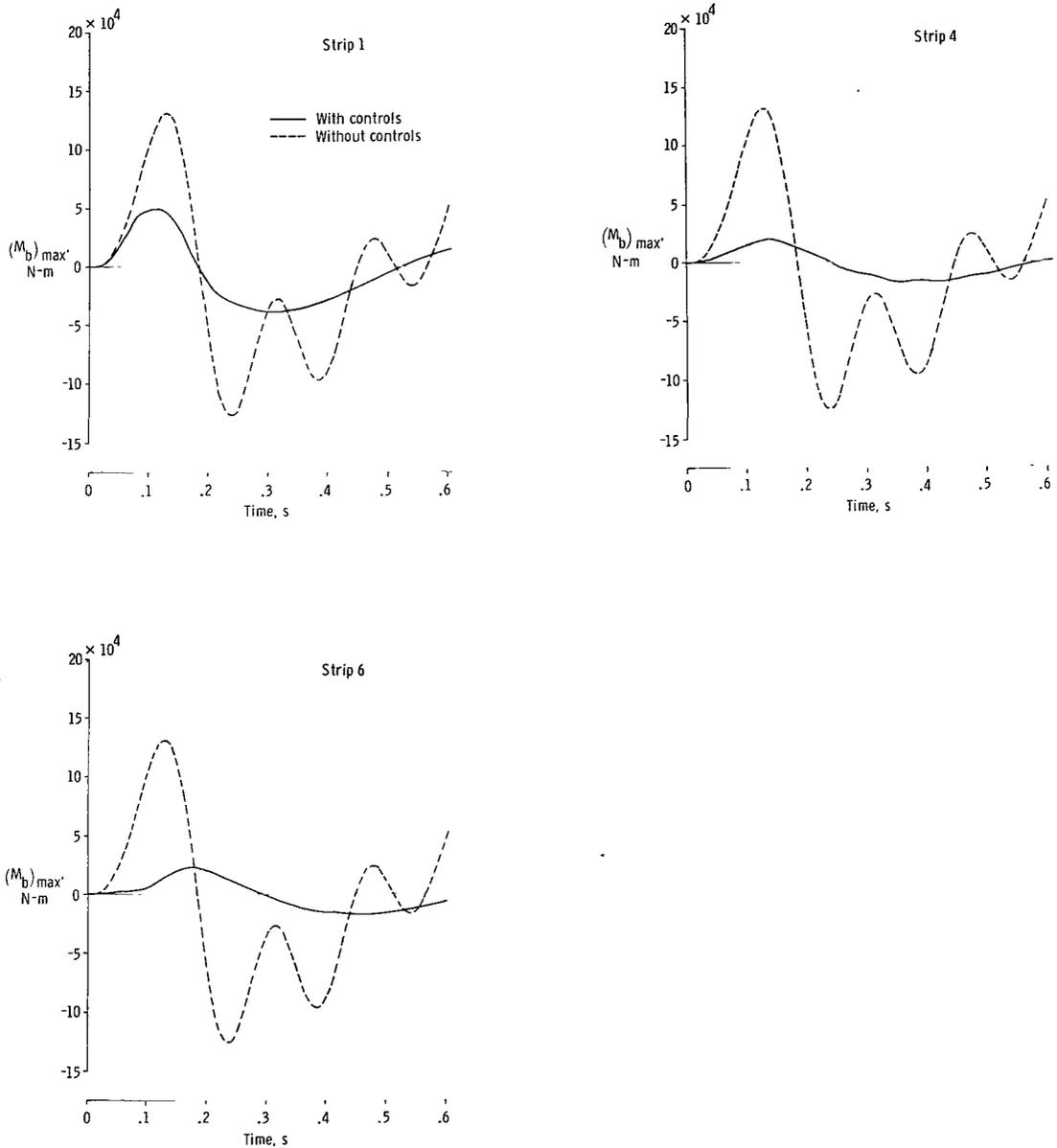
Figure 22.- Variation with time of wing bending moment at station 10 due to a (1 - cos) upgust. Westwind transport with a single L.E.-T.E. active control system (using extended control law) located at various strips along wing and with $\delta_{max} = 0.5$ rad.
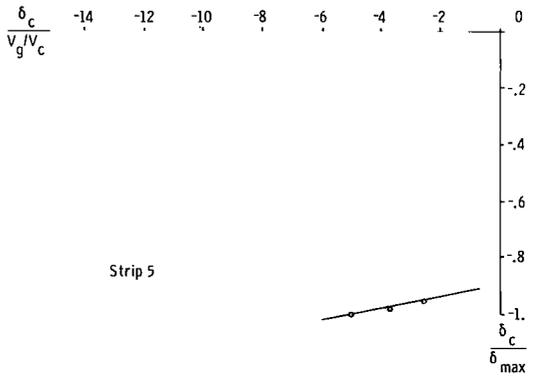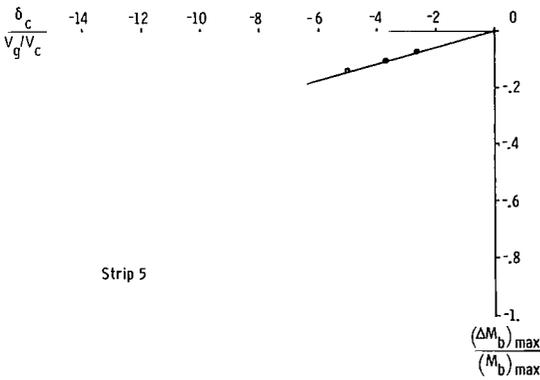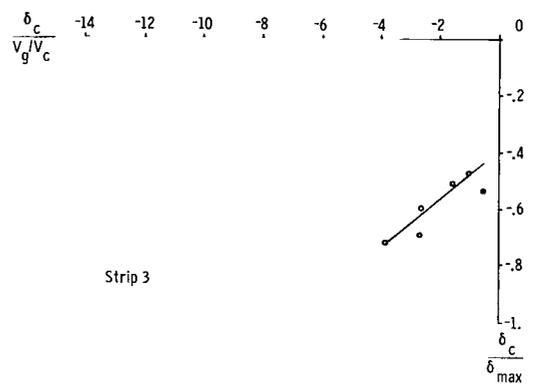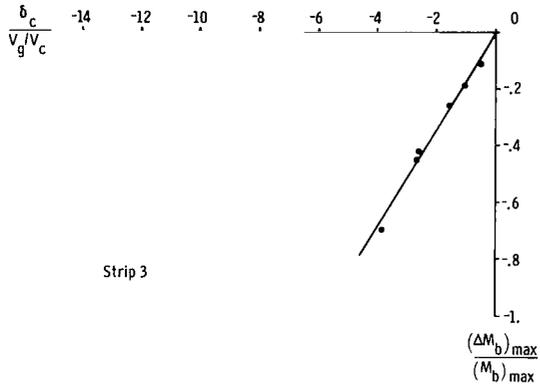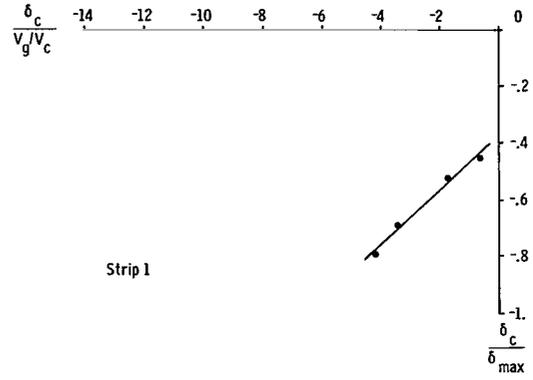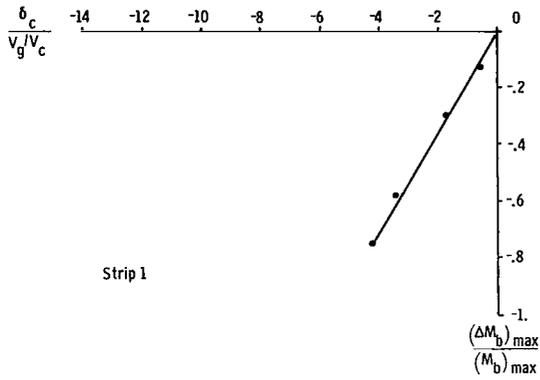
Figure 23.- Variation with control rotation parameter $\dfrac{\delta_c}{V_g/V_c}$ of bending-moment alleviation ratio at station 5 and maximum control rotation ratio. Arava transport with a single L.E.-T.E. active control system (using extended control law) located at various strips along wing.
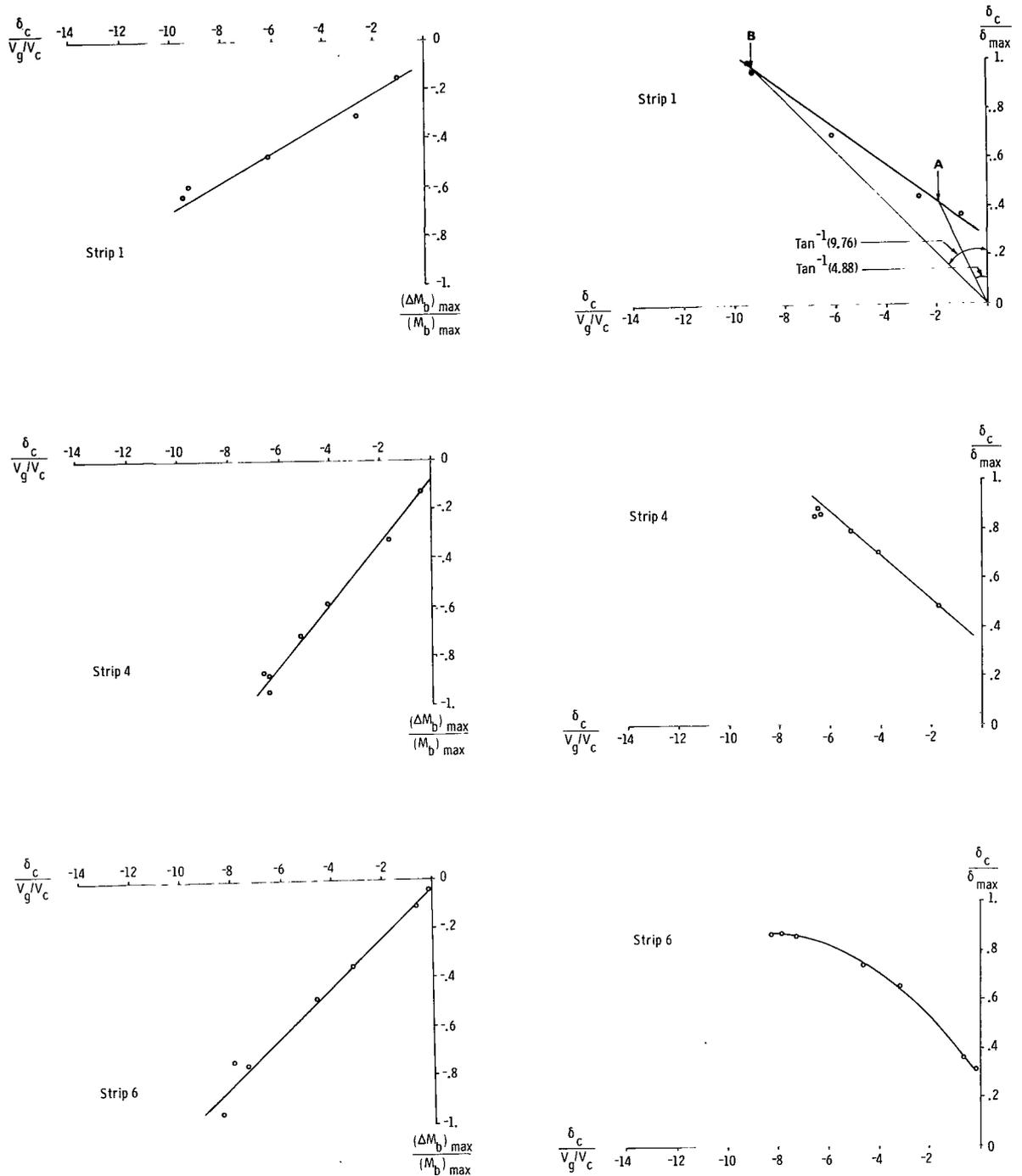
Figure 24.- Variation with control rotation parameter $\dfrac{\delta_c}{V_g/V_c}$ of bending-moment alleviation ratio at station 10 and maximum control rotation ratio. Westwind transport with a single L.E.-T.E. active system (using extended control law) located at various strips along wing.
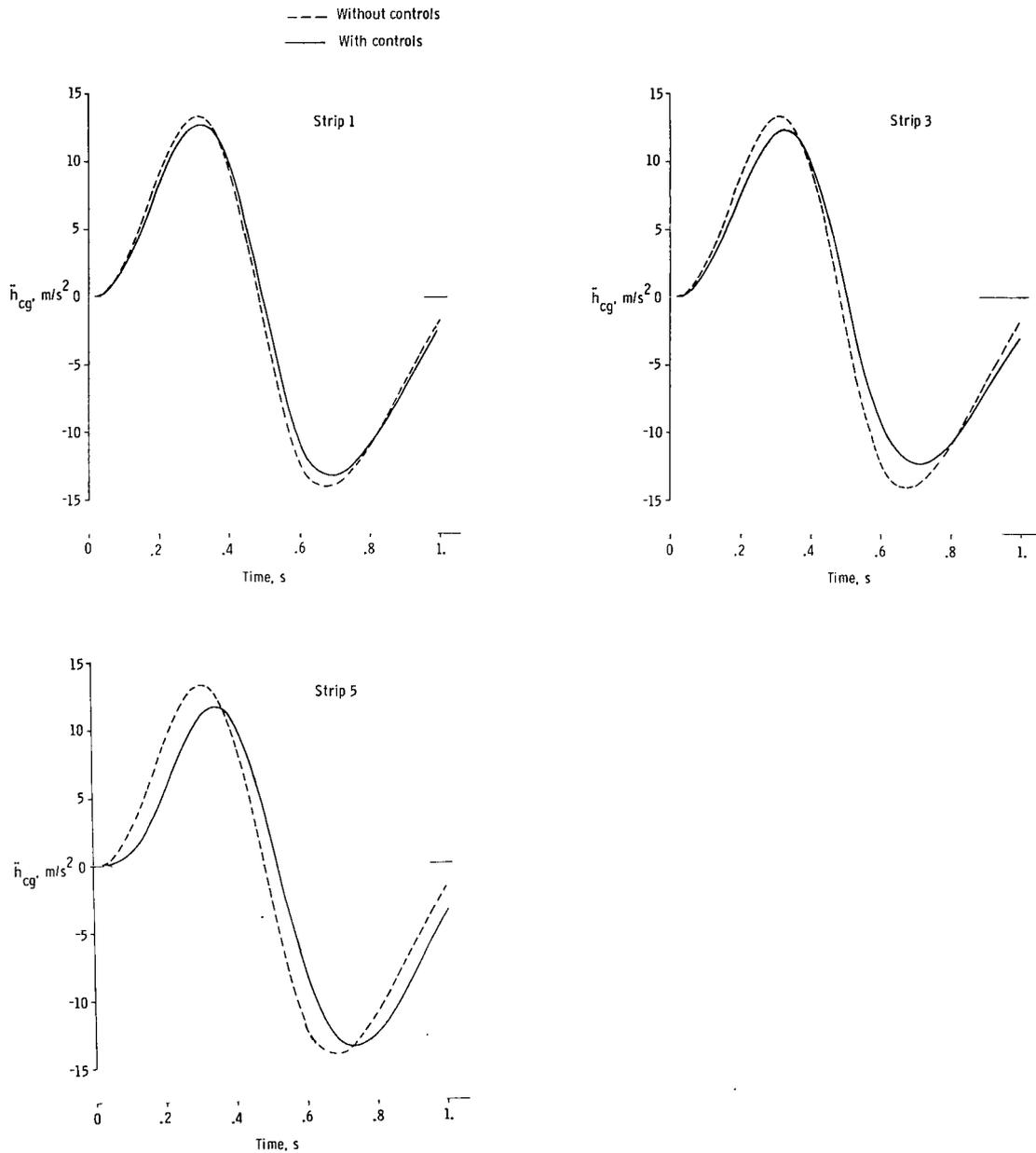
Figure 25.- Variation with time of linear acceleration at center of gravity due to a (1 - cos) upgust. Arava transport with a single L.E.-T.E. active control system (using extended control law) located at various strips along wing and with $\delta_{max} = 0.5$ rad.
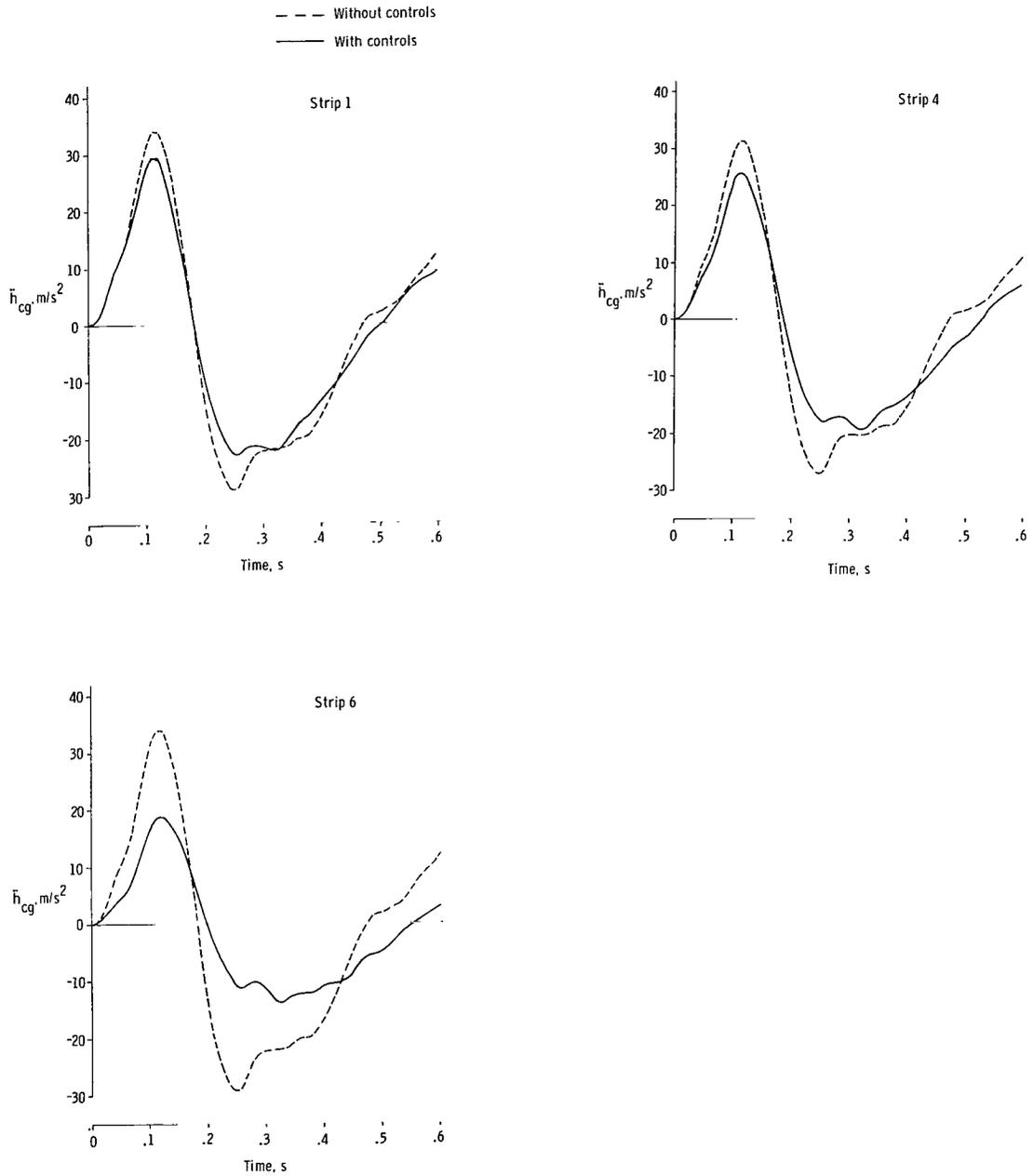
Figure 26.- Variation with time of linear acceleration at center of gravity due to a
(1 - cos) upgust. Westwind transport with a single L.E.-T.E. active control
system (using extended control law) located at various strips along wing and
with δ_{max} = 0.5 rad.
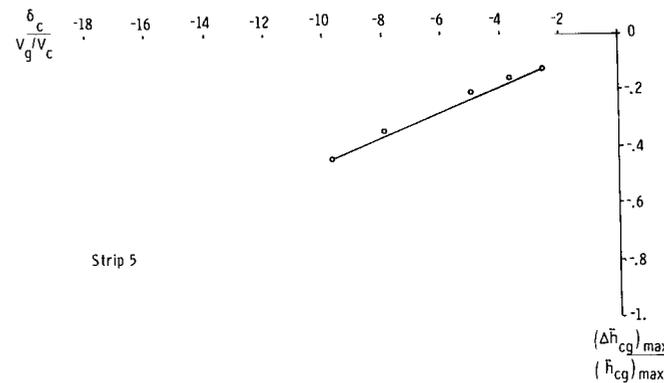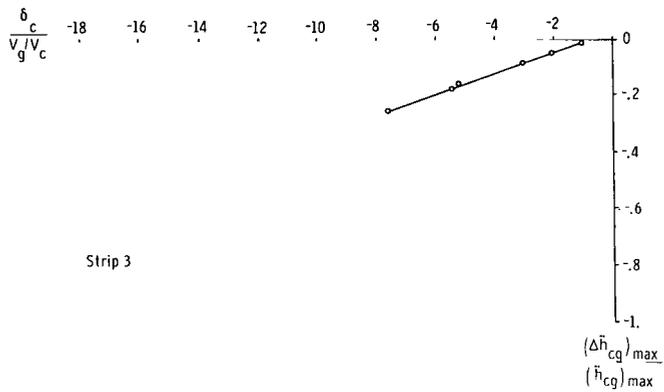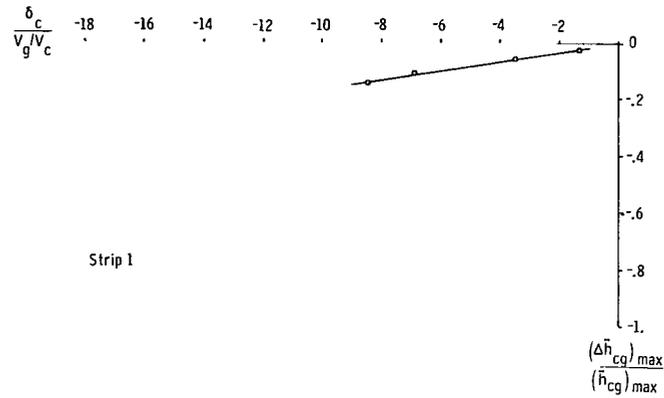
Figure 27.- Variation with control rotation parameter $\dfrac{\delta_c}{V_g/V_c}$ of acceleration alleviation ratio at center of gravity and maximum control rotation ratio. Arava transport with a single L.E.-T.E. active control system (using extended control law) located at various strips along wing.
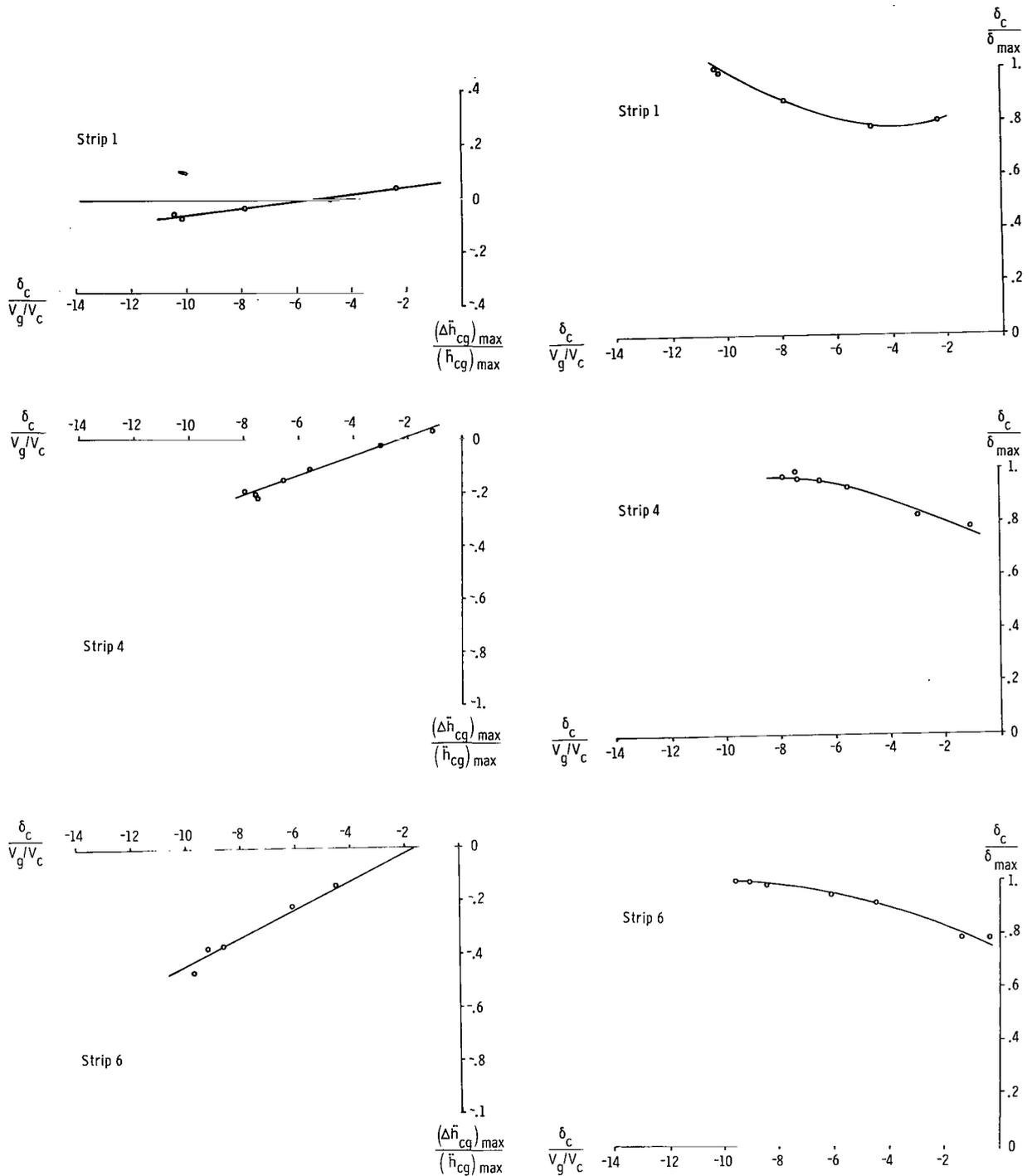
Figure 28.- Variation with control rotation parameter $\dfrac{\delta_c}{V_g/V_c}$ of acceleration alleviation ratio at center of gravity and maximum control rotation ratio. Westwind transport with a single L.E.-T.E. active control system (using extended control law) located at various strips along wing.
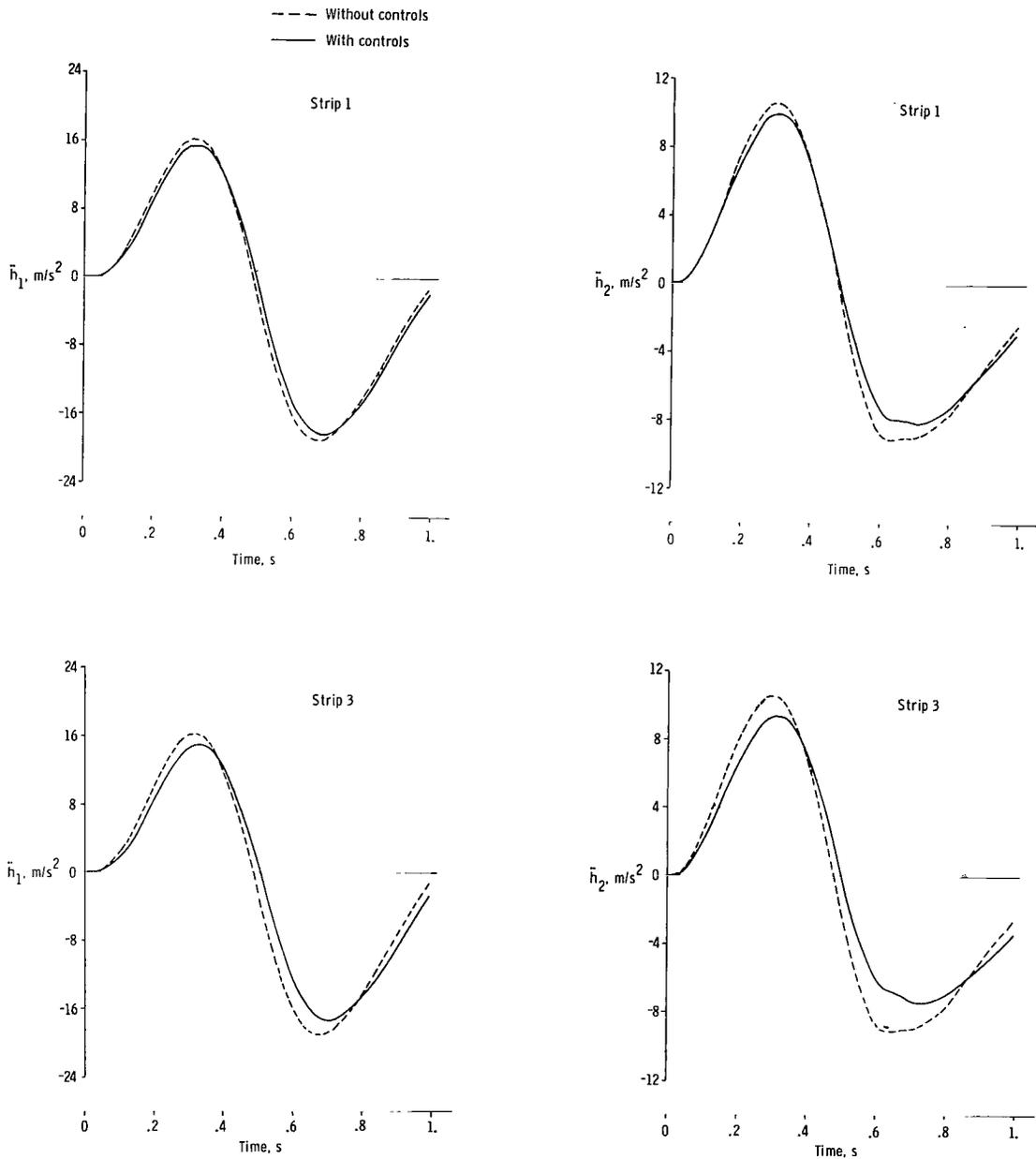
Figure 29.- Variation with time of linear acceleration at point 1 and point 2 due to a
(1 - cos) upgust. Arava transport with a single L.E.-T.E. active control system
(using extended control law) located at various strips along wing and with
δ_{max} = 0.5 rad.
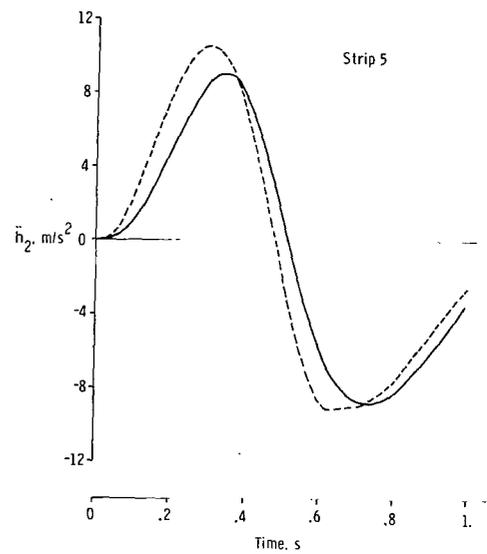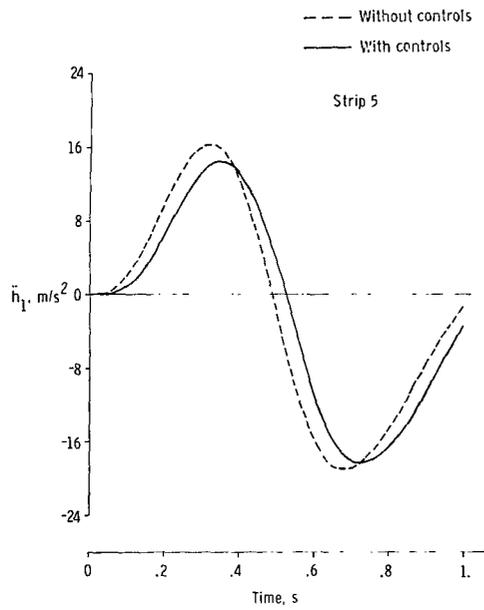
Figure 29.- Concluded.
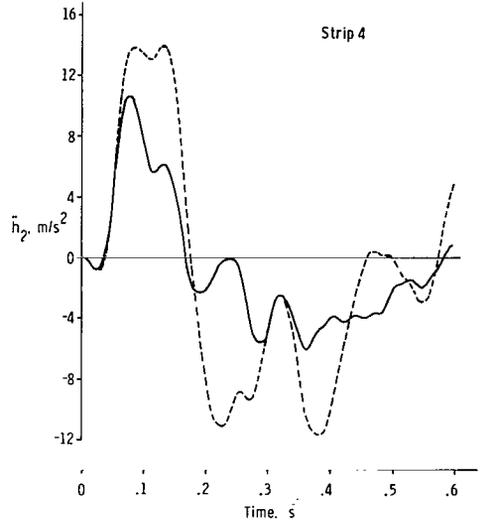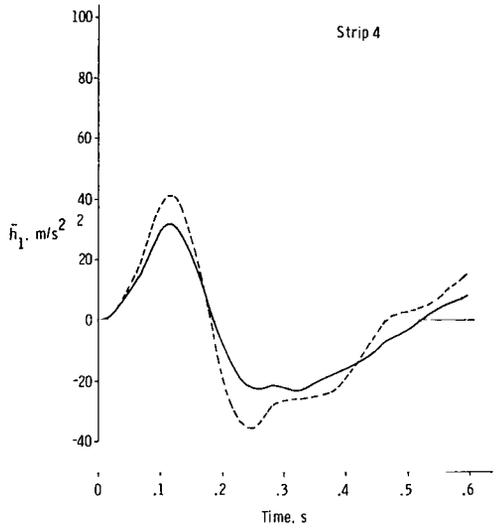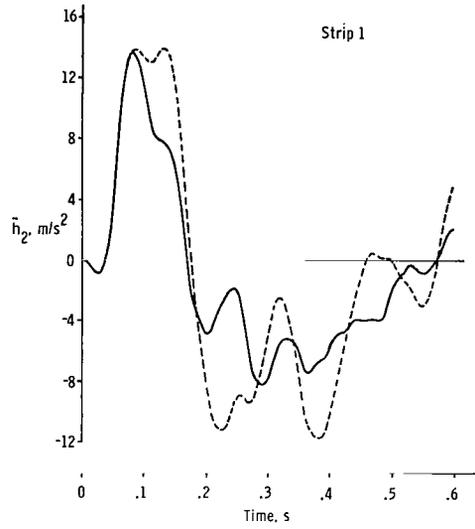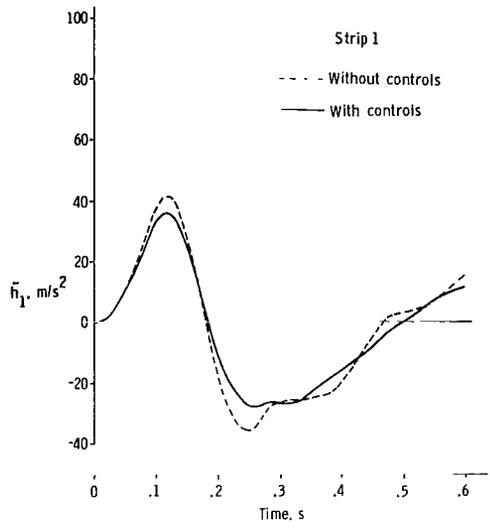
Figure 30.- Variation with time of linear acceleration at point 1 and point 2 due to a
(1 - cos) upgust. Westwind transport with a single L.E.-T.E. active control
system (using extended control law) located at various strips along wing and with
$\delta_{max} = 0.5$.
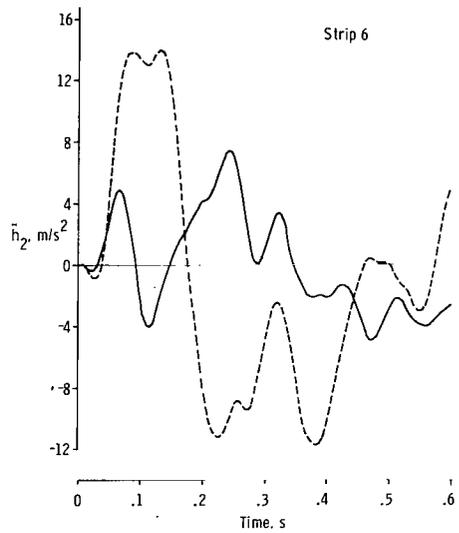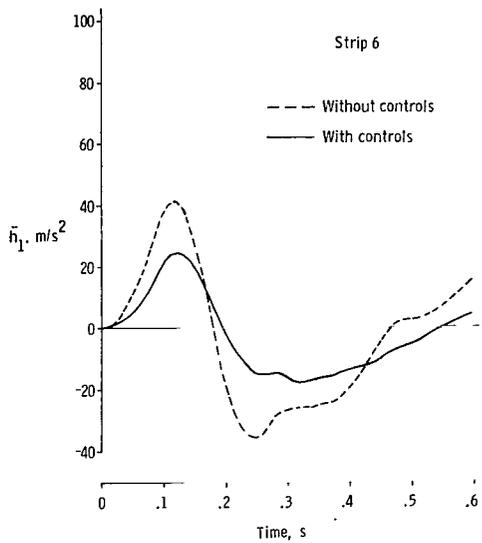
Figure 30.- Concluded.
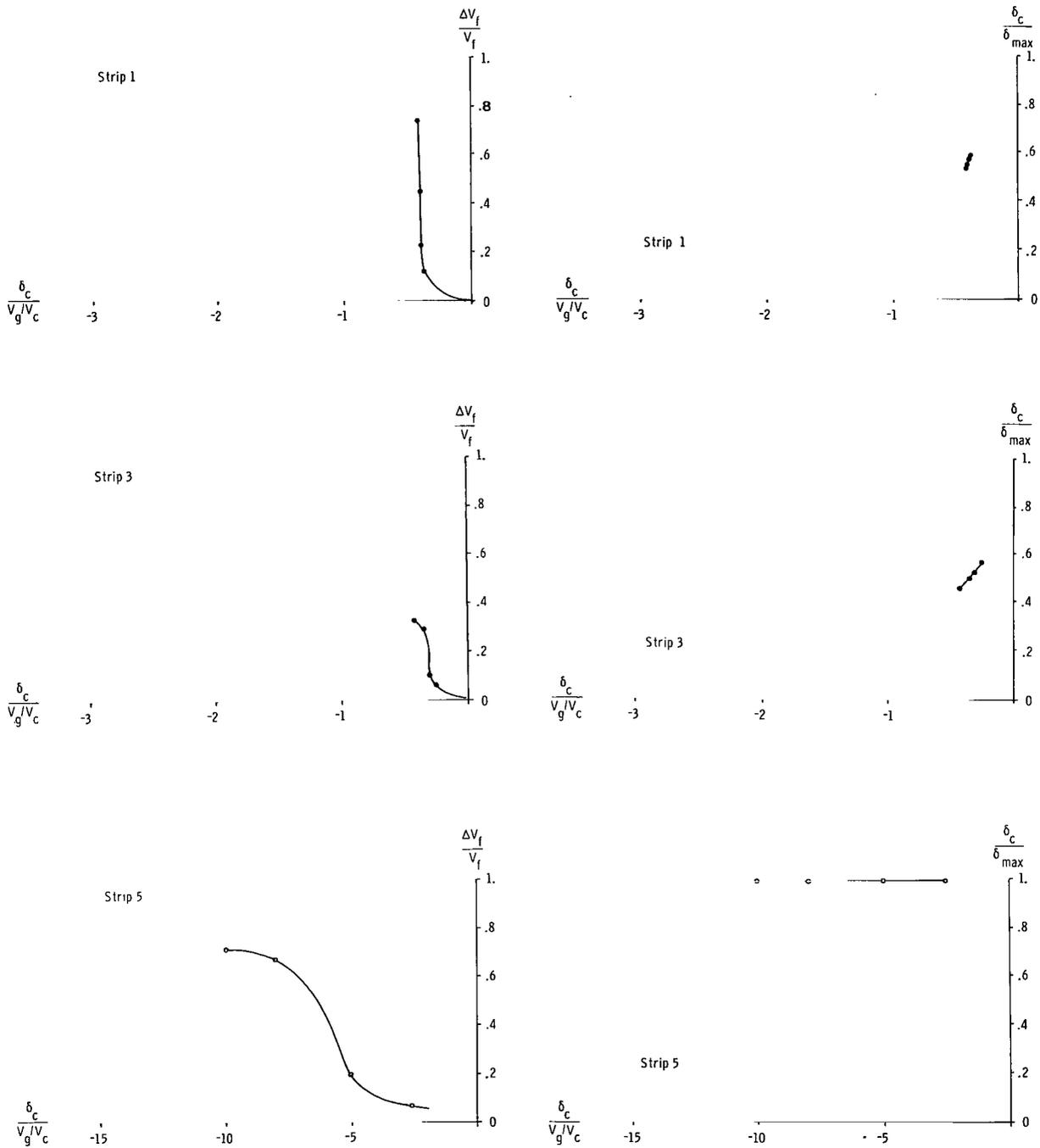
Figure 31.- Variation with control rotation parameter $\dfrac{\delta_c}{V_g / V_c}$ of flutter speed increase ratio and maximum control rotation ratio. Arava transport with a single L.E.-T.E. active control system (using extended control law) located at various strips along wing.
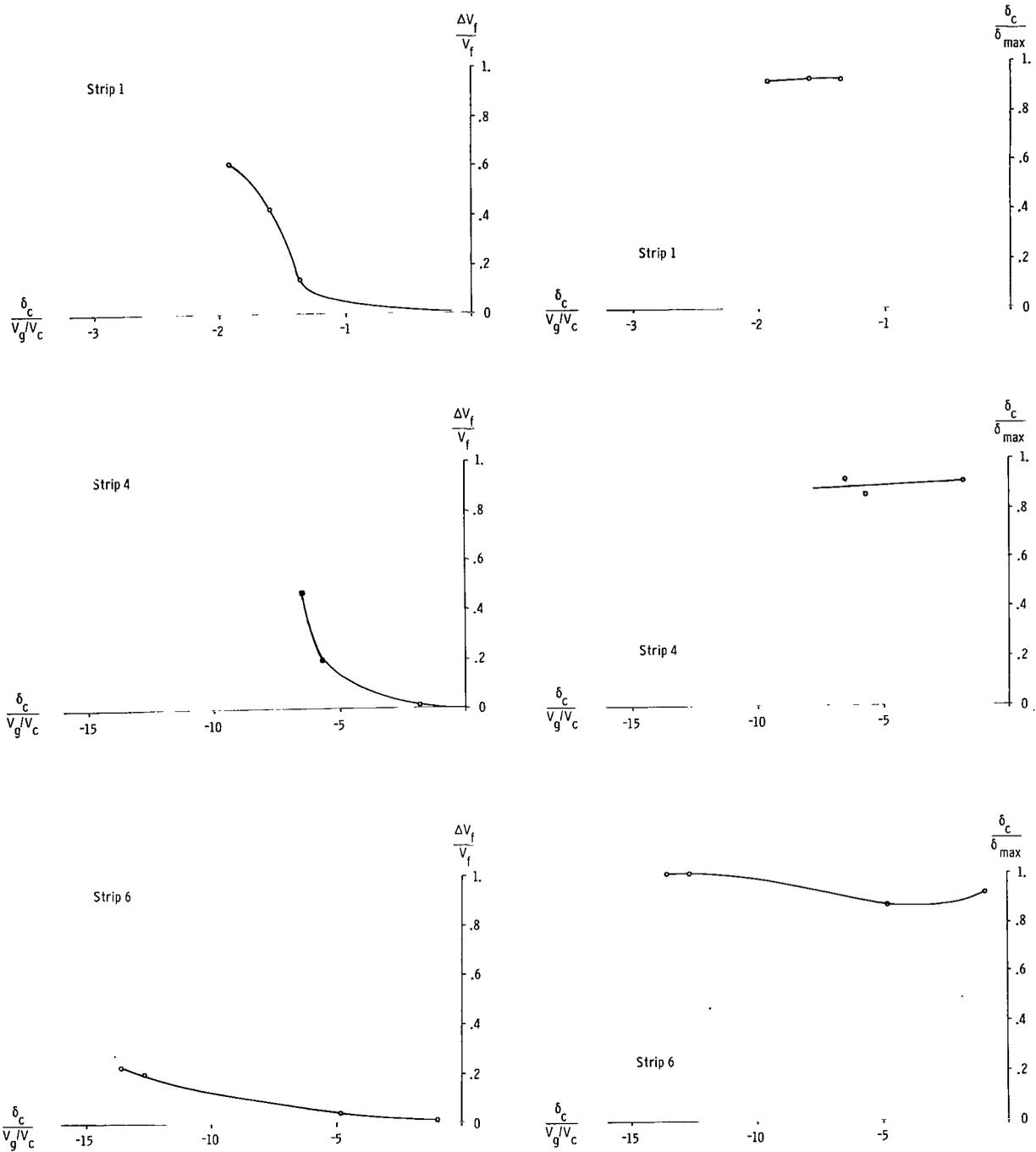
Figure 32.- Variation with control rotation parameter $\dfrac{\delta_c}{V_g/V_c}$ of flutter speed increase ratio and maximum control rotation ratio. Westwind transport with a single L.E.-T.E. active control system (using extended control law) located at various strips along wing.
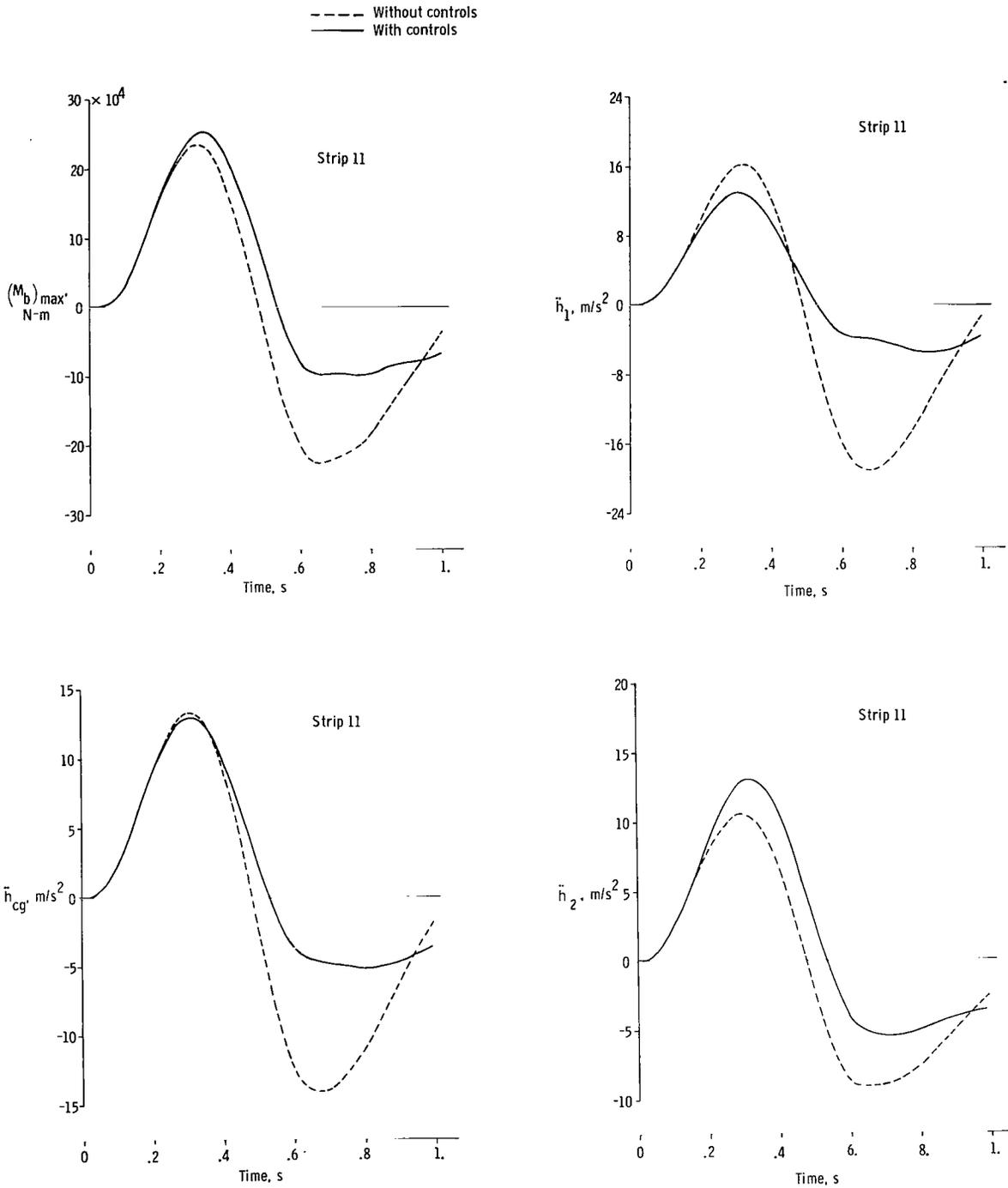
Figure 33.- Variation with time of various gust response parameters due to a (1 - cos) upgust. Arava transport with a single L.E.-T.E. active control system (using extended control law) located at strip 11, near center line of horizontal tail and with δ_{max} = 0.25 rad.
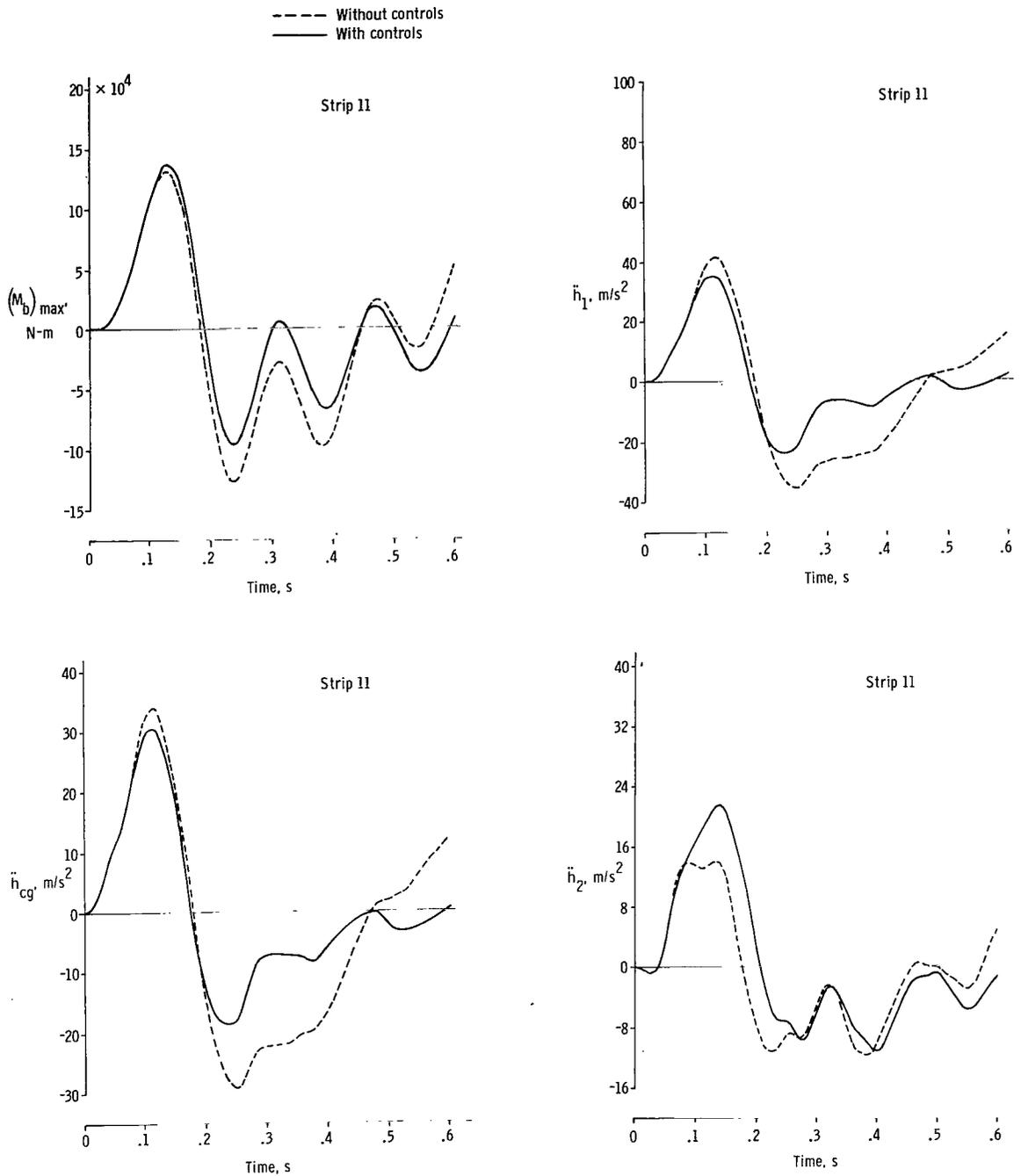
Figure 34.- Variation with time of various gust response parameters due to a (1 - cos) upgust. Westwind transport with a single L.E.-T.E. active control system (using an extended control law) located at strip 11 (at root of horizontal tail) and with $\delta_{max} = 0.5$ rad.
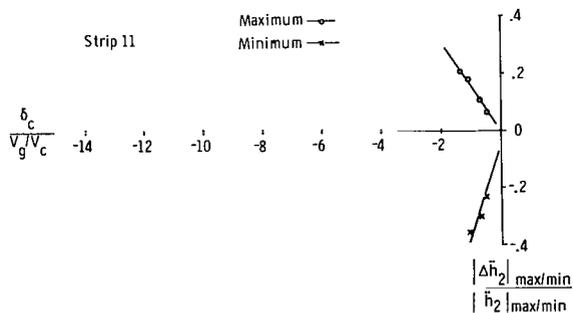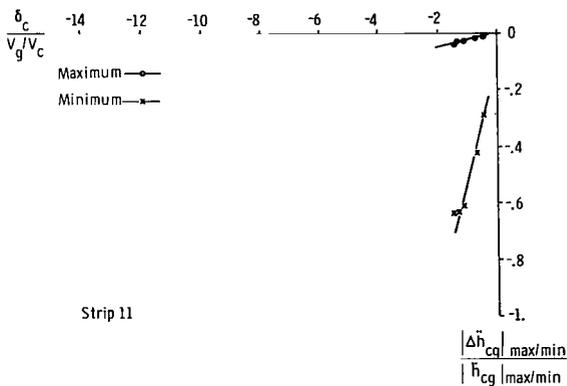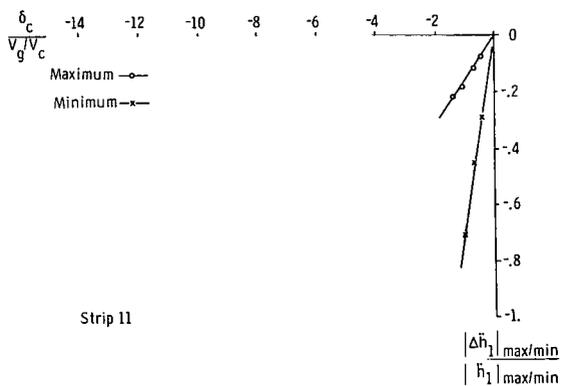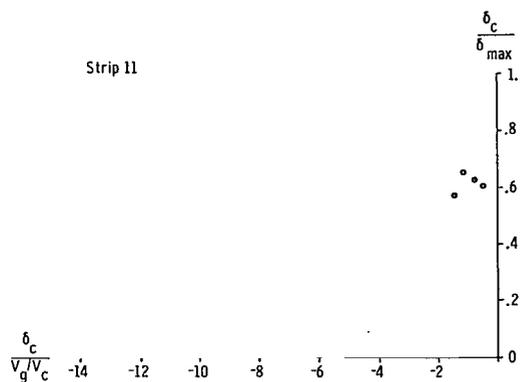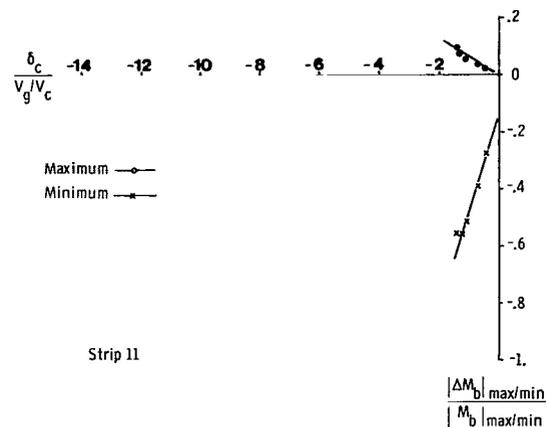
Figure 35.- Variation with control rotation parameter $\dfrac{\delta_c}{V_g/V_c}$ of various gust-alleviation parameter ratios and maximum control rotation ratio due to a (1 - cos) upgust. Arava transport with a single L.E.-T.E. active control system (using an extended control law) located at strip 11 near center line of horizontal tail.
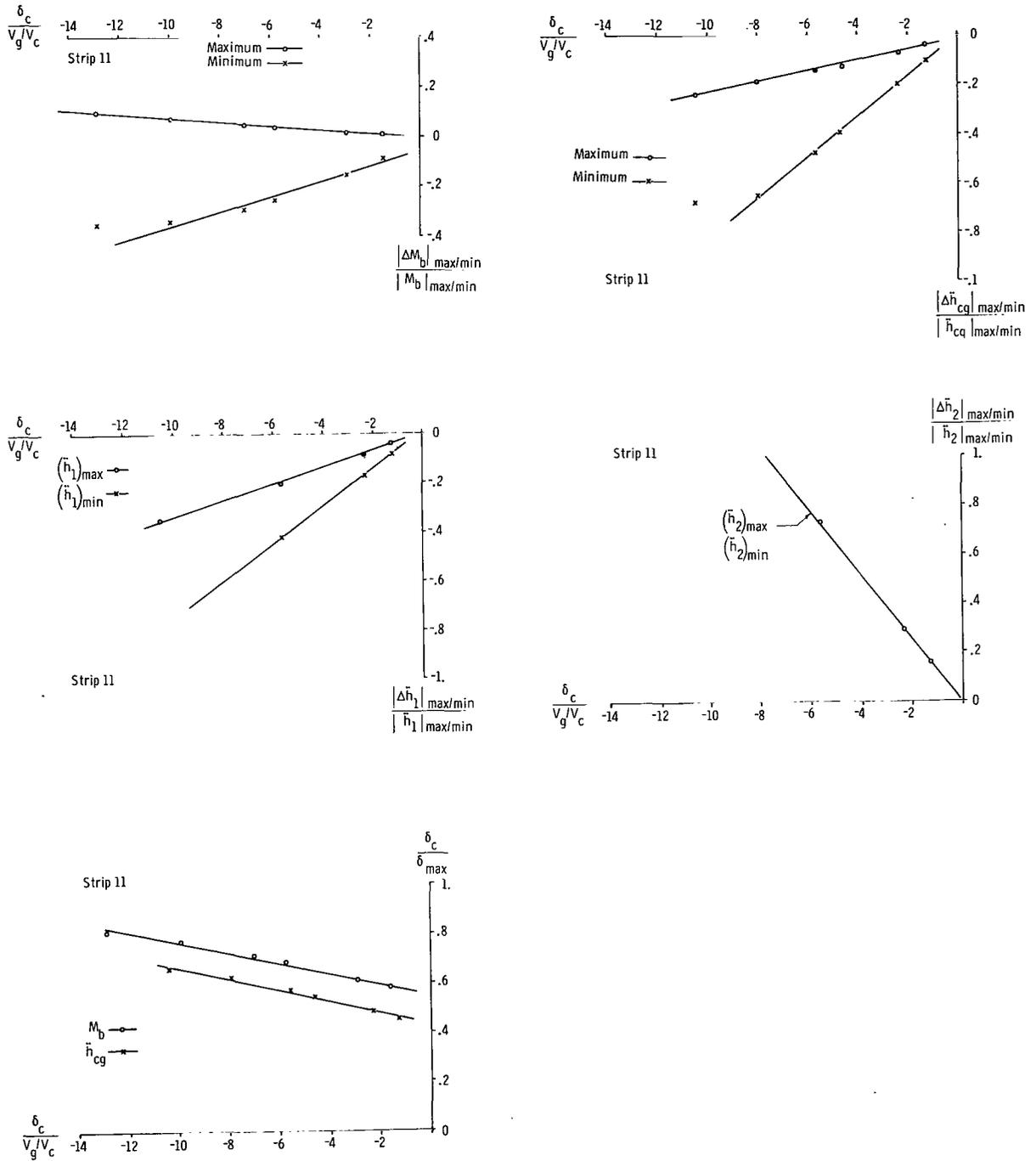
Figure 36.- Variation with control rotation parameter $\dfrac{\delta_c}{V_g/V_c}$ of various gust-alleviation parameter ratios and maximum control rotation ratio due to a (1 - cos) upgust. Westwind transport with a single L.E.-T.E. active control system (using an extended control law) located at strip 11 at root of horizontal tail.

569 001 C1 U   D 760604 S00903DS
DEPT OF THE AIR FORCE
AF WEAPONS LABORATORY
ATTN: TECHNICAL LIBRARY (SUL)
KIRTLAND AFB NM 87117

"The aeronautical and space activities of the United States shall be conducted so as to contribute . . . to the expansion of human knowledge of phenomena in the atmosphere and space. The Administration shall provide for the widest practicable and appropriate dissemination of information concerning its activities and the results thereof."
—NATIONAL AERONAUTICS AND SPACE ACT OF 1958

NASA SCIENTIFIC AND TECHNICAL PUBLICATIONS

TECHNICAL REPORTS: Scientific and technical information considered important, complete, and a lasting contribution to existing knowledge.

TECHNICAL NOTES: Information less broad in scope but nevertheless of importance as a contribution to existing knowledge.

TECHNICAL MEMORANDUMS: Information receiving limited distribution because of preliminary data, security classification, or other reasons. Also includes conference proceedings with either limited or unlimited distribution.

CONTRACTOR REPORTS: Scientific and technical information generated under a NASA contract or grant and considered an important contribution to existing knowledge.

TECHNICAL TRANSLATIONS: Information published in a foreign language considered to merit NASA distribution in English.

SPECIAL PUBLICATIONS: Information derived from or of value to NASA activities. Publications include final reports of major projects, monographs, data compilations, handbooks, sourcebooks, and special bibliographies.

TECHNOLOGY UTILIZATION PUBLICATIONS: Information on technology used by NASA that may be of particular interest in commercial and other non-aerospace applications. Publications include Tech Briefs, Technology Utilization Reports and Technology Surveys.

Details on the availability of these publications may be obtained from:

SCIENTIFIC AND TECHNICAL INFORMATION OFFICE

NATIONAL AERONAUTICS AND SPACE ADMINISTRATION
Washington, D.C. 20546